

DESIGN AND IMPLEMENTATION OF A FIXED POINT DIGITAL
ACTIVE NOISE CONTROLLER HEADPHONE

A THESIS SUBMITTED TO
THE GRADUATE SCHOOL OF NATURAL AND APPLIED SCIENCES
OF
MIDDLE EAST TECHNICAL UNIVERSITY

BY

FATİH ERKAN

IN PARTIAL FULFILLMENT OF THE REQUIREMENTS
FOR
THE DEGREE OF MASTER OF SCIENCE
IN
ELECTRICAL AND ELECTRONICS ENGINEERING

JULY 2009

Approval of the thesis:

**DESIGN AND IMPLEMENTATION OF A FIXED POINT DIGITAL
ACTIVE
NOISE CONTROLLER HEADPHONE**

submitted by **FATİH ERKAN** in partial fulfillment of the requirements for the degree of **Master of Science in Electrical and Electronics Engineering Department, Middle East Technical University** by,

Prof. Dr. Canan Özgen
Dean, Graduate School of **Natural and Applied Sciences** _____

Prof. Dr. İsmet Erkmen
Head of Department, **Electrical and Electronics Engineering** _____

Assoc. Prof. Dr. Tolga Çiloğlu
Supervisor, **Electrical and Electronics Engineering Dept., METU** _____

Examining Committee Members

Prof. Dr. Mübeccel Demirekler
Electrical and Electronics Engineering Dept., METU _____

Assoc. Prof. Dr. Tolga Çiloğlu
Electrical and Electronics Engineering Dept., METU _____

Assist. Prof. Çağatay Candan
Electrical and Electronics Engineering Dept., METU _____

Assist. Prof. Emre Tuna
Electrical and Electronics Engineering Dept., METU _____

Dr. Bekir Ahmet Doğrusöz
ASELSAN _____

Date: 29.07.2009

I hereby declare that all information in this document has been obtained and presented in accordance with academic rules and ethical conduct. I also declare that, as required by these rules and conduct, I have fully cited and referenced all material and results that are not original to this work.

Name, Last name : Fatih Erkan

Signature :

ABSTRACT

DESIGN AND IMPLEMENTATION OF A FIXED POINT DIGITAL ACTIVE NOISE CONTROLLER HEADPHONE

Erkan, Fatih

M. Sc., Department of Electrical and Electronics Engineering

Supervisor: Assoc. Prof. Dr. Tolga Çiloğlu

July 2009, 106 pages

In this thesis, the design and implementation of a Portable Feedback Active Noise Controller Headphone System, which is based on Texas Instruments TMS320VC5416PGE120 Fixed Point DSP, is described. Problems resulted from fixed-point implementation of LMS algorithm and delays existing in digital ANC implementation are determined. Effective solutions to overcome the aforementioned problems are proposed based on the literature survey. Design of the DSP based control card is explained and crucial points about analog-digital-mixed board design for noise sensitive applications are explained. Filtered input LMS algorithm, filtered input normalized LMS algorithm and filtered input sign-sign LMS algorithm are implemented as adaptation algorithms. The advantages and disadvantages of using modified LMS algorithms are indicated. The selection of the parameters of these algorithms is based on theoretical results and experiments. The real time performances of different adaptation algorithms are compared with each other as well as with a commercial analog ANC headphone under different types of artificial and natural noise signals. Moreover, practical conditions such as put on - put off case and dynamic range overflow case are handled with additional software implementations. It is shown that adaptive ANC

systems improve the noise reduction significantly when the noise is within a narrow frequency range and this reduction can be applied to a wider frequency range. It is also shown that the problems of digitally implemented adaptive filters which are based on tracking capability, stability, dynamic range and portability can be fixed to challenge with the analog commercial ANC systems.

Keywords: Filtered Input LMS, Feedback Active Noise Control, Fixed Point Implementation of Active Noise Control, Digital Residual Error, Slowdown Phenomenon in Fixed Point LMS

ÖZ

SABİT NOKTALI SAYISAL AKTİF GÜRÜLTÜ ENGELLEYİCİ KULAKLIK TASARIMI VE UYGULAMASI

Yüksek Lisans, Elektrik ve Elektronik Mühendisliği Bölümü

Tez yöneticisi: Doç. Dr. Tolga Çiloğlu

Temmuz 2009, 106 sayfa

Bu tezde, Sabit Noktalı TMS320VC5416 Sayısal Sinyal İşleyici Tabanlı Taşınabilir Aktif Gürültü Engelleyici Kulaklık tasarım ve uygulaması anlatılmıştır. Sabit-nokta uygulamasından ve sayısal aktif gürültü uygulamasındaki gecikmelerden kaynaklanan problemler belirtilmiştir. Belirtilen problemler için literatür araştırması sonucu etkili çözümler bulunmuştur. Sayısal Sinyal İşleyici tabanlı kart tasarımı irdelenmiş ve gürültü hassasiyeti yüksek analog-sayısal-karışık kart tasarımının kritik noktaları belirtilmiştir. Adaptasyon algoritmaları olarak, filtrelenmiş giriş sinyali kullanımlı LMS, normalize LMS ve sign-sign LMS algoritmaları uygulanmıştır. Kullanılan algoritmaların avantaj ve dezavantajları belirtilmiştir. Bu algoritmaların parametrelerinin seçimi hususunda teorik çıkarımlar ve deneyler kullanılmıştır. Farklı adaptasyon algortimalarının gerçek zamanlı performansları birbirleriyle ve halen piyasada ticari ürün olarak kullanım alanı bulan analog aktif gürültü engelleyici bir kulaklık ile suni ve doğal gürültüler altında kıyaslanmıştır. Bunun ötesinde, kullanım sırasında problem oluşturabilecek, kulaklığın takılıp çıkarılması veya dinamik aralığı aşan gürültü seviyelerine maruz kalınması gibi durumların bertaraf edilmesi için yazılımsal düzeltmeler eklenmiştir. Bu çalışmada gürültü sinyallerinin dar bantta olması durumunda sayısal sistemlerin gürültü azaltımını fark edilir seviyede arttırdığı ve bu artışın daha geniş bantlara da taşınabileceği gösterilmiştir. Ayrıca, sayısal sistemlerin problem yaşadıkları takip edebilme yeteneği, stabil çalışma, dinamik aralık ve

tařınabilirlik konularında geliřtirilebilecekleri ve analog aktif gürültü engelleyici kulaklıklarla rekabet edebilecekleri gösterilmiřtir.

Anahtar Kelimeler: Filtrelenmiř Giriř Sinyali Kullanımlı Geri Besleme, Aktif Gürültü Kontrol Sistemi, Aktif Gürültü Kontrolünün Sabit-Nokta Uygulaması, Sayısal Kalan Hata, Sabit-Nokta LMS uygulamasında Yavařlama Fenomeni

To My Wife

ACKNOWLEDGMENTS

I would like to thank to my supervisor Assoc. Prof. Dr. Tolga ilođlu for his guidance and encouragement.

I also would like to thank to Tbitak for their financial support to this study.

TABLE OF CONTENTS

ABSTRACT	iv
ÖZ	vi
ACKNOWLEDGMENTS	ix
TABLE OF CONTENTS	x
LIST OF TABLES	xiii
LIST OF FIGURES	xiv
LIST OF ABBREVIATIONS	xix
CHAPTERS	
1. INTRODUCTION	1
1.1 Scope of the Thesis	4
1.2 Outline of the Thesis	4
2. ADAPTIVE FILTER THEORY	6
2.1 Wiener Filter Theory	6
2.2 Least Mean Square Algorithm	9
2.3 Recursive Least Square Algorithm vs. Least Mean Square Algorithm	10
2.4 Modified Least Mean Square Algorithms	11
2.4.1 Normalized Least Mean Square Algorithm	11
2.4.2 Sign-Sign Least Mean Square Algorithm	11
3. ADAPTIVE ACTIVE NOISE CONTROL THEORY	13
3.1 Feedforward Active Noise Control	13
3.2 Feedback Active Noise Control	14
3.3 Secondary Path Transfer Function in ANC Systems	16
3.4 Filtered Input LMS Algorithm	17
3.5 Offline Secondary Path Modeling Procedure	19
3.6 Single Channel Feedback Active Noise Control System	21
4. EFFECTS OF FINITE PRECISION ON ADAPTIVE FILTERS	24
4.1 The Quantization Error of MSE in Finite Precision Adaptive Filters	25

4.2	The Slowdown Phenomenon in Finite Precision Adaptation	26
4.3	Advantage of Power-of-Two Step Size Selection in Finite Precision	28
5.	ACTIVE NOISE CONTROL COMPUTER SIMULATIONS	29
5.1	Secondary Path Model Simulations	29
5.2	Noise Cancellation Simulations	31
6.	DESIGN OF PORTABLE DIGITAL ANC HEADPHONE SYSTEM	35
6.1	Schematic Design.....	35
6.2	DSP Configuration	38
6.3	CODEC Configuration.....	39
6.4	DSP Software for ANC Headphone System.....	40
7.	REAL TIME FEEDBACK ACTIVE NOISE CONTROL IMPLEMENTATION	41
7.1	A Practical Approach about Delays in Fx-LMS in ANC Application.....	41
7.2	The Software Architecture of Fx-LMS ANC.....	45
7.3	Fixed Point Limitations in LMS Active Noise Control Implementation	48
7.4	The Discussion of Modified LMS Algorithms in Fixed Point.....	50
7.5	Software Implementation of Offline Secondary Path Modeling.....	51
7.6	Additional Software Implementations	53
8.	PERFORMANCE TESTS OF THE DIGITAL ANC HEADPHONE	55
8.1	Single Tone Experiments	56
8.2	Multiple Tone Experiments	59
8.3	Fan Noise Experiments	64
8.4	Propeller Cabin Noise Experiments	69
8.5	Drill Noise Experiments.....	73
8.6	Tracking Capability Experiments	78
8.7	Convergence Rate for Different LMS Algorithms.....	80
8.8	Digital Residual Error Experiment.....	82
8.9	Drill Noise Experiment: Sub-band Filtering.....	88
8.10	Discussion of the Test Results of Digital ANC Headphone System	90
9.	CONCLUSION	92
9.1	Future Work	94
	REFERENCES.....	96

APPENDICES

A. HARDWARE DESIGN OF DIGITAL ANC HEADPHONE SYSTEM	99
B. TMS320VC5416 DSP CONFIGURATION	101
C. TLV320AIC20K CODEC CONFIGURATION	104

LIST OF TABLES

TABLES

Table 8.1 – The attenuation levels of single tones for digital and analog system.....	58
Table 8.2 – The attenuation levels of multi tone composed of 100 Hz(dominant), 200 Hz(small), 300 Hz(small), 400 Hz(smaller) and 500 Hz(smaller).....	63
Table 8.3 – The attenuation levels of multi tone composed of 200 Hz(dominant), 600 Hz(small), 800 Hz(smaller).....	63
Table 8.4 – The attenuation levels of multi tone composed of 100 Hz(dominant), 400 Hz(small) and 900 Hz(smaller).....	64
Table 8.5 - The attenuation levels of fan noise	68
Table 8.6 - The attenuation levels of propeller cabin noise	73
Table 8.7 - The attenuation levels of drill noise.....	77
Table C.1 – TLV320AIC20K CODEC Write Register Form.....	105
Table C.2 - TLV320AIC20K CODEC Register Content.....	106

LIST OF FIGURES

FIGURES

Figure 2.1 – Wiener Filter Block Diagram	6
Figure 3.1 – Feedforward Active Noise Control System Configuration	13
Figure 3.2 – Feedforward Active Noise Control System Block Diagram	14
Figure 3.3 – Feedback Active Noise Control System Configuration	15
Figure 3.4 – Feedback Active Noise Control Block Diagram	15
Figure 3.5 – Block Diagram of Transfer Functions between Input and Output of Adaptive Feedback Controller	16
Figure 3.6 – Secondary Path Model Transfer Function of Feedback ANC system	16
Figure 3.7 – Filtered Input LMS Algorithm Block Diagram	17
Figure 3.8 – Block Diagram of Secondary Path Modeling in ANC Systems	20
Figure 3.9 - Filtered Input LMS Algorithm Block Diagram.....	22
Figure 3.10 - Filtered Input LMS Algorithm in Feedback System with Primary Signal Estimation Block.....	22
Figure 5.1 – An Accurate Secondary Path Model Estimation of Pure Delay in MATLAB	30
Figure 5.2 – An Improper Secondary Path Model Estimation of Pure Delay in MATLAB due to Step Size Selection Mistake	30
Figure 5.3 – An Improper Secondary Path Model Estimation of Pure Delay in MATLAB due to Insufficient Iteration.....	31
Figure 5.4 – Fourier Transform of Primary Noise Signal in ANC Simulation in MATLAB	32
Figure 5.5 – The Decreasing Characteristic of Error Signal by a Proper Adaptation Process due to Suitable Step Size Selection in MATLAB	32
Figure 5.6 – Adaptation Filter Coefficients of a Converged Simulation in MATLAB ...	33
Figure 5.7 – Faster Convergence due to a Larger Step Size within the Boundary of Convergence in MATLAB.....	33

Figure 5.8 – Convergence Rate with The Accurate Retrieval of Primary Noise in MATLAB	34
Figure 5.9 – Slower Convergence Rate Because of The Inaccurate Retrieval of Primary Noise in MATLAB	34
Figure 6.1 – The Digital ANC System Hardware	36
Figure 6.2 – Generalized Block Diagram of the DSP Code for Fx-LMS Adaptive ANC Headphone System.....	40
Figure 7.1 - The Sampling of Error Signal in Real Time Implementation of ANC Headphone System.....	42
Figure 7.2 - Filtered Input LMS Algorithm in Feedback System.....	42
Figure 7.2 - Overall Block Diagram of Software Implementation for Fx-LMS in Feedback ANC Headphone System	47
Figure 7.3 – Block Diagram of Software Realization of Offline Secondary Path Modeling in ANC Headphone System.....	52
Figure 7.4 – The impulse response of Secondary Path Model of Active ANC Headphone System.....	53
Figure 8.1 – Single 200 Hz Tone in NLMS Experiment “with ANC” and “without ANC”	56
Figure 8.2 – Fourier Transform of Single 200 Hz Tone in NLMS Experiment “without ANC”	57
Figure 8.3 – Fourier Transform of Single 200 Hz Tone in NLMS Experiment “with ANC”	57
Figure 8.4 - Tone of 100 Hz, 200Hz, 300Hz, 400Hz and 500 Hz Composition in NLMS Experiment “with ANC” and “without ANC”	59
Figure 8.5 – Fourier Transform of 100 Hz, 200Hz, 300Hz, 400Hz and 500 Hz Composition in NLMS Experiment “without ANC”	60
Figure 8.6 – Fourier Transform of 100 Hz, 200Hz, 300Hz, 400Hz and 500 Hz Composition in NLMS Experiment “with ANC”	60
Figure 8.7 – Fourier Transform of Multi Tone Signal in LMS Digital Headphone Experiment “with ANC” and “without ANC”	61

Figure 8.8 – Fourier Transform of Multi Tone Signal in LMS Digital Headphone Experiment “with ANC” and “without ANC”	61
Figure 8.9 – Fourier Transform of Multi Tone Signal in Sign-Sign LMS Digital Headphone Experiment “with ANC” and “without ANC”	62
Figure 8.10 – Fourier Transform of Multi Tone Signal in Analog ANC Headphone Experiment “with ANC” and “without ANC”	62
Figure 8.11 - Fan Noise in NLMS Experiment “with ANC” and “without ANC”	65
Figure 8.12 – Fourier Transform of Fan Noise in NLMS Experiment “without ANC” ..	65
Figure 8.13 – Fourier Transform of Fan Noise in NLMS Experiment “with ANC”	66
Figure 8.14 - Fourier Transform of Fan Noise in NLMS Experiment “with ANC” and “without ANC”	66
Figure 8.15 - Fourier Transform of Fan Noise in LMS Experiment “with ANC” and “without ANC”	67
Figure 8.16 - Fourier Transform of Fan Noise in Sign-Sign LMS Experiment “with ANC” and “without ANC”	67
Figure 8.17 - Fourier Transform of Fan Noise in Analog ANC Headphone Experiment “with ANC” and “without ANC”	68
Figure 8.18 - Propeller Cabin Noise in LMS Experiment “with ANC” and “without ANC”	69
Figure 8.19 – Fourier Transform of Propeller Cabin Noise in LMS Experiment “without ANC”	70
Figure 8.20 – Fourier Transform of Propeller Cabin Noise in LMS Experiment “with ANC”	70
Figure 8.21 - Fourier Transform of Propeller Cabin Noise in NLMS Experiment “with ANC” and “without ANC”	71
Figure 8.22 - Fourier Transform of Propeller Cabin Noise in LMS Experiment “with ANC” and “without ANC”	71
Figure 8.23 - Fourier Transform of Propeller Cabin Noise in Sign-Sign LMS Experiment “with ANC” and “without ANC”	72
Figure 8.24 - Fourier Transform of Propeller Cabin Noise in	72
Analog ANC Headphone Experiment “with ANC” and “without ANC”	72

Figure 8.25 - Drill Noise in Sign-Sign LMS Experiment “with ANC” and “without ANC”	74
Figure 8.26 – Fourier Transform of Drill Noise in Sign-Sign LMS Experiment “without ANC”	74
Figure 8.27 - Fourier Transform of Drill Noise in Sign-Sign LMS Experiment “with ANC”	75
Figure 8.28 - Fourier Transform of Drill Noise in NLMS Experiment “with ANC” and “without ANC”	75
Figure 8.29 - Fourier Transform of Drill Noise in LMS Experiment “with ANC” and “without ANC”	76
Figure 8.30 - Fourier Transform of Drill Noise in Sign-Sign LMS Experiment “with ANC” and “without ANC”	76
Figure 8.31 - Fourier Transform of Drill Noise in Analog ANC Headphone Experiment “with ANC” and “without ANC”	77
Figure 8.32 – NLMS Tracking Performance with a Non-stationary Sinusoidal Signal ..	78
Figure 8.33 – LMS Tracking Performance with a Non-stationary Sinusoidal Signal	78
Figure 8.34 – Sign-Sign LMS Tracking Performance with a Non-stationary Sinusoidal Signal	79
Figure 8.35 – Analog ANC Headphone Performance with a Non-stationary Sinusoidal Signal	79
Figure 8.36 – Convergence Rate of NLMS for Single Tone of 300 Hz	80
Figure 8.37 – Convergence Rate of LMS for Single Tone of 300 Hz	81
Figure 8.38 – Convergence Rate of Sign-Sign LMS for Single Tone of 300 Hz	81
Figure 8.39 – Primary Noise for LMS Experiments for level-2 400 Hz signal	82
Figure 8.40 – Residual Error for NLMS Experiment for level-2 400 Hz signal	83
Figure 8.41 – Residual Error for LMS Experiment for level-2 400 Hz signal	83
Figure 8.42 – Residual Error for Sign-Sign LMS Experiment for level-2 400 Hz signal	84
Figure 8.43 – Primary Noise for LMS Experiments for level-1 400 Hz signal	84
Figure 8.44 – Residual Error for NLMS Experiment for level-1 400 Hz signal	85
Figure 8.45 – Residual Error for LMS Experiment for level-1 400 Hz signal	85
Figure 8.46 – Residual Error for Sign-Sign LMS Experiment for level-1 400 Hz signal	86

Figure 8.47 – Primary Noise for LMS Experiments for level-0 400 Hz signal	86
Figure 8.48 – Residual Error for NLMS Experiment for level-0 400 Hz signal	87
Figure 8.49 – Residual Error for LMS Experiment for level-0 400 Hz signal	87
Figure 8.50 – Residual Error for Sign-Sign LMS Experiment for level-0 400 Hz signal	88
Figure A.1 – Serial Port Connections between TLV320AIC20K and DSP	99
Figure B.1 – Block Diagram of Multichannel Buffered Serial Port in TMS320VC5416 DSP	103
Figure C.1 – The Block Diagram of One Channel of TLV320AIC20K CODEC	104

LIST OF ABBREVIATIONS

ANC	: Active Noise Control	McBSP	: Multi Channel Buffered Serial Port
DSP	: Digital Signal Processor	SPCR	: Serial Port Control Register
LMS	: Least Mean Squares	RCR	: Receive Control Register
NLMS	: Normalized Least Mean Square	XCR	: Transmit Control Register
SSLMS	: Sign-Sign LMS Algorithm	PCR	: Pin Control Register
IIR	: Infinite Impulse Response	XRDY	: Transmit Ready
FIR	: Finite Impulse Response	RRDY	: Receive Ready
RLS	: Recursive Least Squares	DMA	: Direct Memory Access
LTI	: Linear Time Invariant	FS	: Frame Synchronization
DAC	: Digital to Analog Converter	MCLK	: Main Clock
ADC	: Analog to Digital Converter	SCLK	: Serial Clock
QE	: Quantization Error	CH	: Channel
DRE	: Digital Residual Error	GPIO	: General Purpose Input Output
LSD	: Least Significant Digit	LSB	: Least Significant Bit
CPU	: Central Processing Unit	Fx-LMS	: Filtered Input Least Mean Square
MSE	: Mean Squared Error	FPGA	: Field Programmable Gate Array
ROM	: Read Only Memory	PROM	: Programmable Read Only Memory
PLL	: Phase Locked Loop	CODEC	: Coder-Decoder Microchip
BGA	: Ball Grid Array		
IFR	: Interrupt Flag Register		
IMR	: Interrupt Mask Register		
CSL	: Chip Support Library		

CHAPTER 1

INTRODUCTION

Acoustic noise has been a serious problem as a result of the development in industry, which introduces fans, engines and noisy machines. Heavy industry workers, pilots or military personnel using noisy vehicles suffer from the noise inherent to their work place.

The basic solution to the acoustic noise has been cancellation by passive elements which are simple earmuffs, enclosures, barriers and acoustical absorbing materials [1]. These passive elements have considerable attenuation over high frequency ranges; however they are ineffective at low frequencies as a result of the increasing wavelength.

Active Noise Control (ANC) is introduced as a superior alternative to passive attenuation [2]. The basic principle of Active Noise Control is to produce an opposing signal having opposite phase and same amplitude with the noise to be reduced [3], [4]. The accuracy in the phase and amplitude matching is critical for the amount of reduction of the noise. Some of the application areas of ANC are duct noise reduction, interior noise reduction in cars and aircrafts and ear protection headphone systems.

According to the properties of the noise source and attenuation zone, ANC systems can be implemented as single channel or multi channel. A single channel ANC system has one output to produce the opposing signal, one input to pick the residual noise signal and depending on the control system may have one reference input to pick the reference noise signal. Headphone systems are good examples to single channel systems. In these systems, noise source is spatial and single secondary source is sufficient for attenuation. Multi channel systems are necessary when noise reduction has

to be achieved in a volume or noise sources can not be modeled as point sources. In this case, the sound field is so complicated that the opposing signal should be generated by a complex array of actuators and multiple error sources are needed. Noise cancellation system in a plane cockpit can be given as an example to multichannel system.

Due to their portability and feasibility, headphone systems are the most preferred solutions to noise cancellation. In 1978, Dorey [5] developed first ANC helmets for aircrew. Most of the commercial ANC headphone products use fixed analog controllers. A constant coefficient cancellation filter is implemented in fixed analog controllers. This cancellation filter is optimized for a predefined frequency range. Fixed analog controllers are preferred for their stability, low power consumption and small sizes. Moreover, there is not a tracking problem in fixed analog controllers. Most of the noise reduction in analog ANC systems is accomplished by mechanical design of the headphone and they are effective only at lower frequency bands.

A more qualitative solution to ANC is Adaptive Active Noise Control. Adaptive ANC systems are based on digital filters which are optimized by adaptation algorithms according to the incoming noise and reference signals. ANC systems are generally implemented with finite impulse response (FIR) filters; because they have quadratic performance surfaces and they are stable.

ANC systems can be classified under two different structures, which are feedforward ANC and feedback ANC. Feedforward ANC systems use one input for error signal, another input for reference signal and one output for secondary source. It is critical that the reference signal be coherent to the noise source in feedforward systems. Feedback ANC systems use one input for error signal and one output for secondary source, because a coherent reference signal is not needed. Headphone systems should be implemented as two independent single channel feedback ANC systems. Feedforward headphone ANC implementation is not feasible, because the movements of user change the transfer function between error microphone and reference microphone.

There are various types of adaptation algorithms for FIR filters such as least mean square (LMS) and recursive least square (RLS). The performance of these algorithms can be compared according to three parameters which are convergence speed, misadjustment and tracking capability. Convergence speed is simply the number of iterations needed for the filter to converge to its optimum state for a specific desired signal and input signal. Misadjustment is the mean deviation of the mean square error from its optimum value. Tracking capability is the ability of the filter to track non-stationary signals. It is difficult to optimize these three parameters simultaneously.

Adaptive filters are implemented in digital signal processors (DSP). Digital signal processors can be fixed point type which are optimized for fixed point arithmetic operations or can be floating point type which can perform floating point operations fast. Floating point processors are superior considering their arithmetic success. On the other hand, fixed point processors dissipate less power than floating point processors and this is vital for portable devices. ANC algorithms can be optimized for both fixed point and floating point environment individually.

Literature survey shows that fixed point implementation of adaptive filters results in severe performance degradation [12]-[15]. This degradation originates from quantization error and slowdown phenomenon. The slowdown phenomenon is defined as stopping or slowing down of the adaptation due to the least significant digit limitation of the digital environment [12]. There exist several theoretical derivations for the quantization error and slowdown phenomenon in literature [12]-[18]. However, real time implementation of adaptive ANC in fixed point digital environment considering quantization error and slowdown phenomenon is not performed. Additionally, the effects of delays existing between the digital and analog parts of the controller in a digitally implemented system are not represented. Moreover, several subjects such as dynamic range and tracking capability of a digitally implemented ANC system are not examined in detail.

1.1 Scope of the Thesis

The main purpose of this study is to design and implement a portable ANC headphone system based on a fixed point DSP. It is aimed to examine the effects of fixed point limitations on LMS algorithm. It is also aimed to represent the effects of delays existing between digital and analog parts of the controller and modify the adaptation software to compensate these effects.

The theory of Wiener filtering, feedback ANC, filtered input LMS algorithm, limitations due to fixed point implementation are examined. Preliminary computer simulations are made for filtered input LMS algorithm in MATLAB. The design and implementation of a digital ANC headphone system is accomplished. A fixed point Texas Instrument TMS320VC5416 DSP and a Texas Instrument TLV320AIC20K CODEC are used on the controller card. Knowles Acoustics SP0103NC microphone and Sennheiser HD265 headphone are used as the analog parts. The resultant system is powered by battery and the portability of the device is provided. The delays existing between digital and analog parts of the controller are mathematically represented. The solutions for the algorithm optimization in fixed point limitations are proposed. The performance tests of designed portable ANC headphone system compared with a commercial analog ANC product are conducted with different noise signals. In addition, modified LMS adaptation algorithms are compared with each other. The effect of slowdown phenomenon is experimentally observed in designed ANC system.

1.2 Outline of the Thesis

Theoretical backgrounds of adaptive filtering and active noise control theory are given in Chapter 2 and Chapter 3 respectively. The effects of finite precision on digitally implemented adaptive filters are given in Chapter 4. Results of MATLAB simulations about filtered input LMS algorithm are shown in Chapter 5. Hardware and embedded software design of the portable DSP based adaptive ANC headphone system is

explained in Chapter 6. In Chapter 7, real time implementation of feedback ANC filtered input LMS algorithm is explained and the delays existing between digital and analog parts of controller are represented. The experiment results of the designed digital headphone system compared with a commercial analog ANC headphone are given in Chapter 8.

CHAPTER 2

ADAPTIVE FILTER THEORY

In this chapter, adaptive filtering problem is investigated beginning from the wiener filter theory. Least Mean Squares (LMS) and Recursive Least Squares (RLS) algorithms are described. The explanation of LMS algorithm is further detailed by describing two modified versions of LMS algorithm which are normalized LMS algorithm (NLMS) and sign-sign LMS algorithm (SSLMS).

2.1 Wiener Filter Theory

The main purpose of the Wiener filter is to reduce the amount of noise in a signal by comparing it with an estimation of the desired signal which is noise free. Wiener Filter has an assumption that the input signal and noise signal are stationary linear stochastic processes.

To derive the expression of a finite impulse response wiener filter, consider a discrete time filter shown in Figure 2.1 [6].

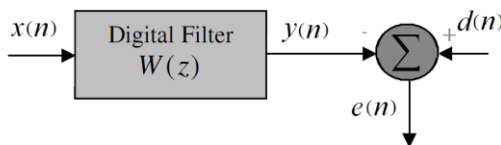


Figure 2.1 – Wiener Filter Block Diagram

$x(n)$: input signal
 $y(n)$: output signal
 $w(n)$: coefficients of wiener filter
 $d(n)$: desired signal
 $e(n)$: error signal

The output $y(n)$ is expressed as

$$y(n) = \sum_{k=0}^{L-1} w_k(n)x(n-k) \quad (2.1)$$

or

$$y(n) = \mathbf{w}(n)^T \mathbf{x}(n) \quad (2.2)$$

where $x(n-k)$ are the input signal samples and w_k are the corresponding weighting elements for the filter coefficients. $\mathbf{x}(n)$ and $\mathbf{w}(n)$ are representing the column vectors consisting of the $x(n-k)$ and w_k elements respectively.

The difference of desired signal $d(n)$ and output signal $y(n)$ is defined as error signal $e(n)$ [6].

$$e(n) = d(n) - y(n) \quad (2.3)$$

The cost function J is defined as the expected value of the square of error signal [6].

$$J = E\{e^2(n)\} \quad (2.4)$$

The purpose of a wiener filter is to minimize the cost function. The optimum filter coefficients can be found by finding the minima of this cost function. Since J is a quadratic function of the filter $w(n)$, the gradient of the cost function with respect to $w(n)$ is

$$\nabla J = -2E\{x(n-k)e(n)\} \quad k=0,1,\dots,L \quad (2.5)$$

The necessary and sufficient condition for the cost function to attain its minimum value is that the corresponding value of error $e(n)$ is orthogonal to each input sample that

enters into the estimation of the desired response at time n . The minimum value of the cost function is reached when gradient of the cost function is zero [6].

$$E\{x(n-k)e_{min}(n)\} = 0 \quad k=0,1,\dots,L \quad (2.6)$$

where e_{min} denotes the minimum error when the filter reaches its optimum state.

Rewriting (2.6) by using (2.1) and (2.3);

$$y(n) = \sum_{j=0}^{L-1} w_{opt}(j) E\{x(n-k)x(n-j)\} = E\{x(n-k)d(n)\}, \quad k = 0,1,2,\dots,L \quad (2.7)$$

where $w_{opt}(n)$ denotes the weighting function at its optimum state and L is the filter length. Defining

$$r(j-k) = E\{x(n-k)x(n-j)\} \quad (2.8)$$

$$p(-k) = E\{x(n-k)d(n)\} \quad (2.9)$$

where $r(j-k)$ is the autocorrelation function of the input signal and $p(-k)$ is the cross-correlation function of the input signal and the desired response, a simpler form of (2.7) can be written as in (2.10) [6].

$$\sum_{j=0}^{L-1} w_{opt}(j)r(j-k) = p(-k), \quad k=0,1,2,\dots,L \quad (2.10)$$

The matrix form of (2.10) is known as Wiener-Hopf equation and can be rewritten as [6]

$$\mathbf{R}\mathbf{w}_{opt} = \mathbf{p} \quad (2.11)$$

where \mathbf{R} is the autocorrelation matrix of input signal $x(n)$, \mathbf{p} is the cross-correlation function of input signal $x(n)$ and desired signal $d(n)$. \mathbf{w}_{opt} is the vector consisting of the

optimum filter coefficients which minimizes $E\{e^2(n)\}$ known as mean squared error (MSE).

2.2 Least Mean Square Algorithm

LMS (least mean square) is an adaptation algorithm which finds the optimal filter coefficients minimizing instantaneous squared values of error signal. LMS algorithm is an approximation to the steepest descent algorithm using expected value of squared error signal. LMS is useful in applications where the entire knowledge of error signal is not available [6].

LMS algorithm finds the filter coefficients iteratively according to (2.12)

$$\mathbf{w}(n+1) = \mathbf{w}(n) + \frac{1}{2}\mu[-\nabla J] \quad (2.12)$$

where $\mathbf{w}(n+1)$ represents the vector consisting of the updated filter coefficients, μ is the step size and J is the cost function. The cost function J is the instantaneous squared value of error signal $e(n)$.

$$J = e^2(n) \quad (2.13)$$

The gradient of the cost function is written using (2.2) and (2.3) as

$$\nabla e^2(n) = -2e(n)\mathbf{x}(n) \quad (2.14)$$

Therefore, the update equation of the filter coefficients is

$$\mathbf{w}(n+1) = \mathbf{w}(n) + \mu[\mathbf{x}(n)e(n)] \quad (2.15)$$

where

$$e(n) = d(n) - y(n) \quad (2.16)$$

and

$$y(n) = \mathbf{w}(n)^T \mathbf{x}(n) \quad (2.17)$$

To prevent the divergence of algorithm the step size μ must satisfy the following condition [6],

$$0 < \mu < 2 / \lambda_{\max} \quad (2.18)$$

where λ_{\max} is the largest eigenvalue of the autocorrelation matrix of $x(n)$, \mathbf{R} .

The boundary for step size selection for convergence is given as follows in [6].

$$0 < \mu < 2 / \sum_{k=0}^{L-1} E\{|x(n-k)|^2\} \quad (2.19)$$

2.3 Recursive Least Square Algorithm vs. Least Mean Square Algorithm

Recursive Least Square Algorithm utilizes information contained in the input data, extending back to the instant of time when the algorithm is initiated [6]. RLS algorithm tries to find optimum filter coefficients so as to minimize sum of error squares. The error signal is defined similar to LMS. However, RLS uses weighting factors for each error sample to calculate the sum of error squares. The convergence rate of RLS is significantly higher than the convergence rate of LMS. Moreover, the rate of convergence is independent from the eigenvalue spread of the autocorrelation matrix of input data in RLS. However, the computational complexity of RLS is high. LMS is preferred rather than RLS for its computational simplicity [7]. On the other hand, LMS suffers from the dependence of its convergence on the eigenvalue spread of the autocorrelation matrix of input data.

2.4 Modified Least Mean Square Algorithms

Considering different properties of LMS algorithms, such as stability, convergence rate and computational requirements of implementation, various types of LMS algorithms are developed.

2.4.1 Normalized Least Mean Square Algorithm

In LMS algorithm, the stability and convergence rate depend on the eigenspread of autocorrelation matrix of reference input $x(n)$. To eliminate this dependency, a modified algorithm called normalized LMS (NLMS) is introduced [6].

$$\mathbf{w}(n+1) = \mathbf{w}(n) + \mu[\mathbf{x}(n) / \|\mathbf{x}^2(n)\|]e(n) \quad (2.20)$$

Considering the adaptation sequence of filter it can be seen that step size μ is dimensionless [6]. Moreover, $\mu / \|\mathbf{x}^2(n)\|$ is actually a time varying step size. NLMS has a faster convergence rate than standard LMS [6]. To prevent divergence the step size μ must satisfy the following condition in normalized LMS algorithm [6].

$$0 < \mu < 2 \quad (2.21)$$

It is important to note that, these discussions about convergence rate and step size choice is considered in infinite precision case. The parameter selection in finite precision is described in Chapter 7, real time implementation of feedback ANC algorithms.

2.4.2 Sign-Sign Least Mean Square Algorithm

To reduce the computational complexity of the standard LMS algorithm, the multiplication of error and input signal in (2.15) can be represented by multiplication of their signs and become as in (2.22) in sign-sign LMS algorithm (SSLMS).

It is obvious that, convergence rate is considerably decreased in SSLMS algorithm. To reduce computational complexity and not to decrease the convergence rate as dramatically as in SSLMS, one can use the sign-data LMS as in (2.23) or sign-error LMS as in (2.24) in which only one of the multiplicative factor is taken as the sign of the signal.

$$\mathbf{w}(n+1) = \mathbf{w}(n) + \mu \text{sign}(\mathbf{x}(n)) \text{sign}(e(n)) \quad (2.22)$$

$$\mathbf{w}(n+1) = \mathbf{w}(n) + \mu \text{sign}(\mathbf{x}(n)) e(n) \quad (2.23)$$

$$\mathbf{w}(n+1) = \mathbf{w}(n) + \mu \mathbf{x}(n) \text{sign}(e(n)) \quad (2.24)$$

CHAPTER 3

ADAPTIVE ACTIVE NOISE CONTROL THEORY

In this chapter, feedforward and feedback ANC systems are explained. In addition, the secondary path in ANC system, filtered input LMS algorithm and offline secondary path modeling are described.

3.1 Feedforward Active Noise Control

In a single channel feedforward active noise control system there are two microphones and one secondary source as seen in Figure 3.1. The reference microphone is placed near the noise source whereas the error microphone is placed near the secondary source. Reference signal from the reference microphone and residual error signal from the error microphone is used for the adaptation of the filter as seen in Figure 3.2 [4].

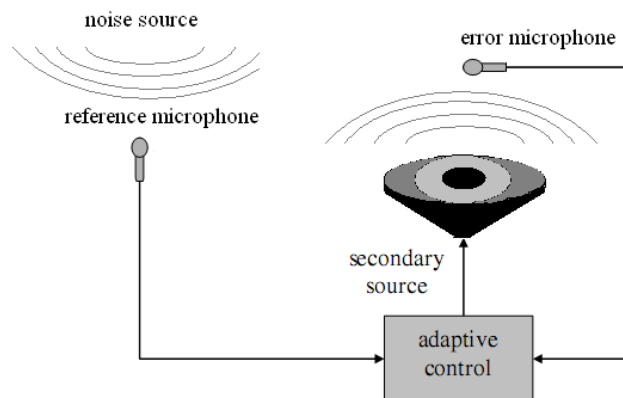


Figure 3.1 – Feedforward Active Noise Control System Configuration

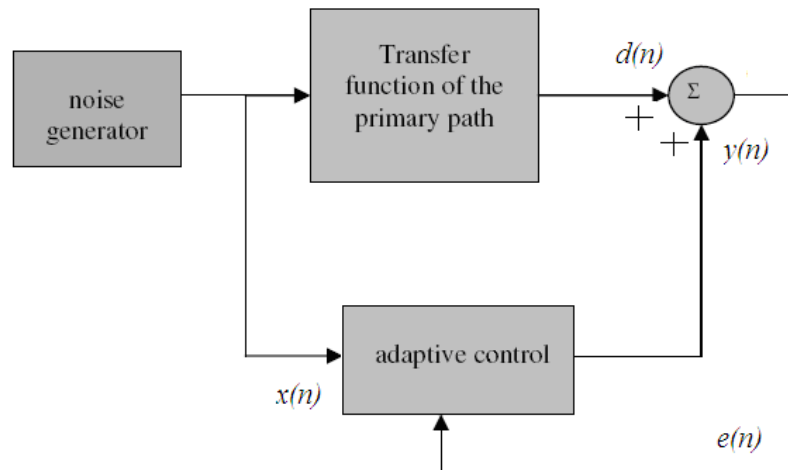


Figure 3.2 – Feedforward Active Noise Control System Block Diagram

- $d(n)$: primary noise signal
- $x(n)$: reference signal
- $y(n)$: adaptive filter output signal
- $e(n)$: error signal

3.2 Feedback Active Noise Control

Feedback ANC system is first proposed by Olson [3]. Since there is no reference microphone, Feedback ANC system generates its own reference signal based on adaptive filter output signal and error signal [4]. Feedback ANC system is required for applications in which it is not possible to sense a reference noise signal coherent to noise source. Headphone system in this study is based on Feedback ANC principle.

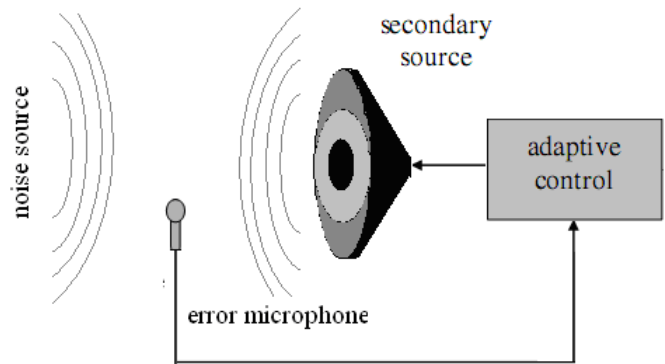


Figure 3.3 – Feedback Active Noise Control System Configuration

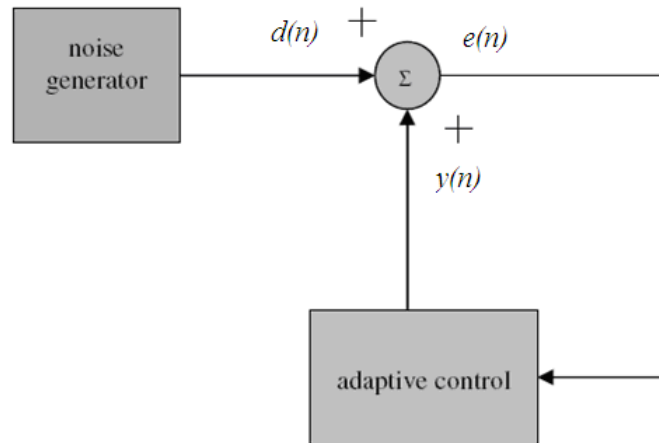


Figure 3.4 – Feedback Active Noise Control Block Diagram

- $d(n)$: primary noise signal
- $y(n)$: adaptive filter output signal
- $e(n)$: error signal

Adaptive feedback ANC estimates the primary noise signal and uses it as the reference signal [4]. As seen in Figure 3.3 and Figure 3.4 the output of the adaptive controller is summed with noise to be reduced and the resultant signal is directly fed back to the controller.

3.3 Secondary Path Transfer Function in ANC Systems

In practical implementations of ANC systems, there exist transfer paths between digital output and digital input of adaptive controller as seen in Figure 3.5 [4].

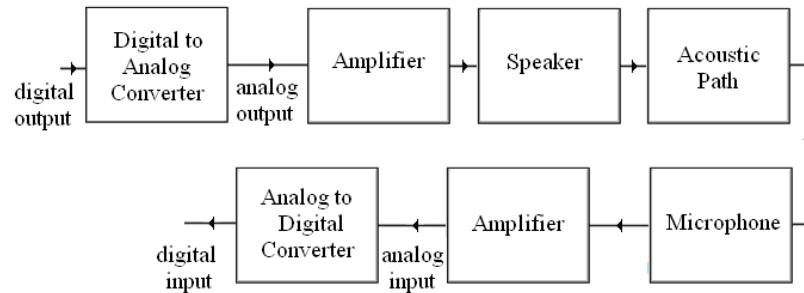


Figure 3.5 – Block Diagram of Transfer Functions between Input and Output of Adaptive Feedback Controller

The contribution of all of the paths in Figure 3.5 creates so-called secondary path. The secondary path of a feedback ANC system can be seen in Figure 3.6.

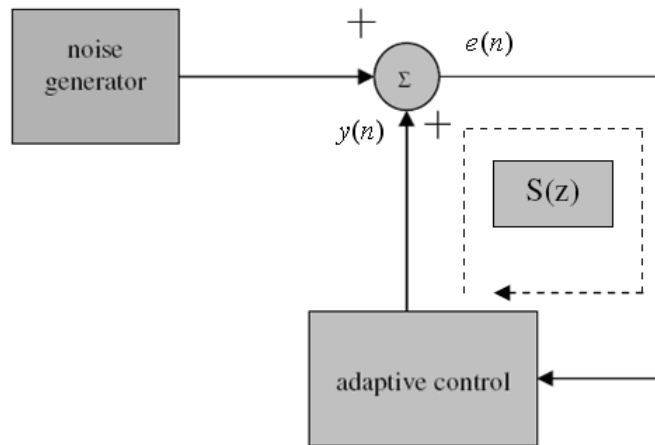


Figure 3.6 – Secondary Path Model Transfer Function of Feedback ANC system

- $e(n)$: error signal
- $y(n)$: output signal
- $S(z)$: secondary path transfer function

3.4 Filtered Input LMS Algorithm

The existence of secondary path in ANC systems necessitates the generation of filtered input LMS algorithm (Fx-LMS). The generalized block diagram of filtered input LMS algorithm is seen in figure 3.7 [4].

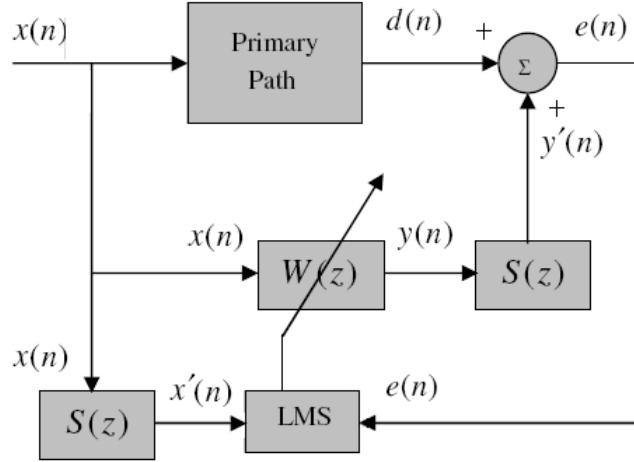


Figure 3.7 – Filtered Input LMS Algorithm Block Diagram

- $x(n)$: input reference signal
- $d(n)$: primary noise signal
- $e(n)$: input error signal
- $y(n)$: output of adaptive filter
- $x'(n)$: adaptation input signal

Considering Figure 3.7, the output of the controller will become $y'(n)$ which is the filtered version of $y(n)$ with secondary path. Thus the error signal is represented as in (3.1) and (3.2)

$$e(n) = d(n) + y'(n) \quad (3.1)$$

$$e(n) = d(n) + s(n) * y(n) \quad (3.2)$$

Inserting (3.3) given below into (3.4) to, a different representation of error signal is reached.

$$y(n) = \mathbf{w}(n)^T \mathbf{x}(n) \quad (3.3)$$

$$e(n) = d(n) + s(n) * (\mathbf{w}(n)^T \mathbf{x}(n)) \quad (3.4)$$

A modification in (3.4) leads to (3.5) and the error signal representation is simplified as in (3.6).

$$e(n) = d(n) + \mathbf{w}^T(n) (s(n) * x(n)) \quad (3.5)$$

$$e(n) = d(n) + \mathbf{w}^T(n) \mathbf{x}'(n) \quad (3.6)$$

where $\mathbf{x}'(n)$ is the vector consisting of adaptation input signal samples and $\mathbf{w}(n)$ is the vector consisting of filter coefficients at instant n .

$$x'(n) = s(n) * x(n) \quad (3.7)$$

$$s(n) = Z^{-1} \{S(z)\} \quad (3.8)$$

The update equation of adaptive filter is as in (3.9)

$$\mathbf{w}(n+1) = \mathbf{w}(n) - (\mu / 2) \cdot \nabla e^2(n) \quad (3.9)$$

Considering (3.6), the gradient of squared of error signal is as in (3.10).

$$\nabla e^2(n) = 2e(n) \mathbf{x}'(n) \quad (3.10)$$

Inserting (3.10) in (3.9), (3.11) is reached.

$$\mathbf{w}(n+1) = \mathbf{w}(n) - \mu e(n) \mathbf{x}'(n) \quad (3.11)$$

Thus, in Fx-LMS the input reference signal to the adaptation algorithm is filtered creating a new signal called adaptation input signal $x'(n)$. The filter is $S(z)$, which is the transfer function of secondary path. The maximum value of step size μ ensuring convergence is [4]:

$$\mu_{\max} = 1 / P_{x'} (L+\Delta) \quad (3.12)$$

where $P_{x'}$ is the power of filtered reference signal $x'(n)$ and Δ is the amount of the delay in the secondary path. $P_{x'}$ is represented by $E\{(x'(n))^2\}$.

In Fx-LMS the system is modeled linear time invariant. A generalized form of Fx-LMS algorithm can be seen in equation (5) of [28]. In this generalized form the system is modeled as linear time varying. The modified Fx-LMS algorithm can be derived from this generalized form as in equation (13) in [28]. In modified Fx-LMS algorithm the convergence rate is increased.

3.5 Offline Secondary Path Modeling Procedure

The secondary path in ANC system should be modeled to implement Fx-LMS algorithm. Assuming that the secondary path is linear time invariant (LTI), a finite impulse response (FIR) filter can be chosen as the modeling filter. The impulse response of secondary path can be estimated by a procedure similar to the process of estimation of adaptive filter of the controller. The estimation can be done prior to the normal operation or during the normal operation. These methods are called offline and online modeling, respectively. In this study, offline secondary path modeling is used.

The secondary path is modeled in offline modeling procedure by sending a wideband signal to the secondary source and comparing a filtered version of this known

signal by the signal picked up from the error microphone. If the adaptation algorithm for the corresponding filter is converged then the filter can be used as a model for the secondary path. The critical points in secondary path modeling are the necessity of wide band frequency characteristics of the sent signal, an optimum number of iteration ensuring convergence and proper gain settings of input and output signals. Generally, white noise is used as the reference signal, because it includes all frequency components equally. Some systems were tried to be implemented by wide band music signals instead of white noise [8]. In this study, white noise is used as output signal. A block diagram of Secondary Path Modeling is given in Figure 3.8 and the modeling procedure is defined below [19].

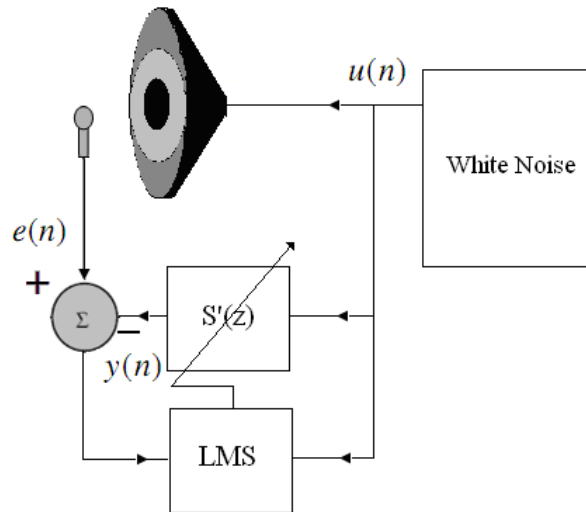


Figure 3.8 – Block Diagram of Secondary Path Modeling in ANC Systems

$u(n)$ represents the white noise signal and $e(n)$ represents the sampled signal. There exist two adaptation signals for LMS algorithm which is $u(n)$ and “ $e(n) - y(n)$ ”, which is the difference between the sampled signal and model filtered signal. A model for the secondary path is used to filter white noise signal and this model is updated according to aforementioned adaptation signals.

The secondary path model $S(z)$ is deviated from its actual value, because it is retrieved from an estimation algorithm. The estimation of secondary path is named $S'(z)$.

Using $S'(z)$, (3.2) and (3.7) can be rewritten as

$$e(n) = d(n) + s'(n) * y(n) \quad (3.13)$$

$$x'(n) = s'(n) * x(n) \quad (3.14)$$

where,

$$s'(n) = Z^{-1}\{S'(z)\} \quad (3.15)$$

Offline secondary path modeling can be used, because even 90° phase error between $S(z)$ and estimation $S'(z)$ is tolerable in the secondary path model estimation [10].

The maximum step size ensuring convergence of filtered input LMS algorithm is as follows [4], [11];

$$\mu_{\max} = 1 / P_{x'}(L+\Delta) \quad (3.16)$$

where $P_{x'}$ is the power of filtered reference signal $x'(n)$ and Δ is the amount of the delay in the secondary path model. Considering (3.16), the delay in secondary path is said to affect the step size upper bound. Thus, to increase the upper bound for step size one should decrease the physical distance between secondary source and error microphone as much as possible.

3.6 Single Channel Feedback Active Noise Control System

Since the adaptive controller in this study is based on feedback ANC system it will be beneficial to have a closer look at feedback ANC and give detailed block diagrams.

Figure 3.9 shows the block diagram of filtered input LMS algorithm [4]. There is no reference microphone in feedback ANC system. The absence of reference signal $x(n)$ is compensated with estimation of primary signal $d(n)$, which is also not trivially accessible. The primary signal $d(n)$ is summed with the output of the controller. The resultant signal is sampled by the error microphone as $e(n)$. Thus, the estimation of primary signal $d(n)$ can be made by using estimation of output signal $y'(n)$. The estimated signal is named $\hat{d}(n)$. The additional blocks for $d(n)$ estimation can be seen in Figure 3.10.

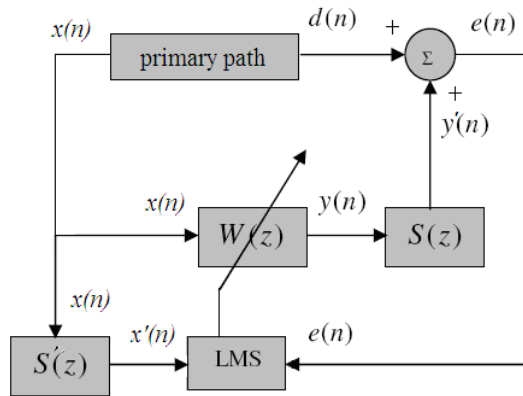


Figure 3.9 - Filtered Input LMS Algorithm Block Diagram

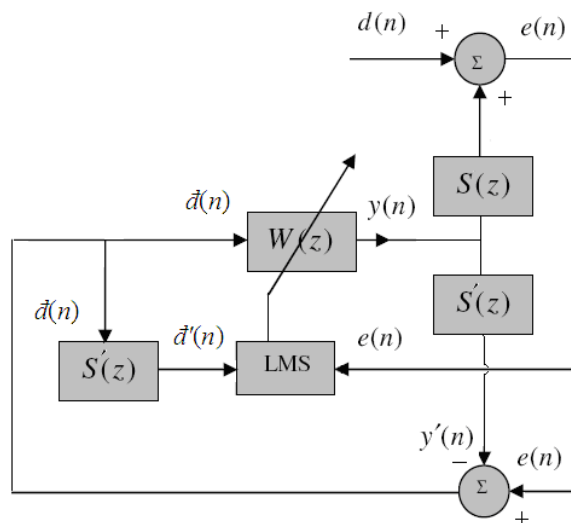


Figure 3.10 - Filtered Input LMS Algorithm in Feedback System with Primary Signal Estimation Block

The estimated primary signal is retrieved as in (3.17) and (3.18).

$$\vec{d}(n) = e(n) - y'(n) \quad (3.17)$$

$$\vec{d}(n) = e(n) - s'(n) * y(n) \quad (3.18)$$

The update equation can be written as in (3.20) using (3.19).

$$e(n) = d(n) + \mathbf{w}^T(n) \vec{d}'(n) \quad (3.19)$$

$$\mathbf{w}(n+1) = \mathbf{w}(n) - \mu e(n) \vec{d}'(n) \quad (3.20)$$

$$\mu_{\max} = 1 / P_{d'}(L+\Delta) \quad (3.21)$$

are reached where $P_{d'}$ is the power of filtered estimated primary signal $\vec{d}'(n)$, L is the order of the adaptive filter and Δ is the amount of delay in secondary path model. Filtered primary signal estimation $\vec{d}'(n)$ is represented as in (3.22) where $s'(n)$ is secondary path model.

$$\vec{d}'(n) = s'(n) * \vec{d}(n) \quad (3.22)$$

(3.22) can be rewritten for normalized LMS as follows:

$$\mathbf{w}(n+1) = \mathbf{w}(n) - \mu e(n) \vec{d}'(n) / \|\vec{d}'(n)\| \quad (3.23)$$

It is critical to note that these results are not actual representations of the real time application. Above analysis belongs to a system with no delay. A more detailed derivation considering the delays inherent to digital implementation will be given in Chapter 7.

CHAPTER 4

EFFECTS OF FINITE PRECISION ON ADAPTIVE FILTERS

In this chapter, the effects of quantization on LMS algorithm implementation are explored by investigating derivations made so far in literature. Moreover, another additional problem originating from fixed point implementation is described which is called slowdown phenomenon.

The input signal $e(n)$ and output signal $y(n)$ in Fx-LMS algorithm from (3.19) to (3.22) are represented by quantized values in a digital signal processor. The procedure of sampling and digitizing the analog signal is accomplished by analog-to-digital Converter (ADC) devices. Similarly, a digital-to-analog converter (DAC) device produces analog signals according to the digital words given by a digital signal processor.

In audio applications, the device containing both ADC and DAC components within encoding, decoding, filtering and interpolation blocks are CODECs. CODECs represent a digital word by 14 bits, 16 bits, 24 bits or 32 bits according to the precision needed specific to application. In this study a 16-bit CODEC is used. 16-bit is sufficient for representing input/output variables since the dynamic range supplied by this resolution is satisfactory. Thus, the algorithm processes the 16-bit samples of input signal and output a 16-bit word. The arithmetic operations are achieved over these 16-bit words in a fixed-point processor. Obviously, the operations can be done by assigning more bits to words to widen the dynamic range. Unfortunately, for higher resolution data the processor uses much more cycles to perform adaptation algorithms. Higher CPU clock rates mean higher power consumption which is unacceptable for portable devices. There exist studies [15] which optimize the bit assignment procedures in fixed point

LMS adaptation algorithms assuring both a minimal MSE and minimal power consumption.

Quantization error is inherent to any digital system. It is shown that adaptation algorithms which are implemented in finite precision digital environments behave significantly different than infinite precision (analog) implemented algorithms due to not only quantization but some further limitations [12].

4.1 The Quantization Error of MSE in Finite Precision Adaptive Filters

To derive an analytical expression for the quantization error, considering the infinite precision and finite precision filters together, filter output equations will be as follows [12]

$$y(n) = \sum_{k=0}^{N-1} w_k(n)x(n-k) \quad (4.1)$$

$$\hat{Y}(n) = \sum_{k=0}^{N-1} \hat{W}_k(n)x(n-k) \quad (4.2)$$

where $\hat{Y}(n)$ and $\hat{W}_k(n)$ are the corresponding digitized values of $y(n)$ and $w_k(n)$ respectively. The quantization error is

$$QE = y(n) - \hat{Y}(n) \quad (4.3)$$

$$= \sum_{k=0}^{N-1} [w_k(n) - \hat{W}_k(n)] \cdot x(n-k) \quad (4.4)$$

The mean-squared QE can be written as

$$E\{QE^2\} = E\left\{ \sum_{k=0}^{N-1} \sum_{m=0}^{N-1} [w_k(n) - \hat{W}_k(n)] \cdot [w_m(n) - \hat{W}_m(n)] \cdot x(n-k) \cdot x(n-m) \right\} \quad (4.5)$$

Assuming that the inputs $\{x_i\}$'s are independent random variables whose root mean square is equal to X_{rms} , (4.5) can be approximated as

$$E\{QE^2\} = E\left\{\sum_{m=0}^{N-1} [w_k(n) - \hat{W}_k(n)]^2\right\} \cdot X_{\text{rms}}^2 \quad (4.6)$$

$$\leq N \cdot \text{LSD}^2 \cdot X_{\text{rms}}^2 \quad (4.7)$$

Rewriting (4.7) removing the power-of-two factors, (4.8) is reached.

$$QE_{\text{rms}} = N^{1/2} \cdot \text{LSD} \cdot X_{\text{rms}} \quad (4.8)$$

The dependence of quantization error on least significant digit value, filter length and the input signal rms value can be seen in (4.8). The result of this derivation will be clearer in the next section.

4.2 The Slowdown Phenomenon in Finite Precision Adaptation

The adaptation algorithms, which update the control variable in negative gradient direction, modify the current filter vector by adding an update term. The update term is the product of a gradient and step-size. Evidently, adaptation ceases when the update term gets smaller in magnitude than the LSD, which is the least significant digit value of the digitizer. This is known as the stopping phenomenon according to [12]. However, a more detailed study shows that this effect is actually slowdown phenomenon [14].

Early termination of the adaptation or adaptation with too low speed due to slowdown phenomenon may result in larger mean square error compared to infinite precision case. In [13] a general derivation of the total output error is made in finite precision case and the optimum step size value for convergence and minimum MSE is

said to be so small that the algorithm does not converge due to the slowdown phenomenon.

When the update term is smaller than LSD the following equation can be written as in [12]

$$|\mu \cdot e_{n_0} \cdot x_{n_0-i}| \leq \text{LSD} \quad (4.9)$$

where μ is the step size and n_0 is the time instant when the LSD value is attained by the update term.

A further assumption that all the taps stop adapting at the same time simplifies the relationship and replaces $|x_{n-i}|$ by its root mean square value, X_{rms} [12].

$$|e_{n_0}| \leq \text{LSD} / (\mu \cdot X_{\text{rms}}) \quad (4.10)$$

$$e_d = \text{LSD} / (\mu \cdot X_{\text{rms}}) \quad (4.11)$$

e_d is defined as the rms digital residual error (DRE). DRE is seen to be inversely proportional to step size and root mean square value of reference signal $x(n)$. The most important conclusion of the DRE expression is that smaller step size values results in larger DRE values and the step size should be larger if the adaptation stops prematurely. In contrast, analog residual error is minimized with a smaller step size [12].

The ratio of DRE to the QE in (4.8) has important results. The ratio of DRE to QE decreases with increasing filter length. It is important to note that longer digital filters seem to be less sensitive to Digital Residual Error, because DRE becomes dominant in the resultant error expression when the length of the filter is decreased. However, increasing the filter length decreases the upper boundary of step size selection. This smaller step size selection makes the DRE larger. Thus DRE can not be decreased simply by decreasing the filter length. On the other hand, when the tap weights get close

to their optimum state the mean square error and the step size have decreased too much and they are using very small correction terms after that point. Considering these, it can be said that a step size decreasing in time should not be used.

In conclusion, contrary to the analog case where the error is minimized by using a small step size, in finite precision case a smaller step size may create a larger digital residual error due to slowdown phenomenon. Thus, there is a trade-off between decreasing analog residual error and decreasing digital residual error. Another difference between infinite and finite precision case is that in finite precision case a constant step size selection made according to the aforementioned issue, gives better result than a time-varying step size which is the optimum selection in infinite precision case [12]. Moreover, in [13] it is shown that if the number of bits used to represent the filter coefficient is higher than the number of bits used for data inputs the dominance of the filter length on the overall quantization error is decreased. This bit assignment proposal is supported in [15]. In [18] equations of optimum step size selection for different algorithms are derived in detail.

4.3 Advantage of Power-of-Two Step Size Selection in Finite Precision

Another important issue, considering the binary digitizing environments is that the step sizes which can be represented as power-of-two are superior because of practical implementation considerations. In this case, multiplication with μ is usually realized as right shifts. The error and input signals are first multiplied in double precision; the result is then shifted and quantized to fixed point precision. The convergence is controlled by the quantized value of the entire weight update term [16], [17].

CHAPTER 5

ACTIVE NOISE CONTROL COMPUTER SIMULATIONS

Preliminary simulations should be made in a flexible environment before real time implementation in order to gain experience about LMS algorithm, offline secondary path modeling and filtered input LMS algorithm. The software environment is chosen as MATLAB and the variables are represented in infinite precision for all simulations.

5.1 Secondary Path Model Simulations

The feasibility of the practical implementation of offline secondary path modelling is investigated. Theory is applied by creating artificial input and output signals in offline secondary path modelling by inserting a predefined delay between these signals. It is aimed to see whether a pure delay secondary path model $S'(z)$ can be estimated by the proposed adaptation process and examine the impulse response of $S'(z)$.

In Figure 5.1, a pure delay $S'(z)$ is estimated accurately, as the result of proper step size selection and sufficient number of iteration. In Figure 5.2, the importance of step size selection is seen. Step size is increased to attain a faster convergence rate. However, the resultant $S'(z)$ is deviated from ideal model. In Figure 5.3, another problem which is early termination of adaptation for offline secondary path model is seen. This problem may be visible due to slowdown phenomenon mentioned in Chapter 4. Thus the same explanation made for the step size selection of finite precision LMS implementation, also applies to finite precision secondary path modelling process.

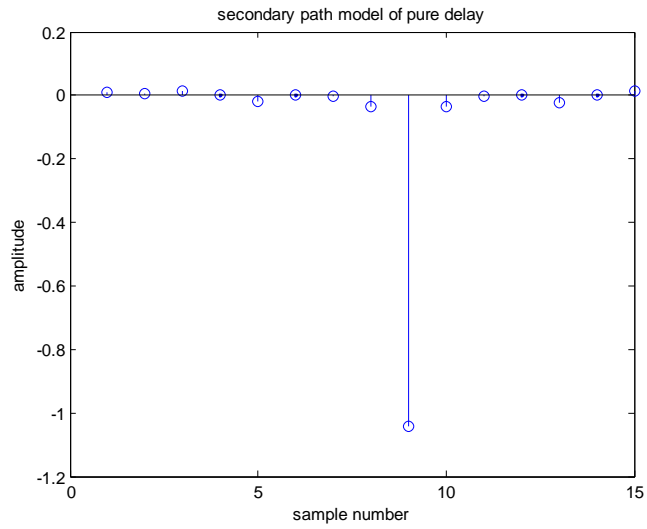


Figure 5.1 – An Accurate Secondary Path Model Estimation of Pure Delay in MATLAB with stepsize 1/1000

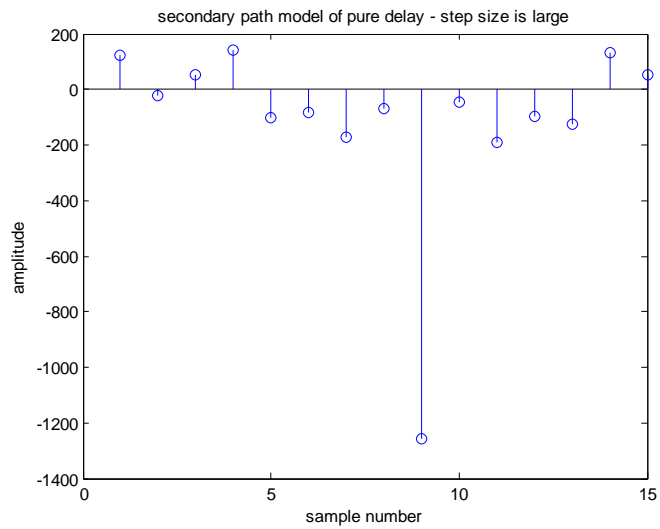


Figure 5.2 – An Improper Secondary Path Model Estimation of Pure Delay in MATLAB with stepsize 1/10000

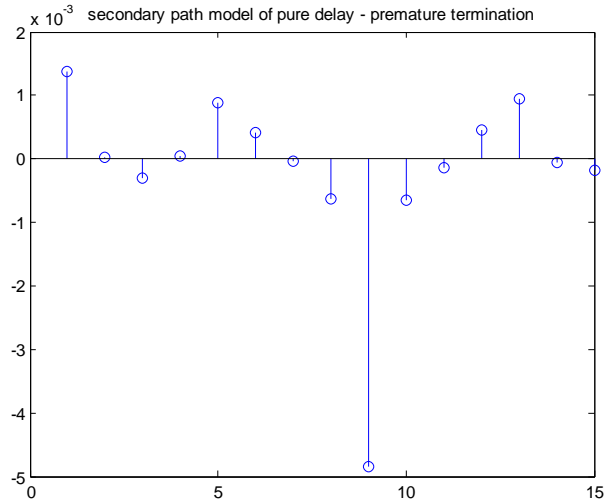


Figure 5.3 – An Improper Secondary Path Model Estimation of Pure Delay in MATLAB due to Insufficient Iteration

5.2 Noise Cancellation Simulations

By using the secondary path model estimation, Fx-LMS algorithm for feedback ANC system is implemented. The acoustic superposition of primary noise signal and secondary source output is artificially made. The crucial points about update coefficient in adaptation equation which is discussed in Chapter 3 are investigated in detail.

In Figure 5.4, the frequency components of tonal noise input to the simulation is seen. In Figure 5.5, it is seen that a proper step size selection and sufficient iteration number results in convergence of the filter coefficients and the error value to decrease to its minimum. Figure 5.6 shows the filter coefficients of this simulation. As can be seen in Figure 5.7 a faster convergence can be achieved with a larger step size within the boundary of step size selection.

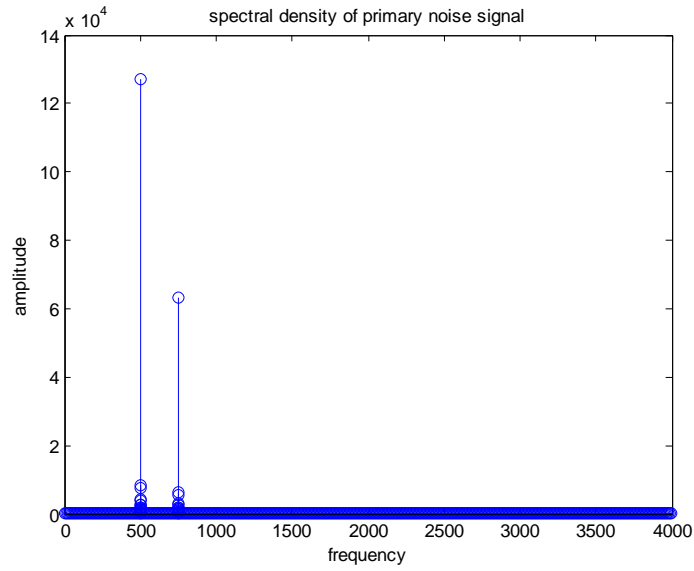


Figure 5.4 – Fourier Transform of Primary Noise Signal in ANC Simulation in MATLAB

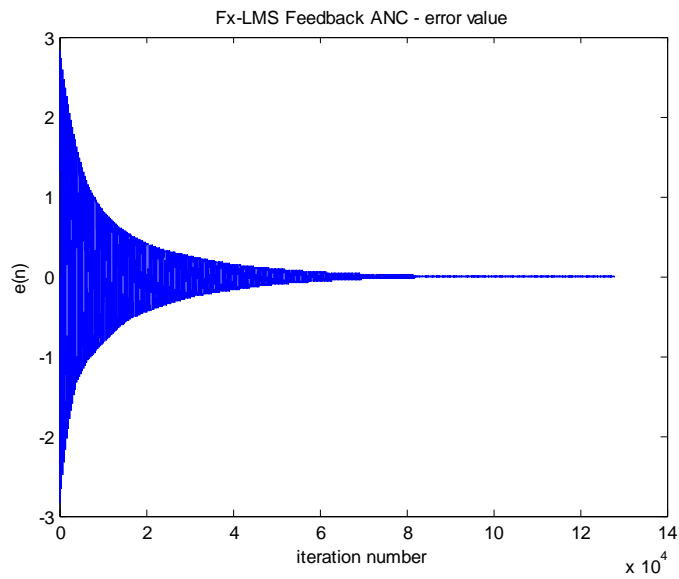


Figure 5.5 – The Decreasing Characteristic of Error Signal by a Proper Adaptation process due to suitable step size selection (1/10000) in MATLAB

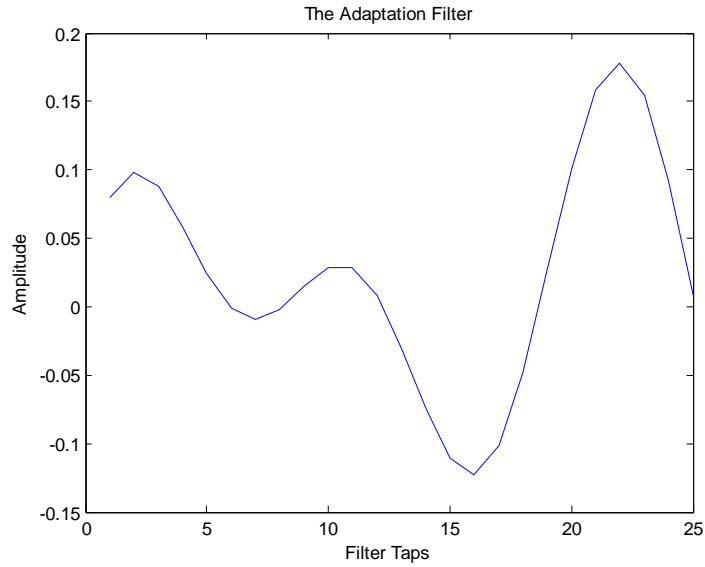


Figure 5.6 – Adaptation Filter Coefficients of a Converged Simulation in MATLAB

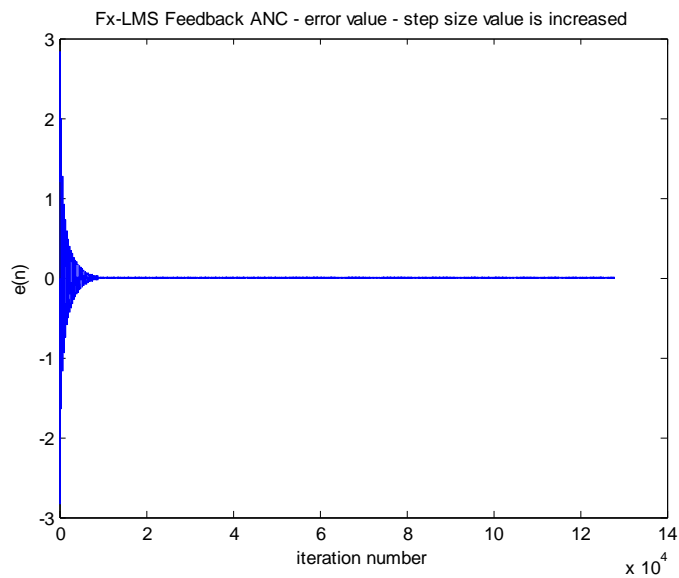


Figure 5.7 – Faster Convergence due to a Larger Step Size (1/5000) within the Boundary of Convergence in MATLAB

An interesting result can be seen in Figure 5.8 and Figure 5.9 which shows the importance of the accurate $\hat{d}(n)$ retrieval. If the primary noise signal is correctly

retrieved, Figure 5.8 is reached. However, if one sample error is inserted in this retrieval process, a slower convergence rate is attained as can be seen in Figure 5.9. It is also possible to show that a more severe retrieval error may result in divergence.

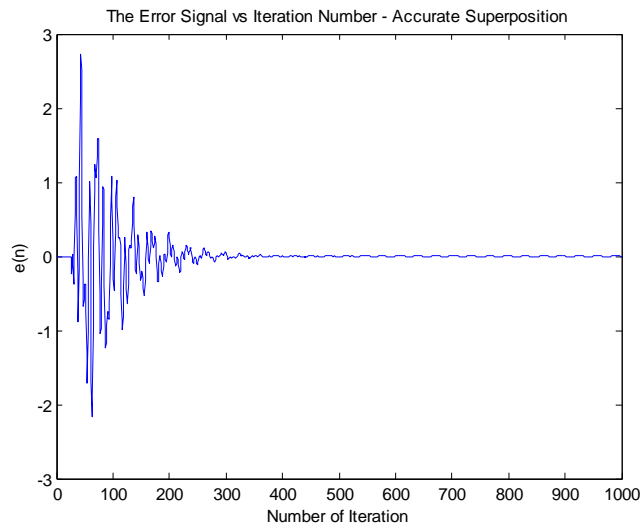


Figure 5.8 – Convergence Rate with The Accurate Retrieval of Primary Noise in MATLAB

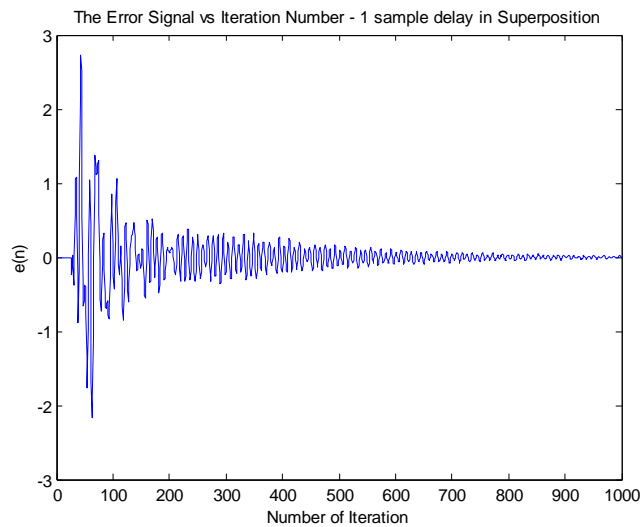


Figure 5.9 – Slower Convergence Rate Because of The Inaccurate Retrieval of Primary Noise in MATLAB

CHAPTER 6

DESIGN OF PORTABLE DIGITAL ANC HEADPHONE SYSTEM

The portable digital ANC headphone system consists of two main parts which are controller card and headset. There are two microphone inputs and one headphone output on the controller card. Another input is line-in for external music sources. In this study the external music source part is not implemented. In each ear cup of the headphone there exists a speaker and an omnidirectional SMD active microphone biased from the controller card. The device is compatible to work with voltages of 3.3V to 5.5V and consumes 150mA. The system can be used actively for 15 - 20 Hours using 2300 mAh batteries.

The operation is based on feedback ANC principle. The noise existing on the microphone diaphragm is sampled as residual error and the opposing signal sample is sent to the headphone. The microphone is directed to the speaker resembling to the position of the ear. The location of the microphone is experimentally decided and stabilized. In [8] and [9] the optimum location of error microphone issue is discussed. The headphone of the system is able to supply audio band frequencies in a flat manner and allow a suitable location for microphone.

6.1 Schematic Design

The main block consists of Texas Instruments TLV320AIC20K CODEC, Texas Instruments TMS320VC5416PGE120 DSP, Knowles Acoustics SP0103NC Active Microphone and Sennheiser HD 265 Headphone. The bias voltage of Microphone is fed

by the CODEC through its MICBIAS output. The input signal is passed through a bandpass filter and fed to the headset (channel-1) and handset (channel-2) inputs of CODEC. These analog inputs are taken and digitized by CODEC. 150 Ohm Analog outputs of the CODEC are connected to the headphone. CODEC produces analog signals according to the digital data taken from DSP. The digital data transfer between DSP and CODEC is accomplished by a multi channel buffered serial port working at 256 KHz. The frequency of the frame synchronization signal of this serial port is 8 KHz which is the sampling frequency of the audio signals. The input digital data is 32-Bit long consisting of two 16-Bit channels corresponding to each CODEC channel. The hardware design of digital ANC headphone system is briefly described in Appendix A. The designed digital ANC headphone is shown in Figure 6.1.



Figure 6.1 – The Digital ANC System Hardware

The design is achieved on a multi layer board. One of the reasons for multi layer design is the existence of Ball Grid Array (BGA) products on the board such as FPGA. Products having BGA layout generally have lots of pins which can not be realized on a standard packet having the pins distributed on the sides of the chip. The pins of a BGA package are simple balls covering the bottom of the chip in an array form and these balls

are so close to each other that the interior pins can not be laid through the outer side of the chip without crossing any line or any other ball. These should be laid on a multi-layer card.

Another reason for multi-layer design is the necessity of stable ground and voltage levels, which is a specific requirement of the implementation. ANC headphone controller card carry sensitive analog and high frequency digital signals which are close to each other. The high speed signals on the board makes transitions between the low voltage and high voltage levels rapidly. During these transitions, there exists a current path between each of these signal nodes to the ground. Every switching between logical levels affects the value of the ground at the instant when the switching is occurred. The ground value on the whole board does not change at the same time at the same level, because each signals current finds it shortest path from its high level node to the ground. Thus, ground levels can represent different voltages on different part of the card. An analog signal which is generally referencing ground and near to aforementioned digital signal path is affected. The analog signals should be isolated from digital swinging.

The most vulnerable analog signal in DSP board is the microphone signal, because the voltage output of a microphone is so low that it can be lost as a result of the stated ground swinging problem. Most electrets microphone suffers from this problem since their voltage levels are in the order of 0.1 – 1mV. However, SP0103NC microphone which is used in this system is an active SMD microphone. It has an embedded gain stage which gives 20dB gain as pre-amplification to the output of its transducer [27]. However, the ground swinging problem is still a problem to be solved.

To eliminate the aforementioned grounding problem and increase the noise immunity of the system, the grounding of the card is made carefully. The problem is solved by distinguishing the grounds for the digital and analog signals and defining a plane for each of them through the whole card. Additionally, another main ground is defined to which the analog and digital grounds are electrically connected at the 4 corners of the card through large vias (defined as drills through layers of the card).

Another solution is defining two different ground regions in the same plane. Then, the circuits using analog ground and digital ground are laid near to analog part and digital part respectively. These two ground parts are electrically connected to each other through only one path. This solution has a drawback of creating an inductance between two ground regions.

Besides distinguishing ground layers, the voltage supplies of digital devices and analog devices are given from different regulators whose outputs are independent. Moreover groundings of these regulators are supplied from their corresponding ground layer.

6.2 DSP Configuration

The configuration of TMS320VC5416 DSP consists of configuration of CPU (central processing unit) registers and some peripheral registers of the serial port between DSP and CODEC. The register description of TMS320VC5416 is given in Appendix B.

The implementation of the ANC system on DSP can be realized in several ways, considering the serial port communication. In this study, specialized multi channel buffered serial ports (McBSPs) of the DSP are used by the CPU itself. The McBSPs are based on the standard serial-port interface found on other 54x devices [20]. The brief description of serial ports in TMS320VC5416 is given in Appendix B. Chip support library (CSL) of DSP is useful for configuration of DSP and signal processing implementation. In this study, general approach is to use CSL wherever appropriate [24].

As a result of configuration of serial port of TMS320VC5416 DSP the write and read processes should be synchronous to XRDY and RRDY signals respectively. XRDY means transmit ready whereas RRDY means receive ready. These are indicator signals toggling from their idle states when the corresponding buffer registers are ready to be

written (XRDY) or to be read (RRDY) [21]. It is crucial to wake the port from reset after configuration and before writing to DXR register.

It is important to note that the data line carries two 16-bit channels together and the synchronization of read/write and signal processing operation is critical. The missing samples on each channel or the placement of each channel samples on the other channel arrays causes the algorithm to easily diverge or the secondary path model not to be properly estimated.

In this study, first XRDY signal is monitored by CPU. CPU waits until the DXR register is suitable for a write, which means DXR register to XSR register copy is accomplished. Afterwards, the data is written to DXR. Similarly when RRDY signals that DRR register is ready to be read, the content of these register is taken by the CPU. The details of this flow is explained in Chapter 7.

6.3 CODEC Configuration

TLV320AIC20K is a specified Texas Instrument CODEC which is optimized for the DSPs of Texas Instrument Company [23]. The resolution of the codec is 16-bit and sampling rate can be maximally 26 KHz. The interior architecture is based on sigma-delta analog-to-digital and digital-to-analog converters. This CODEC carries two independent channels having an ADC and a DAC. The gain settings in the CODEC are critical considering the discussions made so far about secondary path model estimation and accurate sampling of error signal in noise cancellation. These settings are adjusted according to the experiments made with sinusoidal signals with known amplitude and frequency. The specifications and settings of TLV320AIC20K CODEC is given in Appendix C.

6.4 DSP Software for ANC Headphone System

The software starts to apply initialization of DSP's CPU and peripheral registers. This may be done by "gel" files in Code Composer Studio 3.1. Initial values of registers for flash-ROM boot should be carefully assigned. One of the general purpose outputs of DSP is dedicated for reset signal of TLV320AIC20K since a power-up process is necessary for CODEC [23]. First CODEC is initialized. Then, the variables that will be used in following blocks are initialized and the McBSP is configured for CODEC configuration. The CODEC configuration words are written and checked according to [23] and the two main blocks of algorithm start to run consecutively: Offline Secondary Path Modeling and Fx-LMS Adaptive Noise Cancellation Algorithm.

Figure 6.2 shows the main blocks in DSP software. This block diagram does not contain low-level processes such as program loading from flash-ROM or emulator.

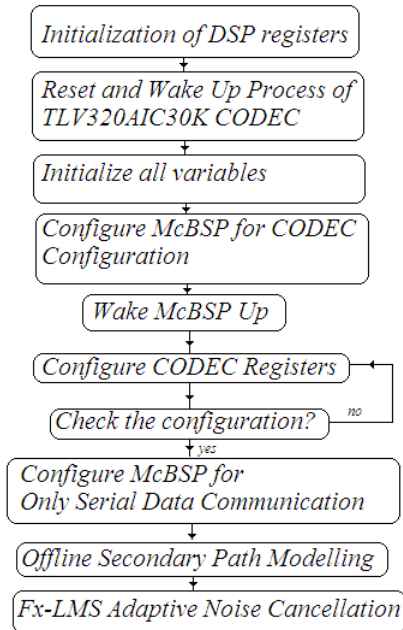


Figure 6.2 – Generalized Block Diagram of the DSP Code for Fx-LMS Adaptive ANC Headphone System

CHAPTER 7

REAL TIME FEEDBACK ACTIVE NOISE CONTROL IMPLEMENTATION

In this chapter software implementation of feedback ANC and offline secondary path modeling are described. The delays existing between digital and analog parts of the controller are represented. The algorithm implementation is modified considering the effects of these delays. The step size selection of LMS algorithm is made considering fixed point implementation. Moreover, software adjustments are proposed to overcome practical problems. One of these problems is changing of secondary path when the headphone is put off. The other problem is divergence of the algorithm when a dynamic range exceeding noise is applied to the system.

7.1 A Practical Approach about Delays in Fx-LMS in ANC Application

There exist delays between digital and analog parts of the ANC system. One of the reasons for these delays is the buffered communication structure between DSP and CODEC. The other reasons are the analog-to-digital and digital-to-analog conversion times of CODEC and the acoustic delays. These delays should be examined, because they affect the update equation of adaptive filter and estimation of primary signal. The actuation component of update equation is the multiplication of stepsize and negative gradient of squared error signal as seen in (7.1).

$$\mathbf{w}(n+1) = \mathbf{w}(n) - (\mu / 2) \cdot \nabla e^2(n) \quad (7.1)$$

The residual error sample $e(n)$ is created by the summation of output of adaptive filter and primary noise signal. The output of adaptive filter is not output from the secondary source just after it is created because of the aforementioned delays. Moreover, the error sample taken into DSP actually belongs to earlier sampling instants because of these delays. In order to calculate the gradient of squared error signal correctly, these delays should be considered. To understand the effects of these delays mathematically, consider the analog signal $e(t)$ and its sampling operation in Figure 7.1 and remember the block diagram of filtered input LMS algorithm in feedback system seen in Figure 7.2.

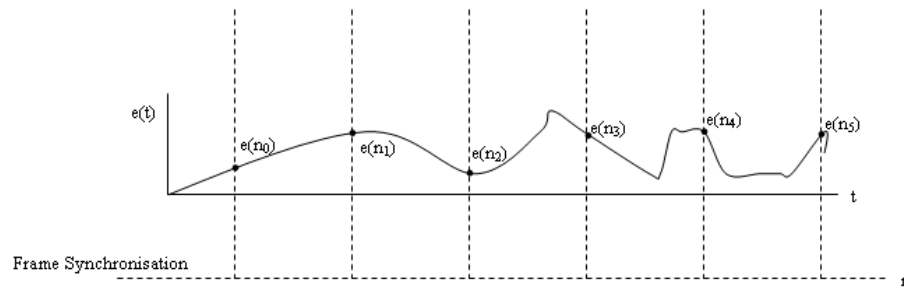


Figure 7.1 - The Sampling of Error Signal in Real Time Implementation of ANC Headphone System

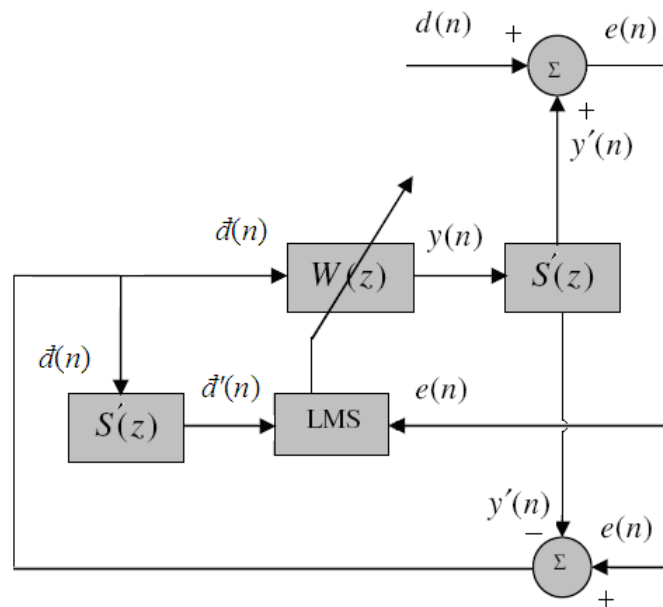


Figure 7.2 - Filtered Input LMS Algorithm in Feedback System

Assume that, A is the delay amount in receive path from microphone to DSP including acoustic delay between noise signal and transducer. Similarly assume that, B is the delay amount in transmit path from DSP to speaker including the delay of the speaker. The delay amount in secondary path model $s(n)$ was defined as Δ in Chapter 3. It is evident that Δ is summation of A and B.

n_A means a time instant after the present time by an amount A, similarly n_B means a time instant before the present time by an amount B. At $n = n_A$, $e(n_0)$ is sampled, because of the delays between microphone and DSP. At $n = n_B$ output sample $y(n_B)$ was created and given to the CODEC. $y(n_B)$ was turned into analog signal at $n = n_0$ because of the delays between DSP and speaker. Thus, $e(n_0)$ was created with contribution of primary noise sample $d(n_0)$ and $y(n_B)$.

$$e(n_0) = d(n_0) + y(n_B) \quad (7.2)$$

At $n = n_A$, $\vec{d}(n_0)$ can be estimated as in (7.3).

$$\vec{d}(n_0) \approx d(n_0) = e(n_0) - y(n_B) \quad (7.3)$$

$\mathbf{w}(n_A)$ in (7.4) represents the adaptive filter coefficients at instant n_A . $y(n_B)$ can be calculated as in (7.5).

$$y(n_A) = \mathbf{w}(n_A)^T \vec{d}(n_0) \quad (7.4)$$

$$y(n_B) = \mathbf{w}(n_B)^T \vec{d}(n_{-(A+B)}) \quad (7.5)$$

Thus, (7.2) can be rewritten as in (7.6).

$$e(n_0) = d(n_0) + \mathbf{w}(n_B)^T \vec{d}(n_{-(A+B)}) \quad (7.6)$$

The update equation at $n = n_A$ is as in (7.7).

$$\mathbf{w}(n_{A+1}) = \mathbf{w}(n_A) - (\mu/2) \cdot \nabla J \quad (7.7)$$

where $J = e^2(n_A)$ and $\mathbf{w}(n_{A+1})$ represents the filter coefficients which will be used for the following cycle. Rewriting (7.7) using (7.8), (7.9) is reached.

$$\nabla J = 2 \cdot e(n_A) \cdot \mathbf{d}(n_{-(A+B)}) \quad (7.8)$$

$$\mathbf{w}(n_{A+1}) = \mathbf{w}(n_A) - \mu \cdot e(n_0) \cdot \mathbf{d}(n_{-(A+B)}) \quad (7.9)$$

$\mathbf{w}(n_A)$ in (7.9) is updated with the error signal resulted from the output signal at instant n_{-B} as seen in (7.3). This output sample is created by $\mathbf{w}(n_{-B})$. This result is inevitable because of the delays existing between input and output signal of digital controller.

The filtered primary signal estimation signal is delayed in modified update equation (7.9). The secondary path model compensates for these delays in update equation, because the delay amount of secondary path model is the summation of A and B. Thus, rewriting (7.9) using $\mathbf{d}'(n_0)$, (7.10) is reached. $\mathbf{d}'(n)$ is the convolution of secondary path model $s(n)$ and estimated primary signal $\mathbf{d}(n)$. $\mathbf{d}'(n)$ is the array consisting of the filtered estimated primary signal samples.

$$\mathbf{w}(n_{A+1}) = \mathbf{w}(n_A) - \mu \cdot e(n_0) \cdot \mathbf{d}'(n_0) \quad (7.10)$$

Although the update equation is not affected by aforementioned delays, the estimation of primary signal should be made considering these delays. The delay between DSP and speaker should be taken into account as seen in (7.3). The effect of one sample estimation mistake on the convergence rate is clearly seen in Chapter 5, Figure 5.8 and Figure 5.9. The estimation of primary signal can be made by using the secondary path filtered $y'(n_0)$ instead of $y(n_{-B})$ as in (3.18) if A is small enough with respect to changes in output signal $y(n)$. Both of $y'(n_0)$ and $y(n_{-B})$ are tried experimentally

in this study and it is seen that there is no significant difference in performance of these implementations.

7.2 The Software Architecture of Fx-LMS ANC

Considering the derivations made for the delays in real time ANC, the following equations are used to realize the feedback ANC in this study.

- $y(n) = \mathbf{w}^T(n) \cdot \mathbf{d}(n)$
- $y'(n) = \mathbf{s}'^T(n) \cdot y(n)$
- $\mathbf{d}'(n) = e(n) - y'(n)$
- $\mathbf{d}'(n) = \mathbf{s}'^T(n) \cdot \mathbf{d}(n)$
- $\mathbf{w}(n+1) = \mathbf{w}(n) - \mu \cdot e(n) \cdot \mathbf{d}'(n)$

$\mathbf{d}(n)$ and $y(n)$ vectors are input and output arrays which are used for convolution with filters. $\mathbf{d}'(n)$ is the vector consisting of filtered estimated primary signal samples. Several experiments are made to decide on the filter length. 128 Tap filters are decided to be used for secondary path model $s'(n)$ and adaptation filter $w(n)$ in implementation of ANC headphone system. The initial values of $w(n)$ and $s'(n)$ are all zeros.

The filtering operations are achieved by FIR function of chip support library (CSL) in TMS320C54x. FIR uses circular addressing modes. In circular addressing, k+1 LSB's of a circular buffer's starting address must be zero where $k = \log_2$ (circular buffer size). Memory alignment should be applied to corresponding arrays in "linker command file" of the project developed in Code Composer Studio 3.1, which is the software environment used in this study. The details of FIR function can be found in [22]. Generally speaking, FIR function achieves convolution of two arrays and stores the result in an output array. The necessary CPU clock cycle for a convolution operation in FIR function is optimized.

Read/write commands should be carefully located to the code. Read operation should be done prior to processing by checking the RRDY signal [21]. Similarly, write operation should be done just after the $y(n) = \mathbf{w}^T(n) \cdot \mathbf{d}(n)$ convolution by checking XRDY signal. The rest of the process should be done in remaining time before the first bit of data of the other channel is started on the line. The 8 KHz frame synchronization signal has 125 μ s period and this period is used by two channels in time division multiplexed structure. Thus one channel resides on 62.5 μ s. Considering that TMS320VC5416 DSP CPU runs at 120MHz, it can be said that the CPU has 7500 cycle for single channel. Experiments showed that CPU has at least 5000 cycle for processing operation. The remaining 2500 cycle is wasted during the CPU waits on XRDY or RRDY signals.

The overall block diagram of software implementation is seen in Figure 7.2 where $w(n)$ is the adaptive filter, $s'(n)$ is the secondary path model, $\hat{d}(n)$ is the estimated primary signal, $d(n)$ is the primary noise signal, $y(n)$ is the output signal and $\hat{d}'(n)$ is the filtered estimated primary input signal. $\mathbf{d}'(n)$ is the vector consisting of filtered estimated primary input signal samples.

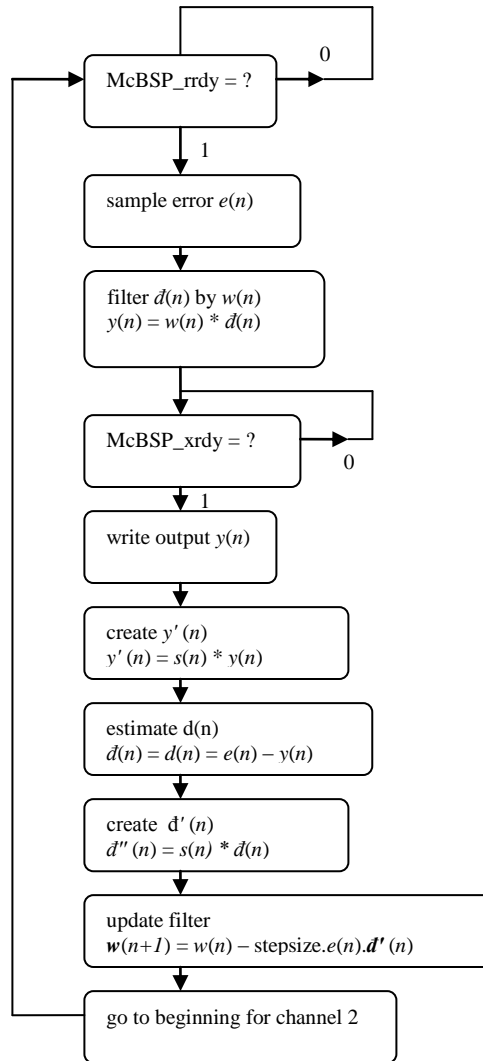


Figure 7.2 - Overall Block Diagram of Software Implementation for Fx-LMS in Feedback ANC Headphone System

It is well known that assembler coding in a DSP environment minimizes the process time. However, complicated expressions are too difficult to implement without help of C optimizers. In this study, only the convolution operation is achieved by an assembly coded FIR function.

7.3 Fixed Point Limitations in LMS Active Noise Control Implementation

Fixed point limitations affect the step size selection in LMS algorithm. Additionally, software implementation of LMS includes some multiplication and division operation which can produce overflow or rounding errors in finite precision environment.

The resolution for the variables are chosen as 16-bit for input and output signals according to the CODEC digital data format. In order to prevent some additional unexpected error, all the other variables are defined in 16-bit resolution. The multiplications in DSP are done using a 40-bit accumulator. The multiplication of two 16-bit integers results in a 32-bit integer. Summation of these 32-bit integers may need higher order bits. The 40-Bit accumulator is split into three parts which are guard bits, high order bits and low order bits. Guard bits (most significant 8 bits) are used for the filtering operation including multiplication and addition of long filter coefficients. The result of a multiplication is most accurate if the high order 16 bits are returned as the result.

Division operation in fixed point is different than multiplication, because the rounding error is produced by division. Rounding error may seem to be solved by pre-multiplications but the upper dynamic limit of defined resolution generally puts a restriction on the multiplication results. To prevent this, it must be ensured that the prior multiplications are done in 40-bit accumulator and division is operated on the high resolution value before it is normalized to 16-bit.

There exist multiplications in update equation (7.11). Although, the step size is seen to be multiplied with the other components, it is generally a dividing factor. For strong primary signals the upper boundary for step size selection is too small.

$$\begin{aligned}
\mathbf{w}(n+1) &= \mathbf{w}(n) - \mu \mathbf{d}'(n) e(n) \\
&= \mathbf{w}(n) - [\mathbf{d}'(n) \cdot e(n)] / [1/\mu] \quad (7.11)
\end{aligned}$$

The upper boundary on the step size is determined by calculating the power of filtered primary signal estimation $\mathbf{d}'(n)$ (3.22). The signed 16-bit integer values are between -32768 and 32767. Experiments showed that upper bound on step size is around 1/1000000 for a strong sinusoidal whose peak-to-peak amplitude value is 20000. The multiplication of filtered estimated primary sample and error sample should be divided by 1000000 in order to realize that step size value; however this division factor can not be represented in 16-bit resolution. The following equation can be used although there exists round-off error;

$$\begin{aligned}
\mathbf{w}(n+1) &= \mathbf{w}(n) - \mu \mathbf{d}'(n) e(n) \\
&= \mathbf{w}(n) - [\mathbf{d}'(n) / C_1] \cdot [e(n) / C_2] \quad (7.12)
\end{aligned}$$

where $C_1.C_2 = 1/\mu$.

C_1 and C_2 can be represented in 16-bit resolution correctly. Each division result should be kept as 16-bit integers independently and the multiplication should be done with these division results.

If C_2 is selected too high in (7.12) in order to guarantee the convergence, the error signals smaller than this high threshold stop adaptation temporarily. Digital residual error becomes dominant with respect to quantization error due to the slowdown phenomenon defined in Chapter 4. C_1 and C_2 should be selected by experimental results so that convergence for strong primary noise signals is ensured and weak primary noise signals do not result in high digital residual error. If the value of C_1 or C_2 can not satisfy these requirements, one should alter the gain settings of microphone input and/or speaker output.

C_1 and C_2 are selected as 2048 (2^{11}) in LMS algorithm in order to realize the division by shifting the binary value of $e(n)$ and $\hat{d}'(n)$. C_1 constant in (7.12) becomes power of $\hat{d}'(n)$ signal in NLMS. The initial C_1 is chosen as 2048 in NLMS. Afterwards, the squared value of the bottom element of $\hat{d}'(n)$ array is subtracted from C_1 and the new incoming sample is added to it. C_2 is also chosen as 2048 in NLMS. In SSLMS, the filter coefficients are increased or decreased by 1 according to the signs of error and filtered estimated primary noise signal. A dead zone of 1024 is inserted for $e(n)$ signal in order to prevent the sign-sign LMS algorithm to update the filter coefficients for too small residual error signals. Inside aforementioned dead zone the filter coefficients are not updated.

C_1 and C_2 are selected considering the input/output signal levels in several experiments. These experiments showed that C_2 and/or C_1 value should follow an adaptive way to maximize the dynamic range, because a strong primary noise signal needs a smaller step size for convergence and smaller step size values increase the digital residual error for smaller primary signals due to slowdown phenomenon. This makes the overall ANC system ineffective for low level noise signals or divergent for high level primary noises.

7.4 The Discussion of Modified LMS Algorithms in Fixed Point

Normalized LMS has an adaptive step size effective to both low level and high level primary noise signals. The value of aforementioned divider factor (C_1, C_2) is increased with increasing primary noise signal level. However, time-varying stepsize is a drawback for NLMS in fixed point implementation considering discussions made in Chapter 4. On the other hand, in NLMS the power of filtered estimated primary signal should be calculated. The multiplication and addition operation during this calculation results in overflow errors if the samples of estimated primary signal are not normalized to a lower level. Since the power of filtered estimated primary signal is a dividing factor,

an overflow error results in divergence. The main advantage of NLMS is its increased rate of convergence as seen in theoretical explanations in Chapter 2.

Convergence rate is decreased in sign-sign LMS. The main advantage of sign-sign LMS is that a higher reduction than the other algorithms can be attained for weaker signals by introducing a smaller dead zone.

7.5 Software Implementation of Offline Secondary Path Modeling

Offline secondary path modeling is implemented according to explanations made in Chapter 3. Fixed point limitations also apply to secondary path modeling. Gain settings and iteration number are optimized for the most accurate modeling. White noise samples are created by random generator function in DSP library. The result of this function is scaled and biased according to some experimental results guaranteeing the convergence.

The block diagram of offline secondary path modeling is seen in Figure 7.3

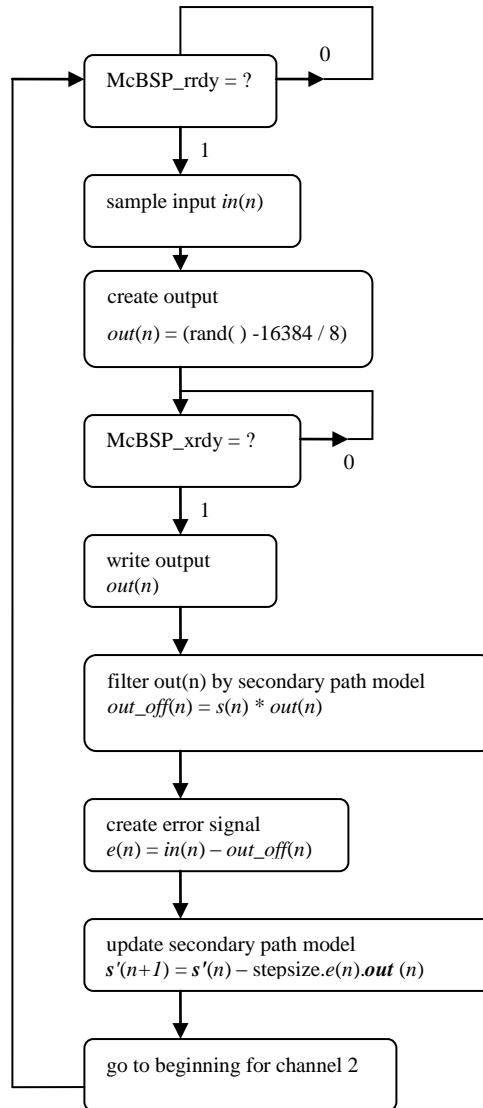


Figure 7.3 – Block Diagram of Software Realization of Offline Secondary Path Modeling in ANC Headphone System

A similar step size selection procedure to LMS implementation is followed.

$$s(n+1) = s(n) + [\mathbf{out}(n) / C_1] \cdot [e(n) / C_2] \quad (7.13)$$

is reached where $out(n)$ is the output white noise signal. As the result of several experiments, both C_1 and C_2 are chosen as 2048. Offline secondary path modeling lasts

for 10 seconds in this implementation. Figure 7.4 shows the impulse response of secondary path model of one channel obtained in real time experiments.

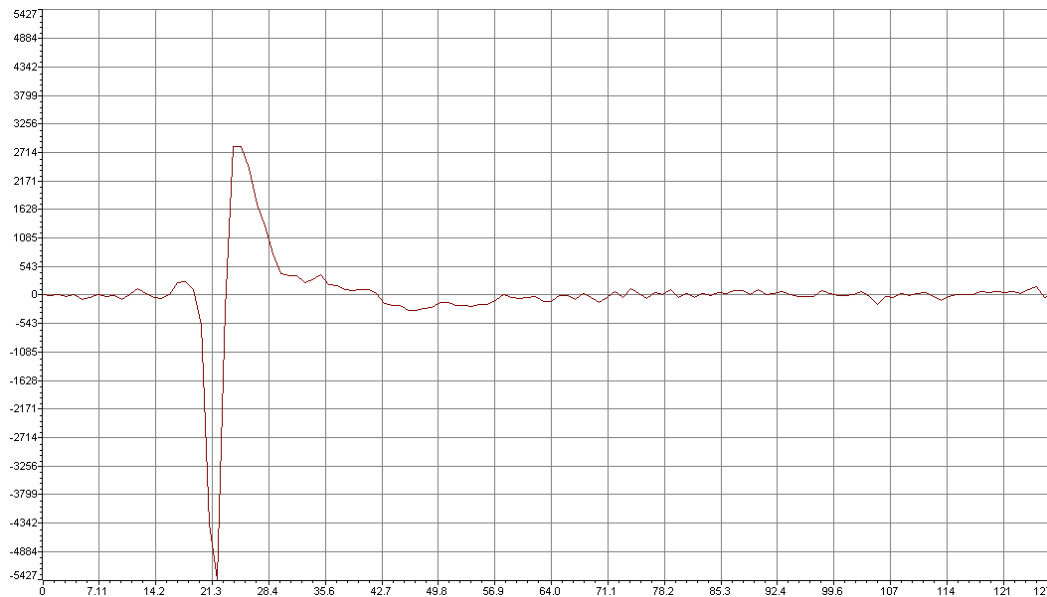


Figure 7.4 – The impulse response of Secondary Path Model of Active ANC Headphone System

7.6 Additional Software Implementations

The designed digital ANC system may lose its stability when these two conditions occur:

- A large primary noise signal exceeding dynamic range of digital ANC system is applied.
- The secondary path is changed when user puts off the headphone.

The first problem is solved by increasing the high level threshold. This is done by decreasing the gain of the microphone. However, this resulted in the degradation in the sensitivity of the system to low level noises. Another solution to this problem is to automatically control the gain of the input by modifying the ADC gain settings of the

CODEC. However, this results in the changing of the secondary path model which should be compensated with a new modeling. Unfortunately, it is impossible to stop the system and make another offline secondary path modeling. CODEC should be reset and all registers should be reconfigured with a cost of 10 samples for each channel. An adaptive step size selection procedure is tried in order to increase dynamic range. The step size value is decreased when the estimated primary noise power decreased below a predefined limit. Similarly step size value is increased when estimated primary noise power increased above a predefined limit. This adjustment is difficult to implement because of its computational complexity.

In this study the second problem is solved by a software machine which handles the task of checking error signal and resets the corresponding channel's parameters when a predefined range is exceeded by error signal. By this adjustment, the stability is rearranged if the headphone is put on again.

CHAPTER 8

PERFORMANCE TESTS OF THE DIGITAL ANC HEADPHONE

A test set up is constructed to compare the designed digital ANC headphone system with a commercial analog ANC system which is designed by BOSE (Model QC-1). The test set up consists of a Sennheiser ME102 omnidirectional microphone and its corresponding amplifier connected to the microphone input of the computer. A MATLAB code records the data in wave format. Adaptive ANC system is activated while the record is being made. The parts represented as “with ANC” and “without ANC” are transformed into frequency domain and results are compared. The non-stationary signal tests are done twice for each system; one for “with ANC” and the other one for “without ANC” and the results are drawn together.

The test signals are stationary single tones, fan noise, propeller cabin noise and drill noise. An artificial sinusoidal signal with changing frequency and amplitude is also used for tracking capability test. Mainly, the attenuation levels of digital ANC headphone based on LMS, normalized LMS and sign-sign LMS algorithms are compared with each other as well as with Bose analog ANC headphone. In addition, the tracking capability, the convergence rate and digital residual error are examined.

It is experimentally shown that the location of the test microphone may change the results significantly. Moreover, the listener position to the noise source may dramatically affect the primary noise signal levels. These contributions result in erroneous comparisons between different LMS algorithms. The listener position, the test microphone location and noise level should stay unchanged for a specific test in order to

minimize these errors. Additionally, the test microphone should be as close as possible to the error microphone of digital ANC.

8.1 Single Tone Experiments

Figure 8.1 shows the error signal recorded during a single tone NLMS digital ANC headphone experiment. Higher amplitudes (amplitude of power of error signal) belong to the part “without ANC” and the lower amplitudes belong to the part “with ANC”. The single frequency component of the test noise is 200Hz. Fourier transform of the samples between 0 and 10000 is plotted in Figure 8.2 and the Fourier transform of the samples between 90000 and 100000 is plotted in Figure 8.3. The attenuation level of 200 Hz single tone is 25.5 dB ($10 \cdot \log(434.0245 / 1,225)$).

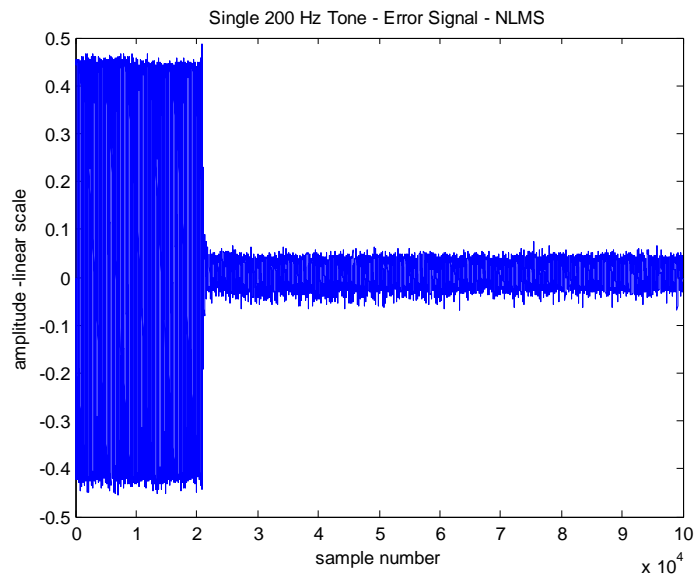


Figure 8.1 – Single 200 Hz Tone in NLMS Experiment “with ANC” and “without ANC”

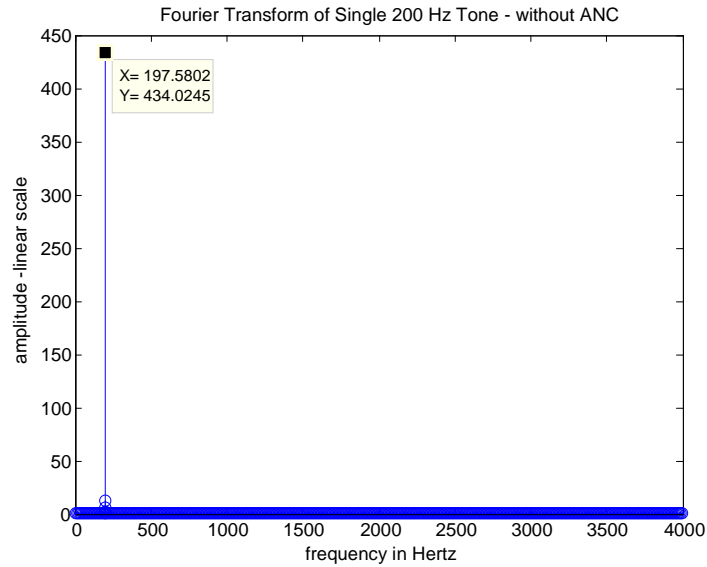


Figure 8.2 – Fourier Transform of Single 200 Hz Tone in NLMS Experiment “without ANC”

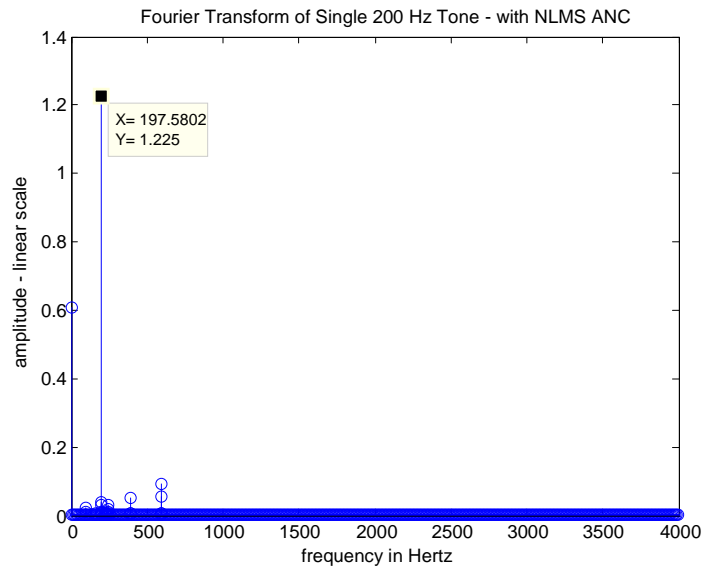


Figure 8.3 – Fourier Transform of Single 200 Hz Tone in NLMS Experiment “with ANC”

Similar experiments are made with NLMS, LMS and SSLMS for other single tone signals from 100Hz up to 1100 Hz for. Additionally, the Bose ANC headphone is tested with these signals. The results of ANC experiments with single tones for different

LMS algorithms and analog ANC headphone is shown in Table 8.1. It is important to note that the attenuation levels may significantly change (about 5-6 dB) with a change in the location of test microphone.

Table 8.1 – The attenuation levels of single tones for digital and analog system

ANC system frequency	Digital ANC Headphone - NLMS	Digital ANC Headphone – LMS	Digital ANC Headphone – Sign-Sign LMS	Analog ANC Headphone
100Hz	33.5 dB	28.6 dB	30.1 dB	14.6 dB
200Hz	25.5 dB	30.6 dB	21.2 dB	11.9 dB
300Hz	29.7 dB	24.0 dB	30.0 dB	10.4 dB
400Hz	24.0 dB	30.1 dB	21.5 dB	14.1 dB
500Hz	22.1 dB	31.4 dB	21.5 dB	6.5 dB
600Hz	19.0 dB	20.0 dB	18.9 dB	3.6 dB
700Hz	19.8 dB	21.1 dB	18.8 dB	1.5 dB
800Hz	18.4 dB	16.5 dB	17.3 dB	-1.8 dB
900Hz	14.9 dB	24.8 dB	28.9 dB	-4.3 dB
1000Hz	16.2* dB	14.7 dB*	12.9 dB*	-5.4 dB
1100Hz	10.8* dB	16.0 dB*	7.3 dB*	-4.7 dB

*for these frequencies the attenuation levels are not stable.

These single tone experiments show that digital ANC headphone system is considerably superior to the analog ANC headphone system when the noise is narrow band. Analog ANC headphone system increases frequency components higher than 700Hz - 800Hz. In contrast, digital ANC system can extend the attenuation band up to 1000Hz successfully. Furthermore, digital ANC is successful in narrowband signals in the optimized working region of analog headphone which resides between 100Hz and

400Hz. LMS showed the most successful results of all the other algorithms. This is a result of the constant step size optimizing the implementation for fixed point environment [12].

8.2 Multiple Tone Experiments

Figure 8.4, Figure 8.5, Figure 8.6 and Figure 8.7 show the results of the experiments made with digital ANC headphone NLMS method for the multi tone of 100Hz, 200Hz, 300Hz, 400Hz and 500Hz composition. The attenuation levels are calculated as 17.3dB for 100Hz, 33.5 dB for 200Hz, 24.1dB for 300Hz, 28.5dB for 400Hz and 21.7 dB for 500 Hz. In Figure 8.8, Figure 8.9 and Figure 8.10, the corresponding results for LMS, SSLMS and analog ANC headphone can be seen respectively.

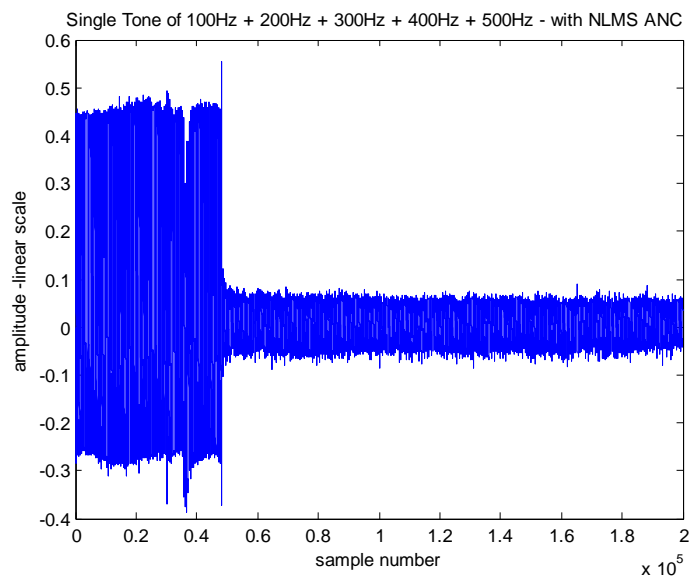


Figure 8.4 - Tone of 100 Hz, 200Hz, 300Hz, 400Hz and 500 Hz Composition in NLMS Experiment “with ANC” and “without ANC”

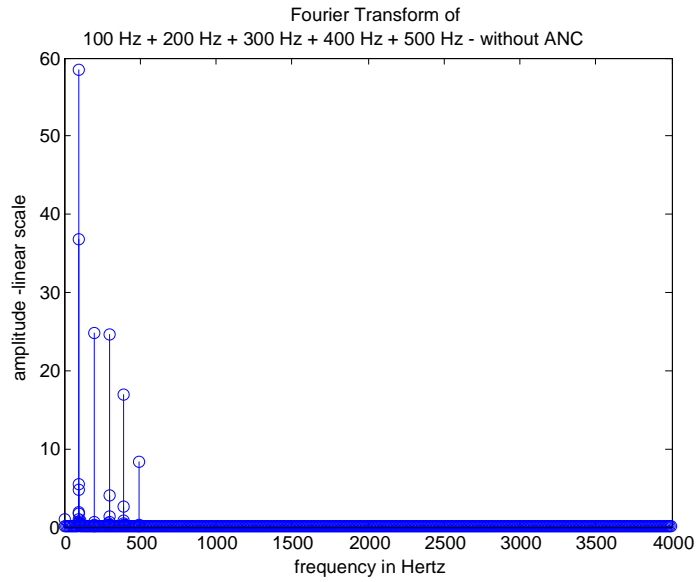


Figure 8.5 – Fourier Transform of 100 Hz, 200Hz, 300Hz, 400Hz and 500 Hz Composition in NLMS Experiment “without ANC”

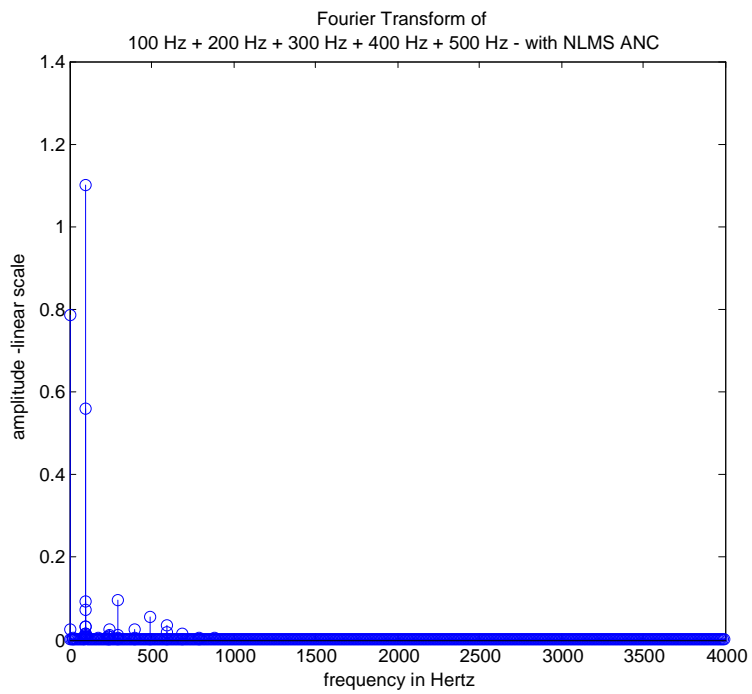


Figure 8.6 – Fourier Transform of 100 Hz, 200Hz, 300Hz, 400Hz and 500 Hz Composition in NLMS Experiment “with ANC”

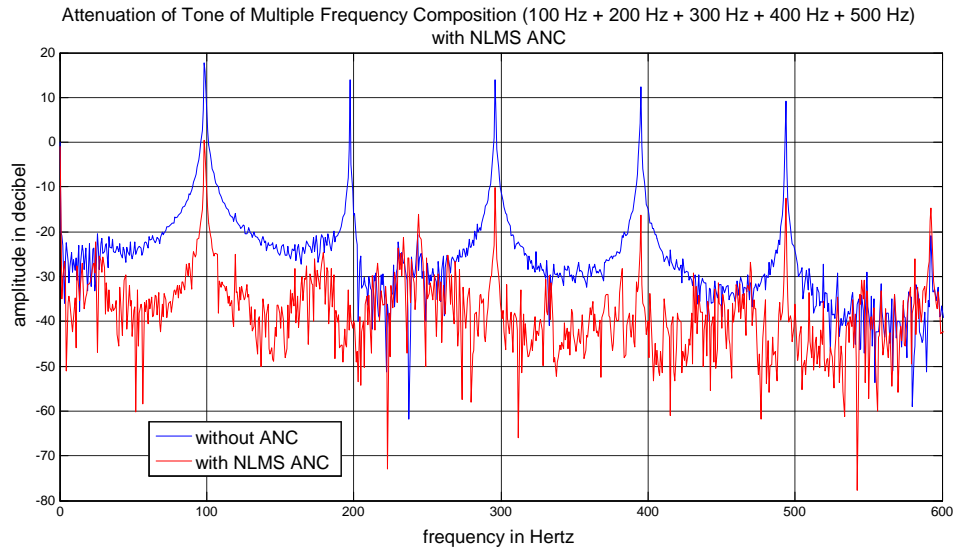


Figure 8.7 – Fourier Transform of Multi Tone Signal in LMS Digital Headphone
Experiment “with ANC” and “without ANC”

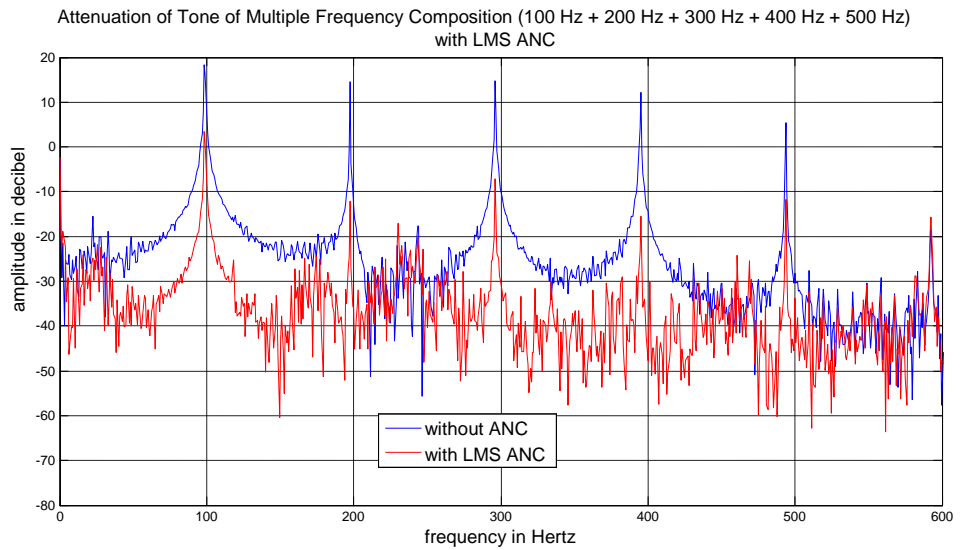


Figure 8.8 – Fourier Transform of Multi Tone Signal in LMS Digital Headphone
Experiment “with ANC” and “without ANC”

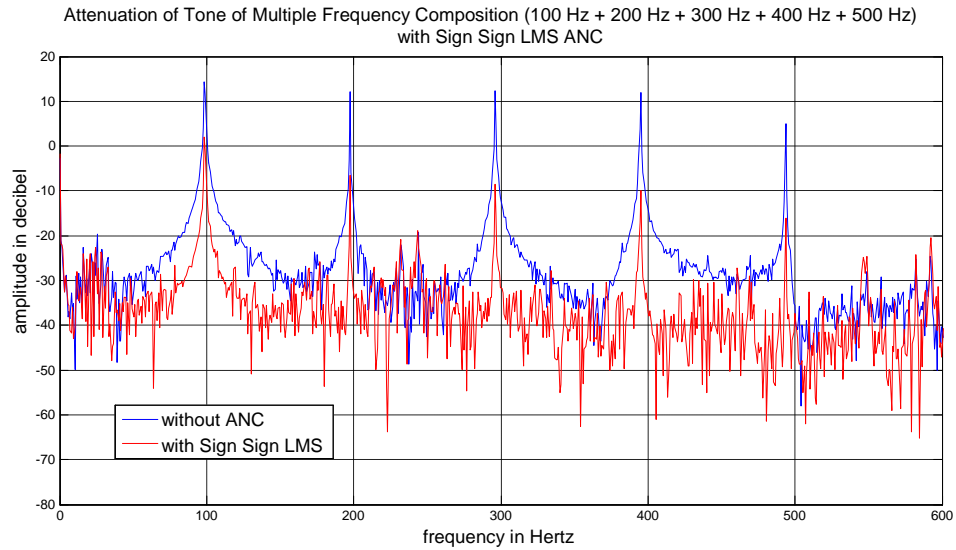


Figure 8.9 – Fourier Transform of Multi Tone Signal in Sign-Sign LMS Digital Headphone Experiment “with ANC” and “without ANC”

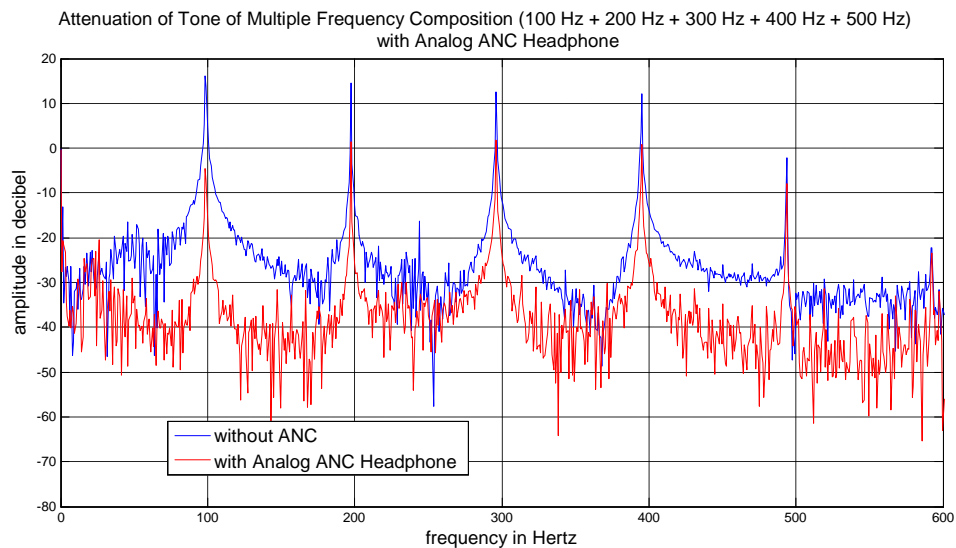


Figure 8.10 – Fourier Transform of Multi Tone Signal in Analog ANC Headphone Experiment “with ANC” and “without ANC”

The results of multi tone experiments are listed in Table 8.2. Similar experiments are made for various multi tones and the results are shown in Table 8.3 for 200Hz, 600Hz and 800Hz composition and in Table 8.4 for 100Hz, 400Hz and 900Hz composition.

Table 8.2 – The attenuation levels of multi tone composed of 100 Hz(dominant), 200 Hz(small), 300 Hz(small), 400 Hz(smaller) and 500 Hz(smaller)

ANC system frequency	Digital ANC Headphone – NLMS	Digital ANC Headphone – LMS	Digital ANC Headphone – Sign-Sign LMS	Analog ANC Headphone
100Hz	17.3 dB	14.7 dB	12.7 dB	21.0 dB
200Hz	33.5 dB	26.5 dB	18.9 dB	12.3 dB
300Hz	24.1 dB	21.9 dB	20.1 dB	10.6 dB
400Hz	28.5 dB	27.6 dB	22.0 dB	11.6 dB
500Hz	21.7 dB	17.2 dB	21.6 dB	4.6 dB

Table 8.3 – The attenuation levels of multi tone composed of 200 Hz(dominant), 600 Hz(small), 800 Hz(smaller)

ANC system frequency	Digital ANC Headphone – NLMS	Digital ANC Headphone – LMS	Digital ANC Headphone – Sign-Sign LMS	Analog ANC Headphone
200Hz	22.0 dB	27.5 dB	24.7 dB	18.6 dB
600Hz	14.0 dB	13.2 dB	12.1 dB	-1.4 dB
800Hz	12.8 dB	13.4 dB	13.1 dB	-1.3 dB

Table 8.4 – The attenuation levels of multi tone composed of 100 Hz(dominant), 400 Hz(small) and 900 Hz(smaller)

ANC system frequency	Digital ANC Headphone – NLMS	Digital ANC Headphone – LMS	Digital ANC Headphone – Sign-Sign LMS	Analog ANC Headphone
100Hz	15.1 dB	24.0 dB	15.1 dB	21.5 dB
400Hz	19.1 dB	19.2 dB	19.1 dB	10.1 dB
900Hz	9.5 dB	6.9 dB	7.3 dB	-6.3 dB

The experiments with multi tones showed that additional frequency components degrade the attenuation levels attained for each frequency in single tone experiments. However, the digital systems still perform better than analog ANC headphone especially for frequencies higher than 100-150 Hz. Analog ANC headphone is good at attenuating 100 Hz components when the noise has multiple frequency components; however it is ineffective for frequencies higher than 400Hz. The attenuation levels of LMS are better than modified LMS algorithms.

8.3 Fan Noise Experiments

Figure 8.11, Figure 8.12, Figure 8.13 and Figure 8.14 show the results of the experiments made with digital ANC headphone NLMS method for fan noise whose main frequency components are 125 Hz and 374 Hz. The ANC starts to run nearly after 6000th sample. The attenuation levels are calculated as 21.3dB for 125 Hz and 19.3 dB for 374 Hz. The corresponding results for LMS, SSLMS and analog ANC headphone can be seen in Figure 8.15, Figure 8.16 and Figure 8.17 respectively. These results are listed in Table 8.5.

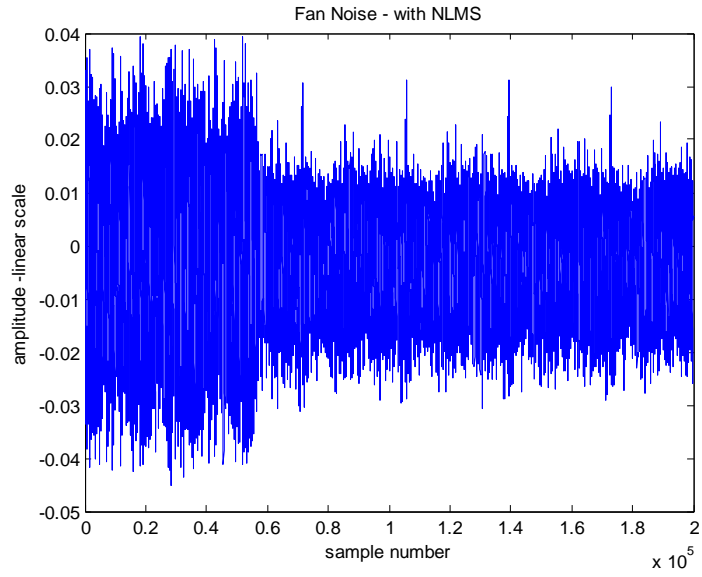


Figure 8.11 - Fan Noise in NLMS Experiment “with ANC” and “without ANC”

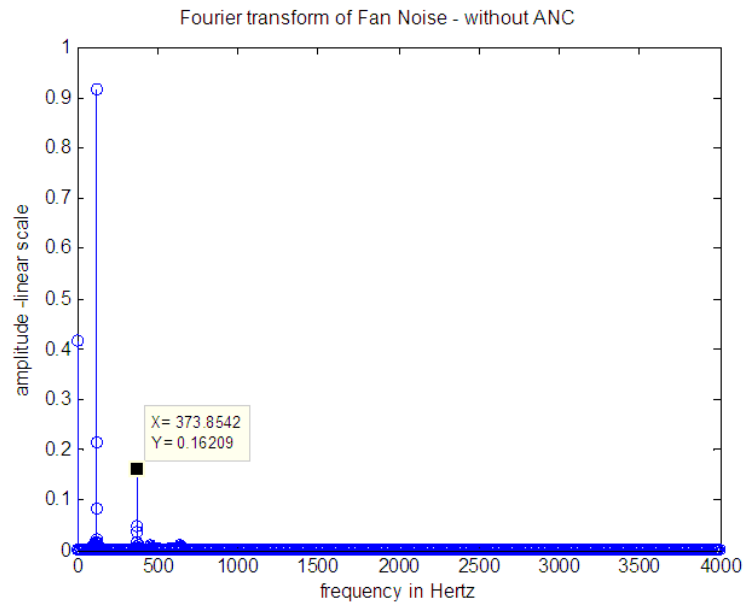


Figure 8.12 – Fourier Transform of Fan Noise in NLMS Experiment “without ANC”

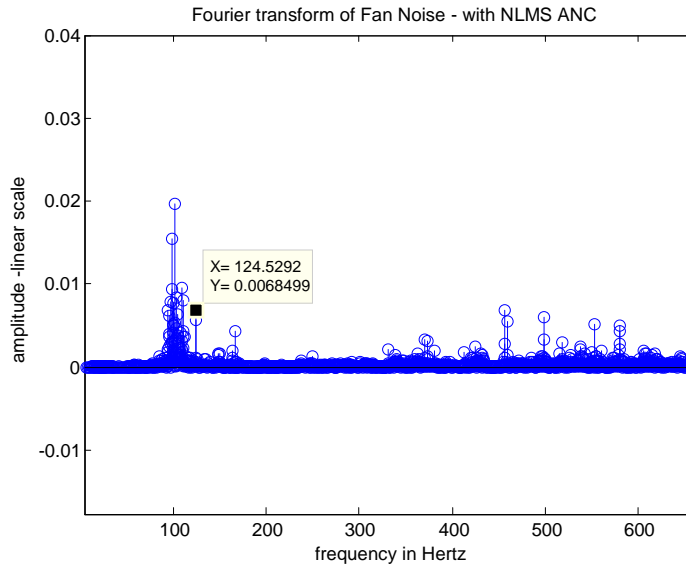


Figure 8.13 – Fourier Transform of Fan Noise in NLMS Experiment “with ANC”

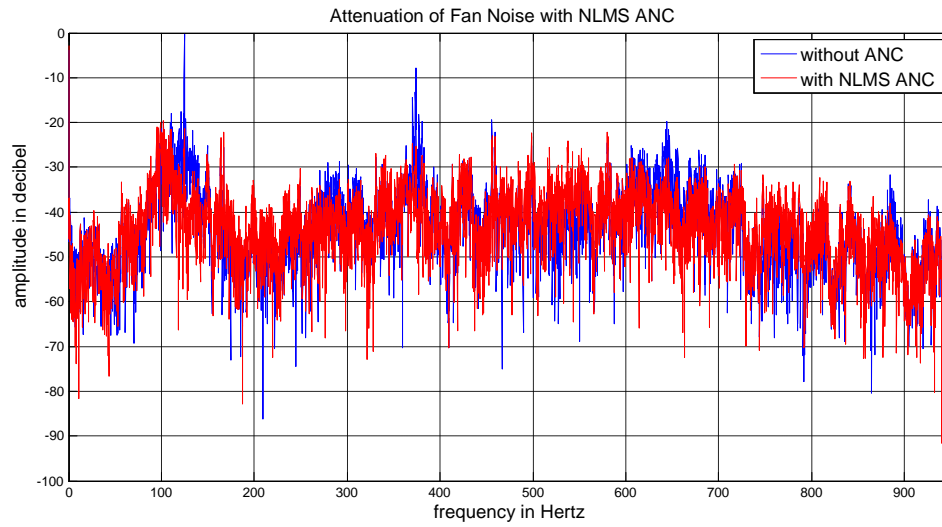


Figure 8.14 - Fourier Transform of Fan Noise in NLMS Experiment “with ANC” and “without ANC”

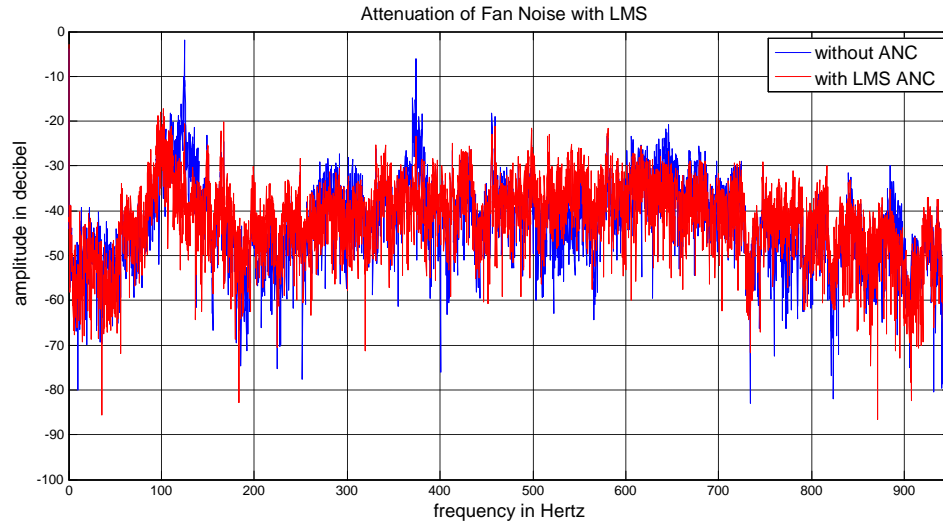


Figure 8.15 - Fourier Transform of Fan Noise in LMS Experiment “with ANC” and “without ANC”

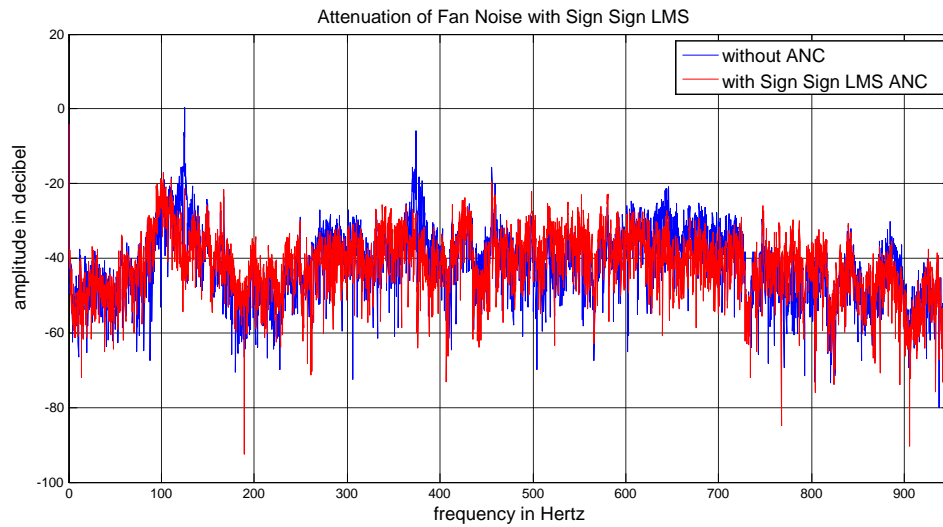


Figure 8.16 - Fourier Transform of Fan Noise in Sign-Sign LMS Experiment “with ANC” and “without ANC”

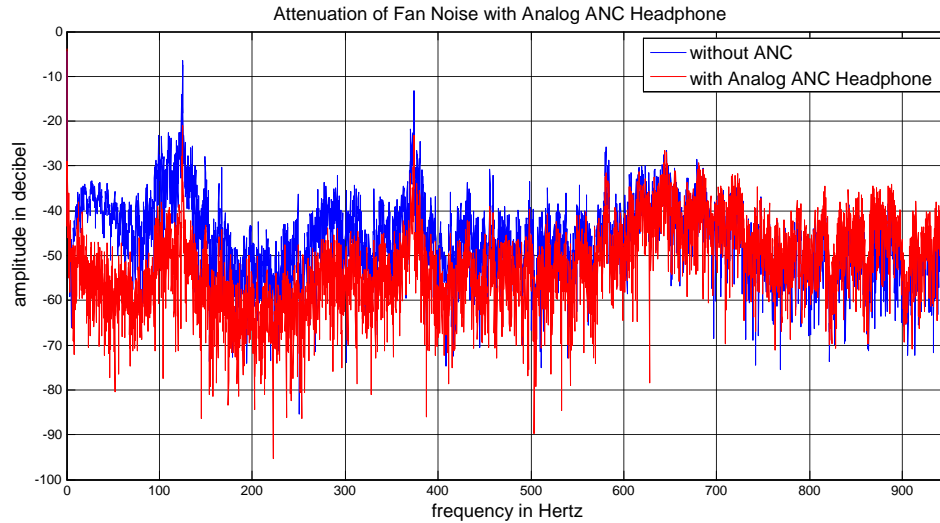


Figure 8.17 - Fourier Transform of Fan Noise in Analog ANC Headphone Experiment
 “with ANC” and “without ANC”

Table 8.5 - The attenuation levels of fan noise

ANC system frequency	Digital ANC Headphone – NLMS	Digital ANC Headphone – LMS	Digital ANC Headphone – Sign-Sign LMS	Analog ANC Headphone
125 Hz	21.3 dB	20.7 dB	22.4 dB	16.6 dB
374 Hz	19.3 dB	18.5 dB	18.3 dB	18.7 dB

The attenuation levels of the dominant frequency components are greater in digital ANC headphone. On the other hand, the attenuation levels of analog ANC headphone for weaker components smaller than 400 Hz is higher. Thus generally speaking, the digital ANC system is good at reducing the dominant frequencies of this wideband fan noise. The optimized filter coefficients in digital ANC try to decrease power of error signal. The main components are attenuated whereas the audible weaker components on the band are unaffected. On the other hand it can be seen that the frequency band between 600Hz and 700Hz is attenuated about 5-10 dB by digital ANC systems whereas the same frequency band is unaffected by analog ANC system.

Actually digital ANC system attenuated even 850-900 Hz band whereas the analog ANC system increases noises at these frequencies.

8.4 Propeller Cabin Noise Experiments

Figure 8.18, Figure 8.19, Figure 8.20 and Figure 8.21 show the results of the experiments of LMS algorithm with propeller cabin noise whose main frequency components are 83 Hz and 249 Hz. The attenuation level is calculated as 18.8 dB for 83 Hz and 19.3 dB for 249 Hz. In Figure 8.22, Figure 8.23 and Figure 8.24 the corresponding results for normalized LMS, sign-sign LMS and analog ANC headphone can be seen respectively. These results with the other systems experiment results are listed in Table 8.6.

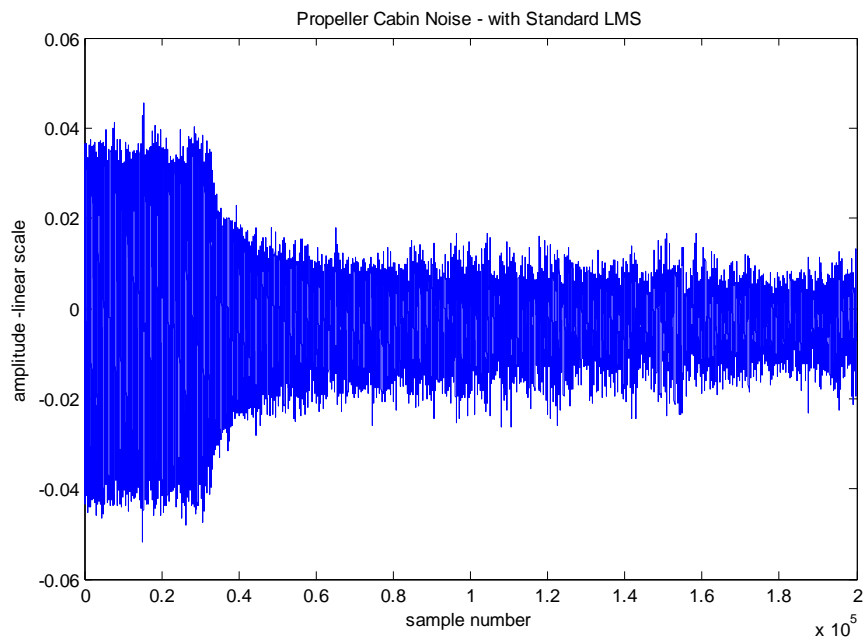


Figure 8.18 - Propeller Cabin Noise in LMS Experiment “with ANC” and “without ANC”

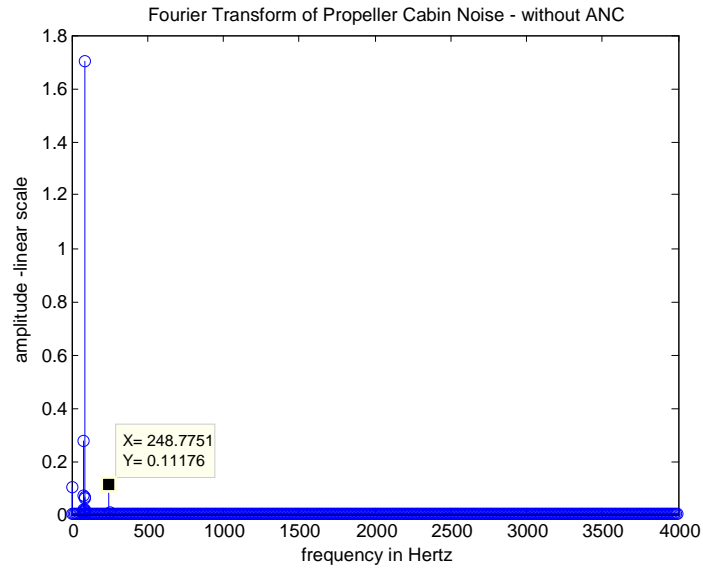


Figure 8.19 – Fourier Transform of Propeller Cabin Noise in LMS Experiment “without ANC”

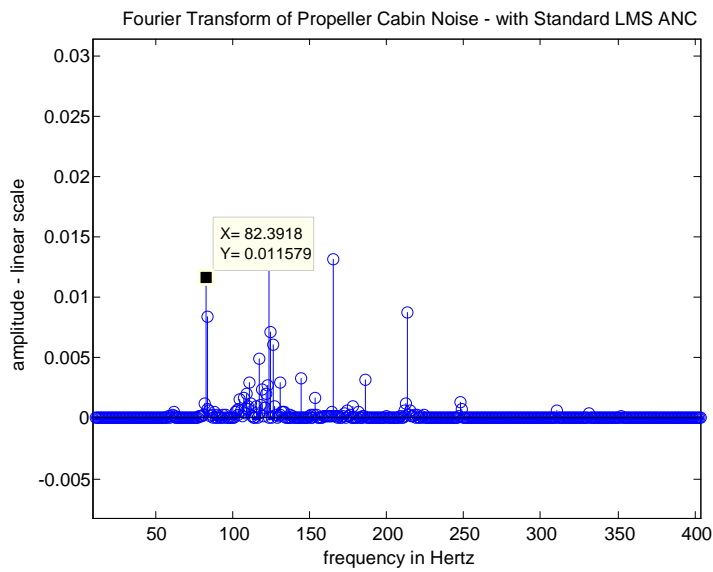


Figure 8.20 – Fourier Transform of Propeller Cabin Noise in LMS Experiment “with ANC”

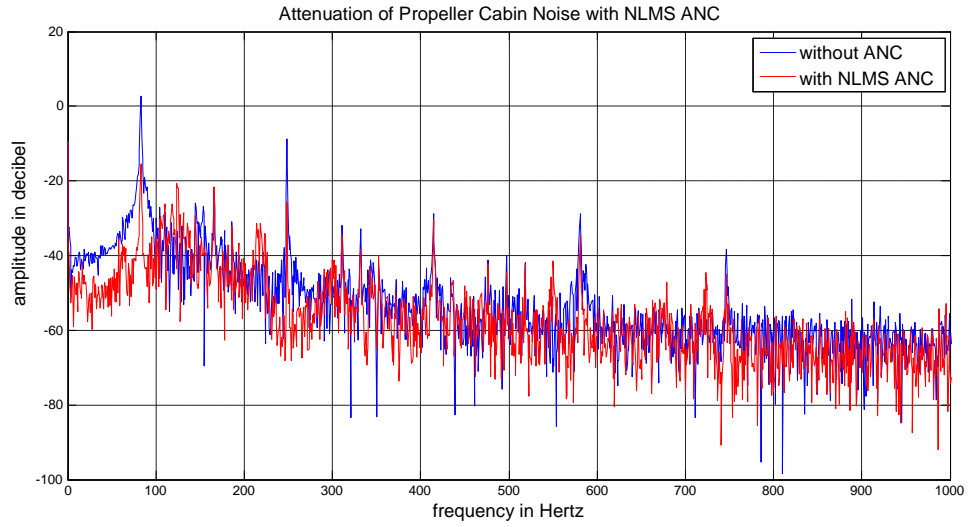


Figure 8.21 - Fourier Transform of Propeller Cabin Noise in NLMS Experiment “with ANC” and “without ANC”

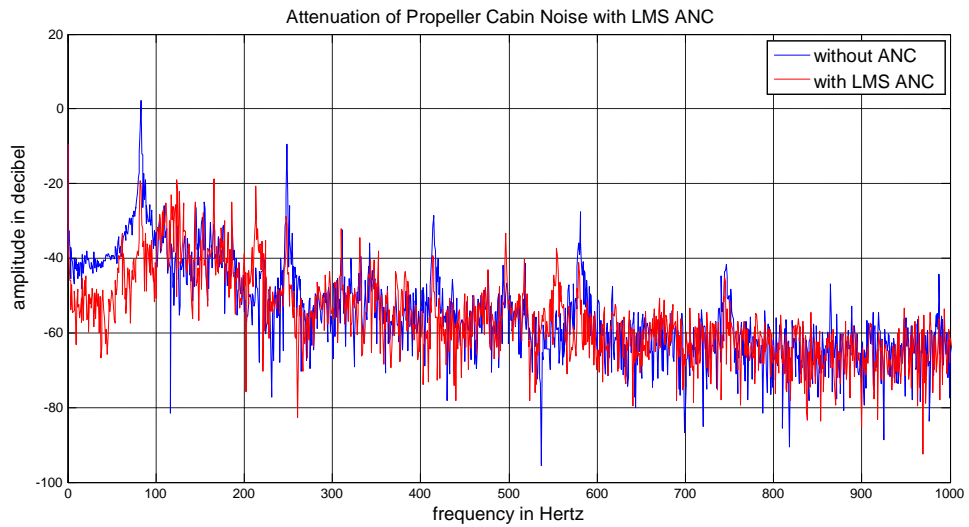


Figure 8.22 - Fourier Transform of Propeller Cabin Noise in LMS Experiment “with ANC” and “without ANC”

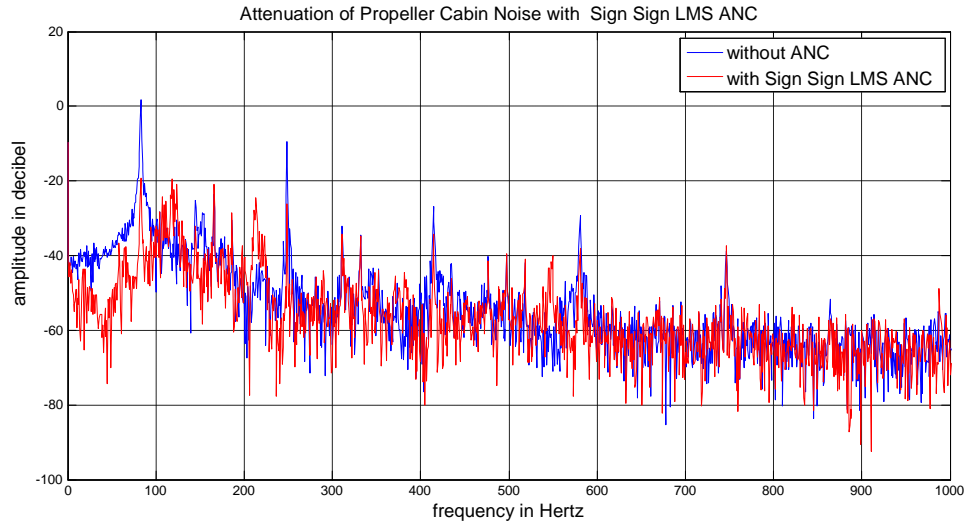


Figure 8.23 - Fourier Transform of Propeller Cabin Noise in Sign-Sign LMS Experiment “with ANC” and “without ANC”

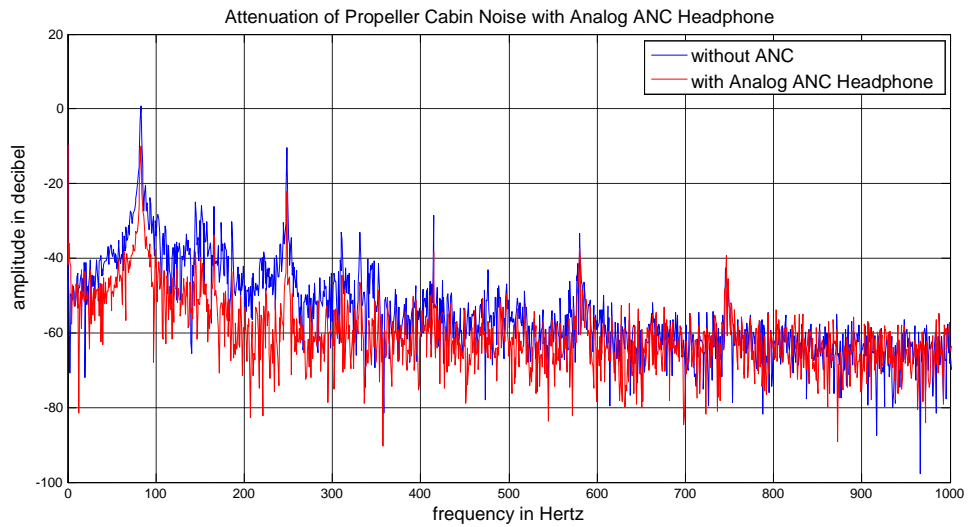


Figure 8.24 - Fourier Transform of Propeller Cabin Noise in Analog ANC Headphone Experiment “with ANC” and “without ANC”

Table 8.6 - The attenuation levels of propeller cabin noise

ANC system frequency	Digital ANC Headphone – NLMS	Digital ANC Headphone – LMS	Digital ANC Headphone – Sign-Sign LMS	Analog ANC Headphone
83 Hz	18.8 dB	21.7 dB	21.2 dB	12.5 dB
249 Hz	19.3 dB	19.2 dB	16.7 dB	9.4 dB

The attenuation levels of dominant frequency components are higher in digital system in propeller cabin noise experiment. However, analog system attenuates weaker signals in the frequency band 50Hz – 300Hz. The digital system with optimized filter coefficients mainly attenuates the dominant frequency components.

8.5 Drill Noise Experiments

Figure 8.25, Figure 8.26, Figure 8.27 and Figure 8.28 show the results of the experiments of sign-sign LMS algorithm with drill noise whose main frequency component is 450 Hz. The attenuation level is calculated as 10.8 dB for 450 Hz. In Figure 8.29, Figure 8.30 and Figure 8.31 the corresponding results for NLMS, LMS and analog ANC headphone can be seen respectively. These results with the other systems experiment results are listed in Table 8.7.

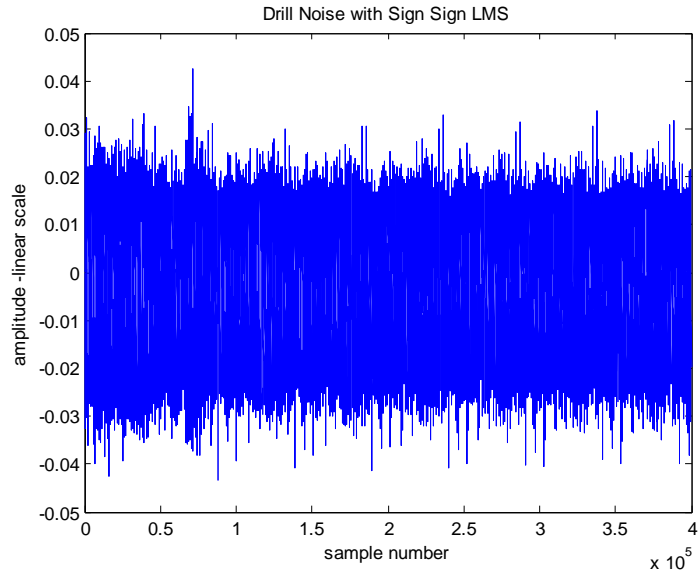


Figure 8.25 - Drill Noise in Sign-Sign LMS Experiment “with ANC” and “without ANC”

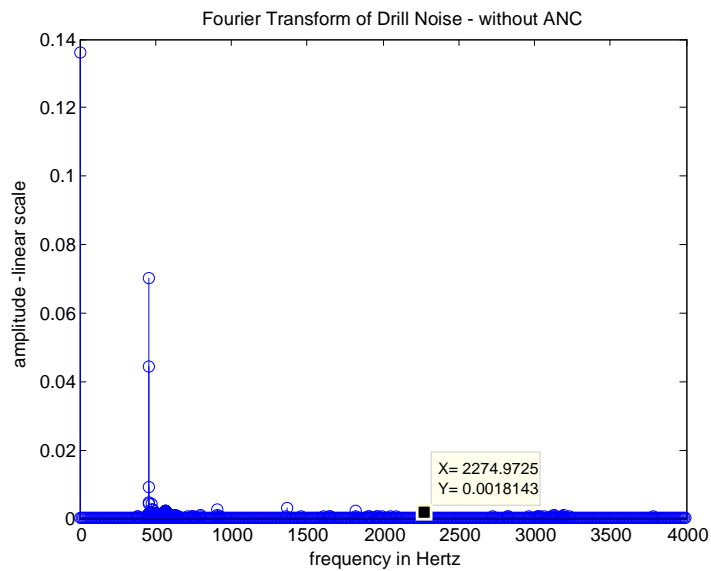


Figure 8.26 – Fourier Transform of Drill Noise in Sign-Sign LMS Experiment “without ANC”

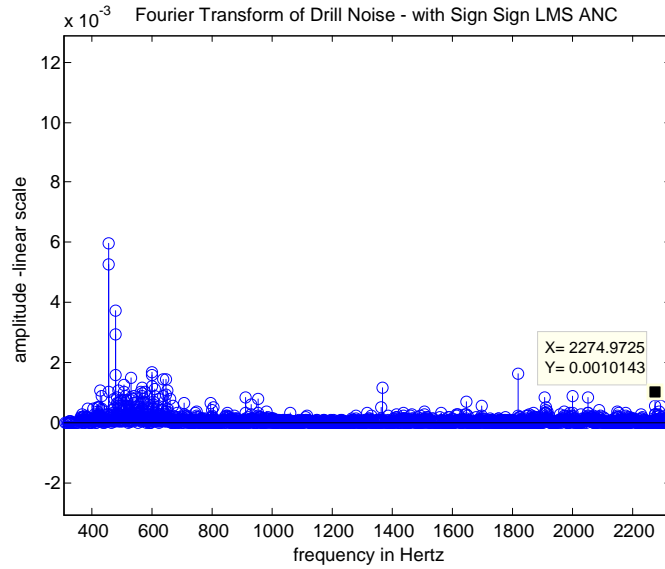


Figure 8.27 - Fourier Transform of Drill Noise in Sign-Sign LMS Experiment “with ANC”

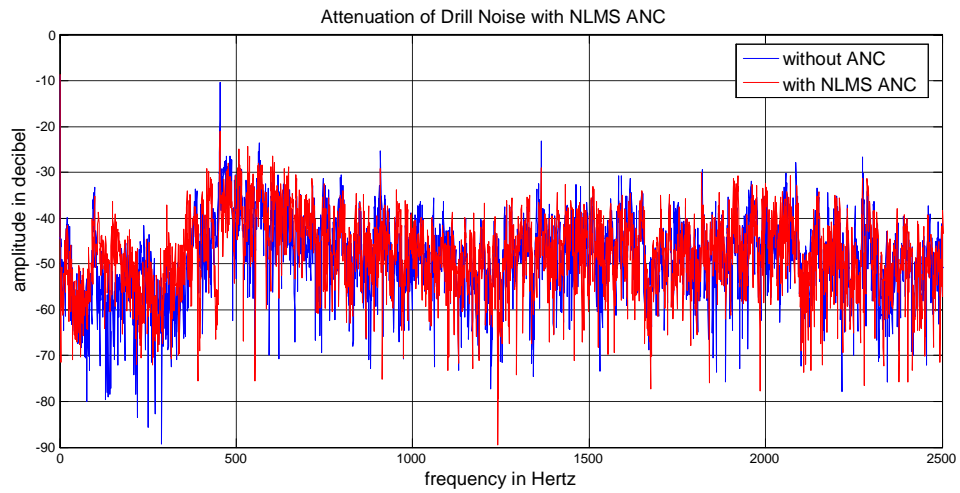


Figure 8.28 - Fourier Transform of Drill Noise in NLMS Experiment “with ANC” and “without ANC”

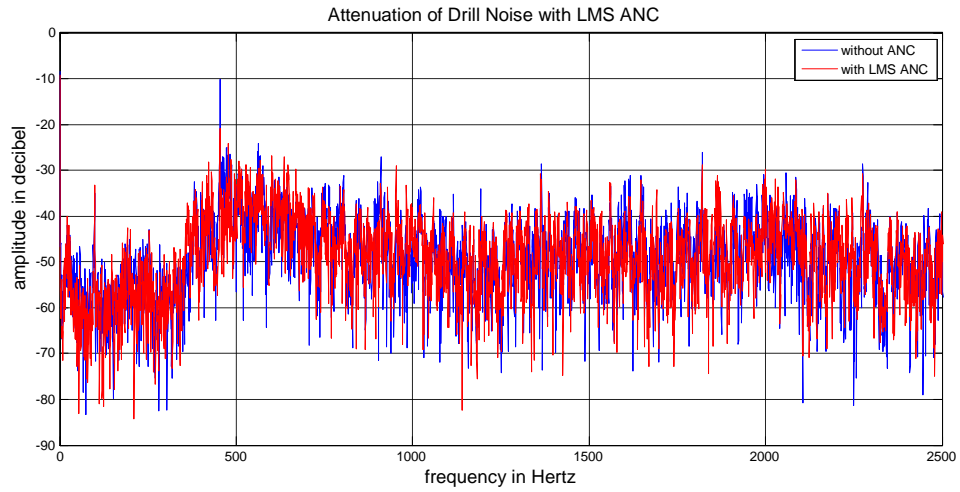


Figure 8.29 - Fourier Transform of Drill Noise in LMS Experiment “with ANC” and “without ANC”

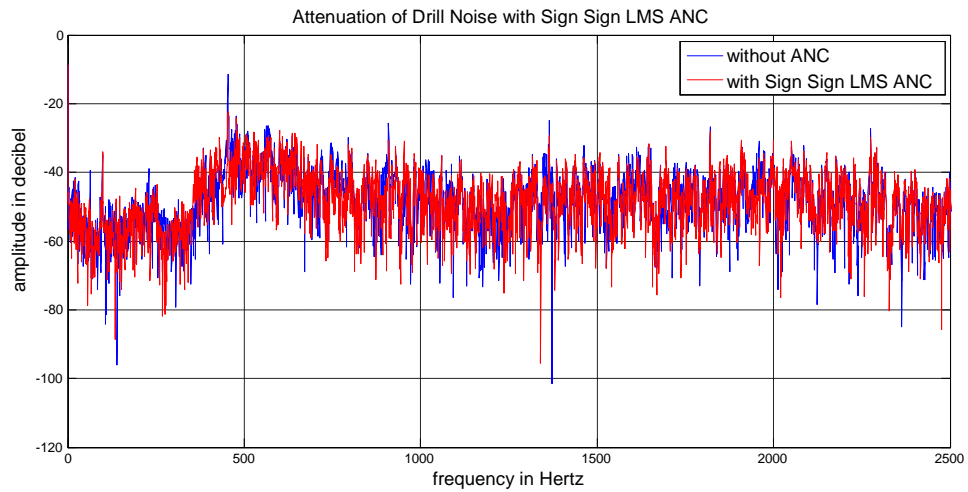


Figure 8.30 - Fourier Transform of Drill Noise in Sign-Sign LMS Experiment “with ANC” and “without ANC”

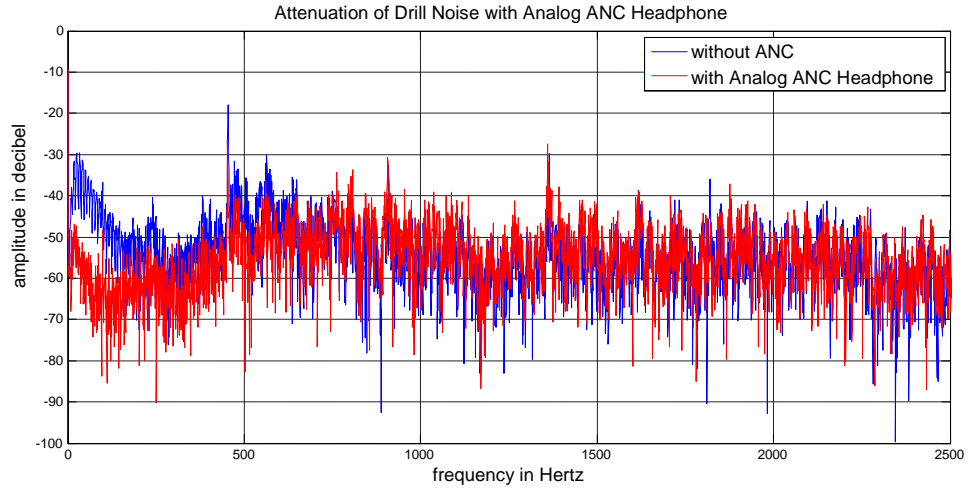


Figure 8.31 - Fourier Transform of Drill Noise in Analog ANC Headphone Experiment
“with ANC” and “without ANC”

Table 8.7 - The attenuation levels of drill noise

ANC system frequency	Digital ANC Headphone – NLMS	Digital ANC Headphone – LMS	Digital ANC Headphone – Sign-Sign LMS	Analog ANC Headphone
450 Hz	10.8 dB	10.8 dB	10.7 dB	8.4 dB
910 Hz	4.0 dB	5.9 dB	5.4 dB	-1.8 dB
1363 Hz	5.9 dB	2.1 dB	4.5 dB	-2.4 dB
2275 Hz	4.7 dB	2.0 dB	2.5 dB	*

*this high frequency component is cancelled mechanically by Analog ANC headphone.

The attenuation of dominant frequency component between 100Hz and 500Hz in digital ANC system is higher in drill noise experiment. Attenuation levels of weaker frequency components between 50-400Hz are higher in analog system. However, the drill noise has higher frequency components especially distributed around 450 Hz, 900 Hz, 1300 Hz and 2250 Hz. Thus, analog ANC headphone is ineffective for this noise type whereas digital ANC headphone continues attenuation. On the other hand, drill noise is a very difficult noise type for digital adaptive ANC system because of its wideband characteristics. Most of the frequency component of drill noise is unaffected.

8.6 Tracking Capability Experiments

Tracking is the ability of the algorithm to track non-stationary signals. Figure 8.32, Figure 8.33, Figure 8.34 and Figure 8.35 show the results of each system under a non-stationary sinusoidal signal.

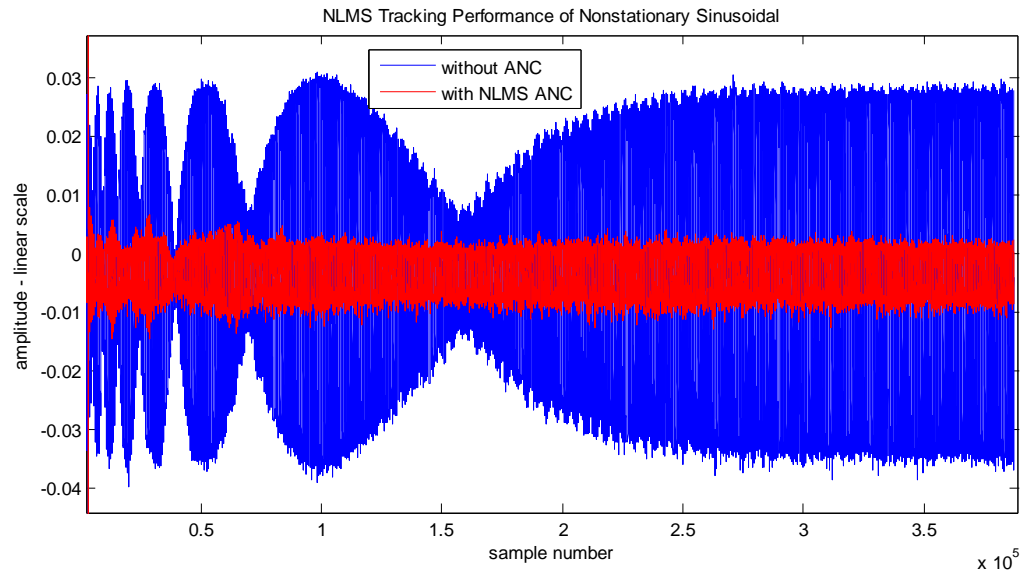


Figure 8.32 – NLMS Tracking Performance with a Non-stationary Sinusoidal Signal

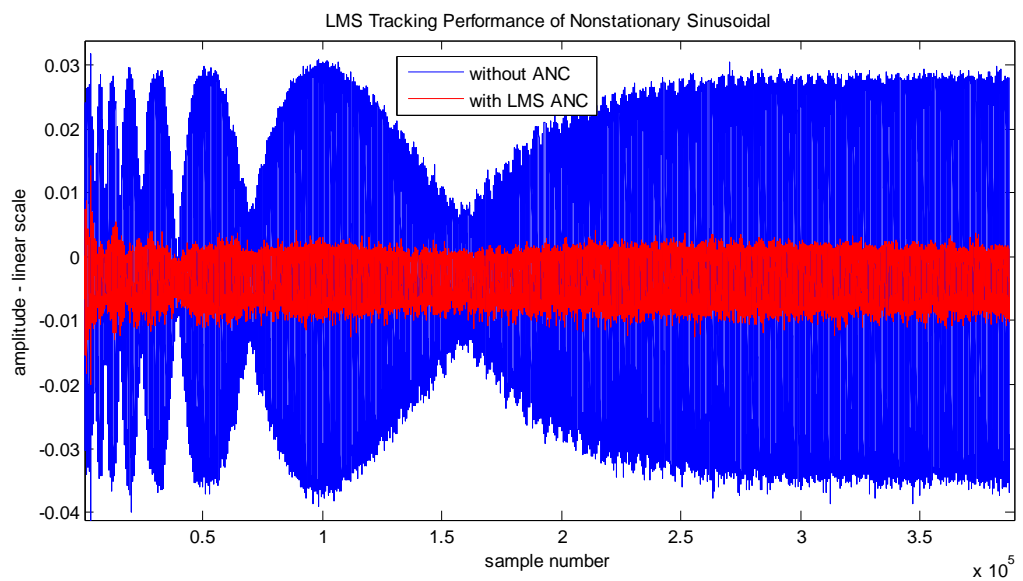


Figure 8.33 – LMS Tracking Performance with a Non-stationary Sinusoidal Signal

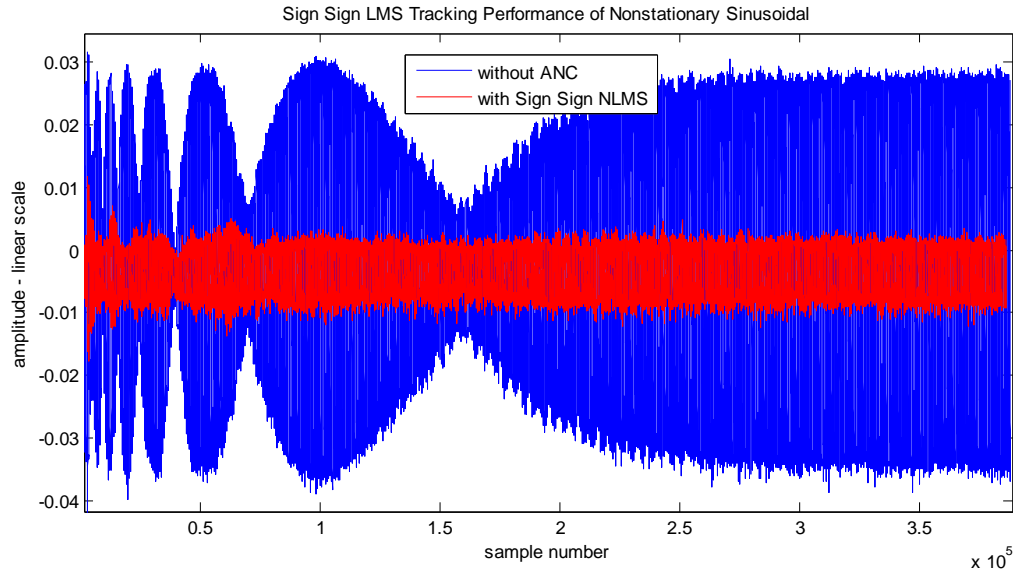


Figure 8.34 – Sign-Sign LMS Tracking Performance with a Non-stationary Sinusoidal Signal

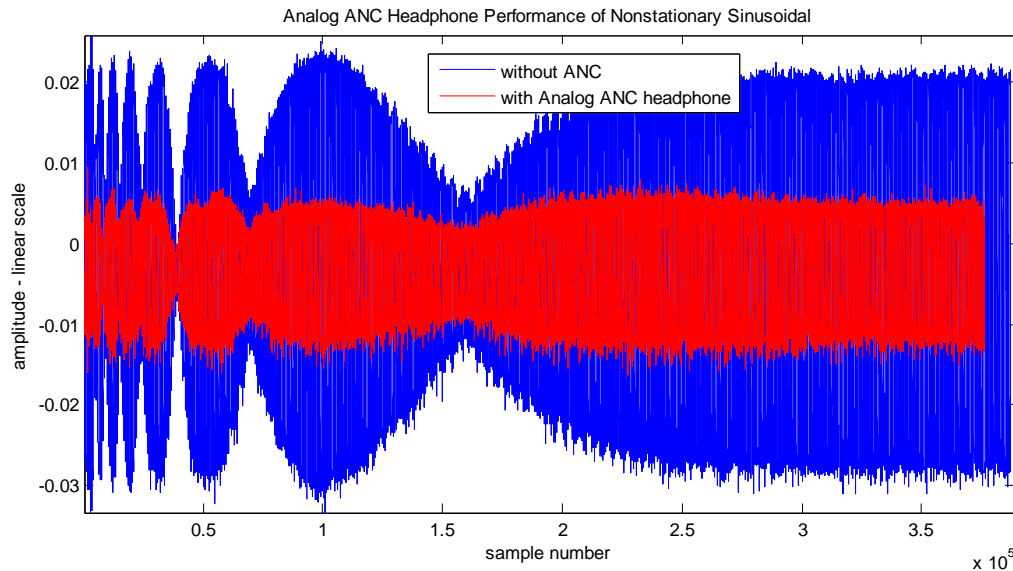


Figure 8.35 – Analog ANC Headphone Performance with a Non-stationary Sinusoidal Signal

The attenuation levels are better in digital ANC headphone than analog ANC headphone as seen in above figures. Digital ANC system preserves attenuation even though the primary noise levels are changed. This situation can be observed between the

samples 160000 and 250000. The responses of the system before the 50000th sample shows that the digital system tracks the decreasing slope of primary error signal. LMS adaptation shows the best performance in tracking capability. Analog ANC headphone is successful in the non-stationary signal experiment, because there is not a tracking problem in fixed analog controllers.

8.7 Convergence Rate for Different LMS Algorithms

The following experiments are made to see the convergence rate for different LMS algorithms. Figure 8.36, Figure 8.37 and Figure 8.38 are plotted in same scale showing convergence rate for single tone of 300 Hz.

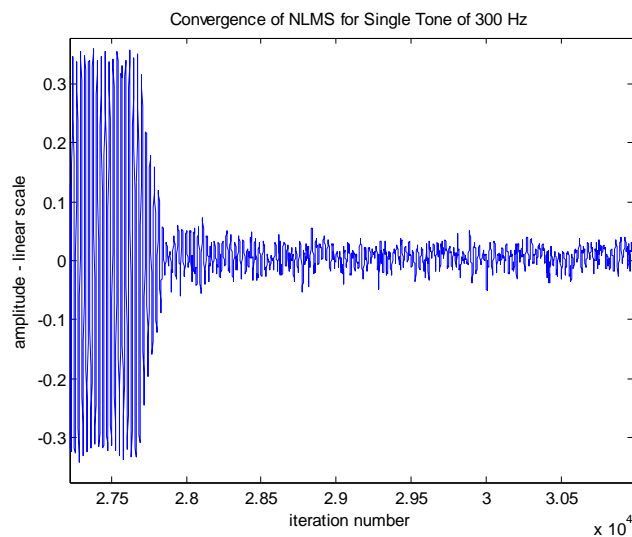


Figure 8.36 – Convergence Rate of NLMS for Single Tone of 300 Hz

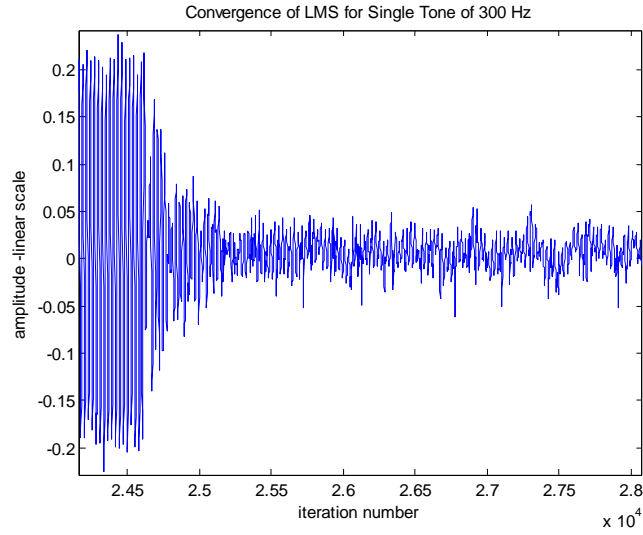


Figure 8.37 – Convergence Rate of LMS for Single Tone of 300 Hz

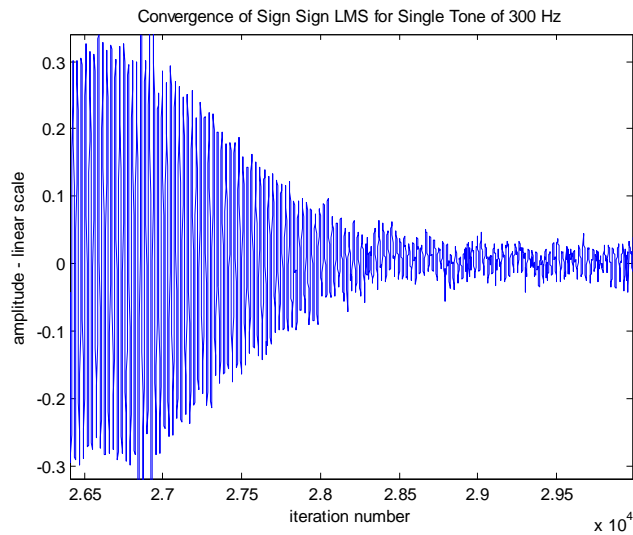


Figure 8.38 – Convergence Rate of Sign-Sign LMS for Single Tone of 300 Hz

As expected from theoretical discussions, NLMS has a faster convergence rate than LMS and SSLMS has the slowest convergence rate.

8.8 Digital Residual Error Experiment

Three different primary noise levels are given to digital ANC headphone and the attenuation amount in each step is observed. These three primary noise signals are named as level-2, level-1 and level-0 with decreasing power. The minimum signal level that can be attenuated by each algorithm is tried to be determined. The graphics are drawn in the DSP debugger environment in real time.

The Fourier transform of a primary noise signal of level-2 400 Hz is given in Figure 8.39. The residual error levels are seen for NLMS, LMS and SSLMS algorithms respectively in Figure 8.40, Figure 8.41 and Figure 8.42. Similarly a weaker 400 Hz signal (marked as level-1 amplitude) seen in Figure 8.43 is applied to the systems and the responses in Figure 8.44, Figure 8.45 and Figure 8.46 are recorded. The last group of figures from Figure 8.47 to Figure 8.50 shows the results for the weakest primary test signal (marked as level-0 amplitude) for which the algorithms are on the edge of stopping or severely slowing down.

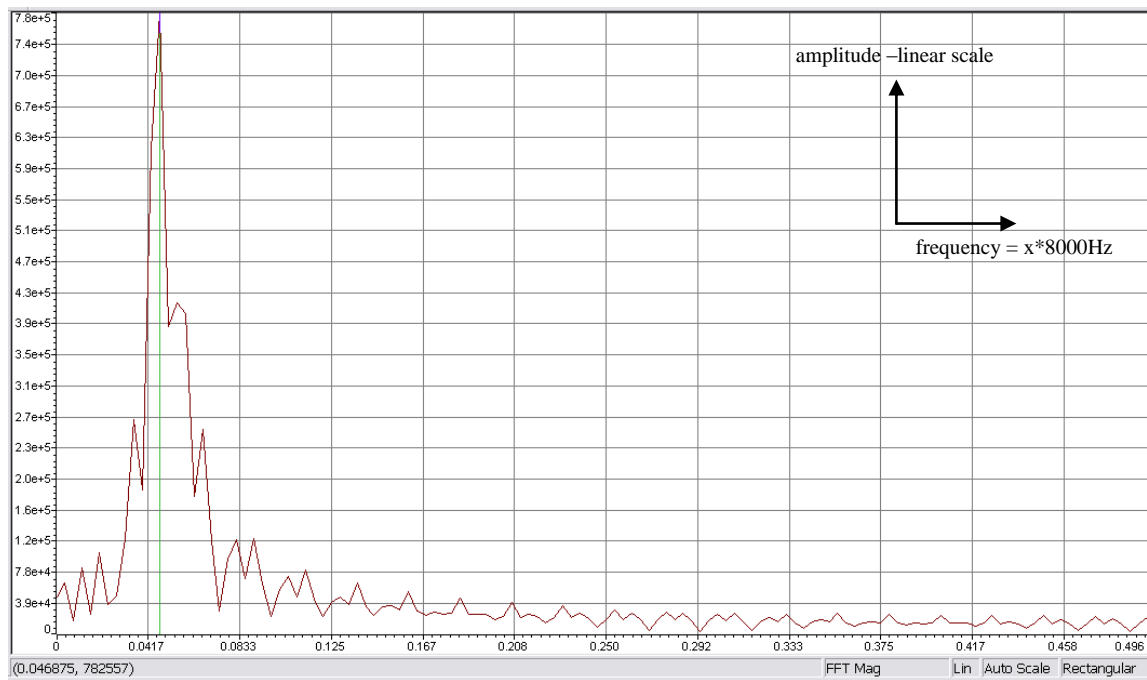


Figure 8.39 – Primary Noise for LMS Experiments for level-2 400 Hz signal

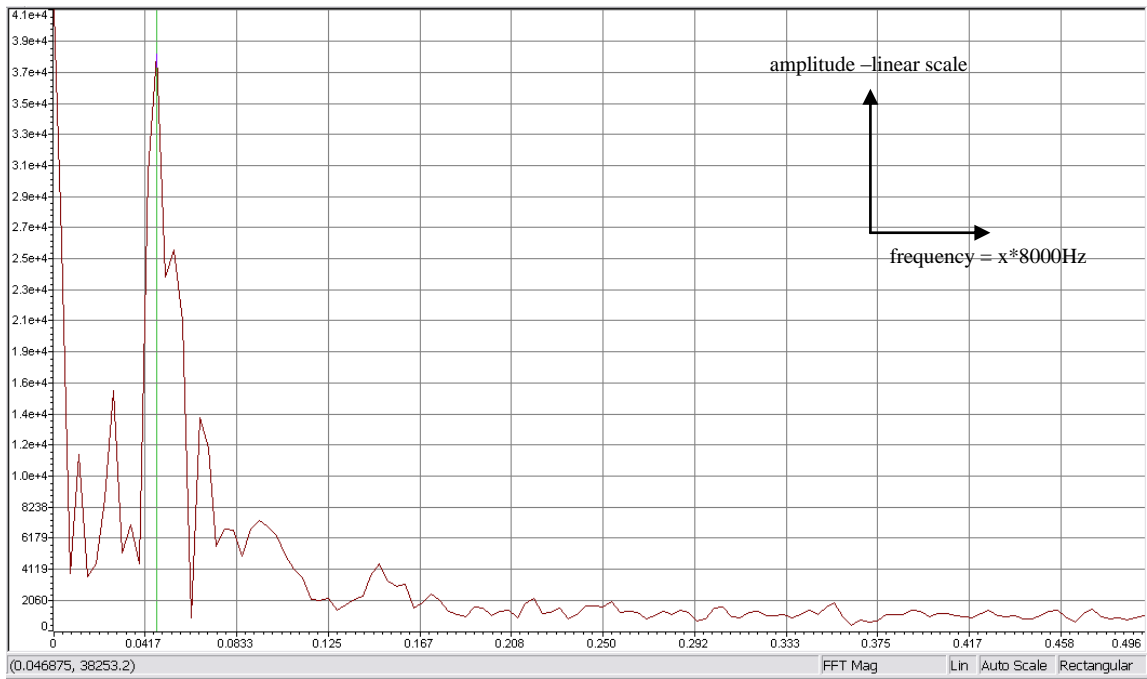


Figure 8.40 – Residual Error for NLMS Experiment for level-2 400 Hz signal

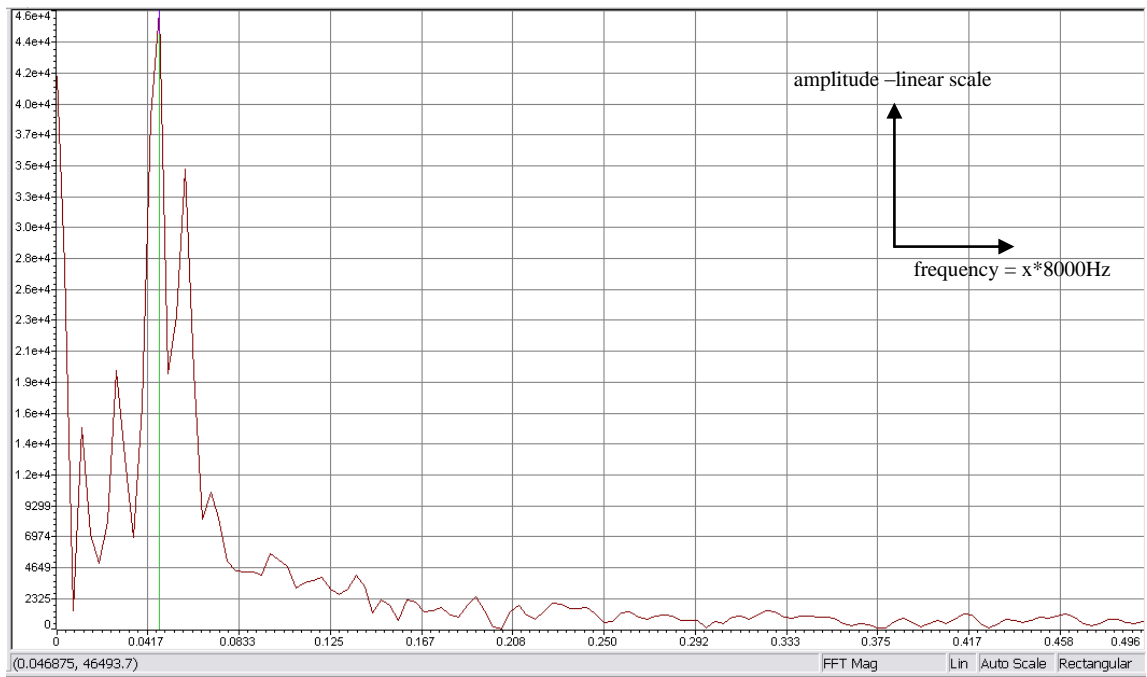


Figure 8.41 – Residual Error for LMS Experiment for level-2 400 Hz signal

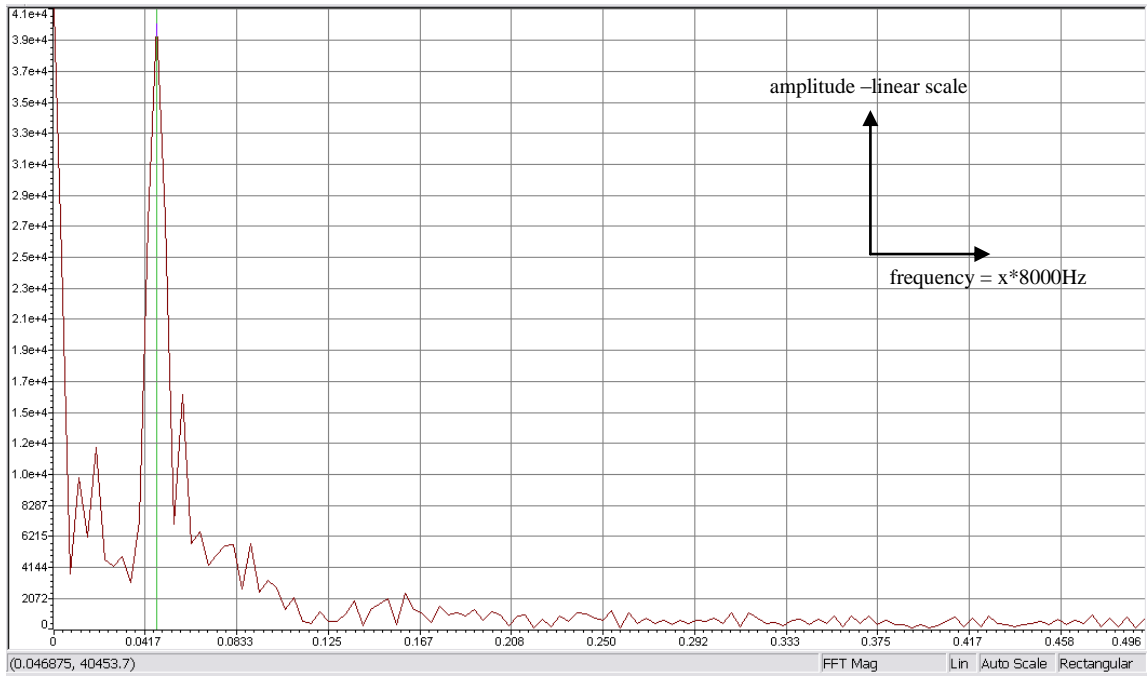


Figure 8.42 – Residual Error for Sign-Sign LMS Experiment for level-2 400 Hz signal

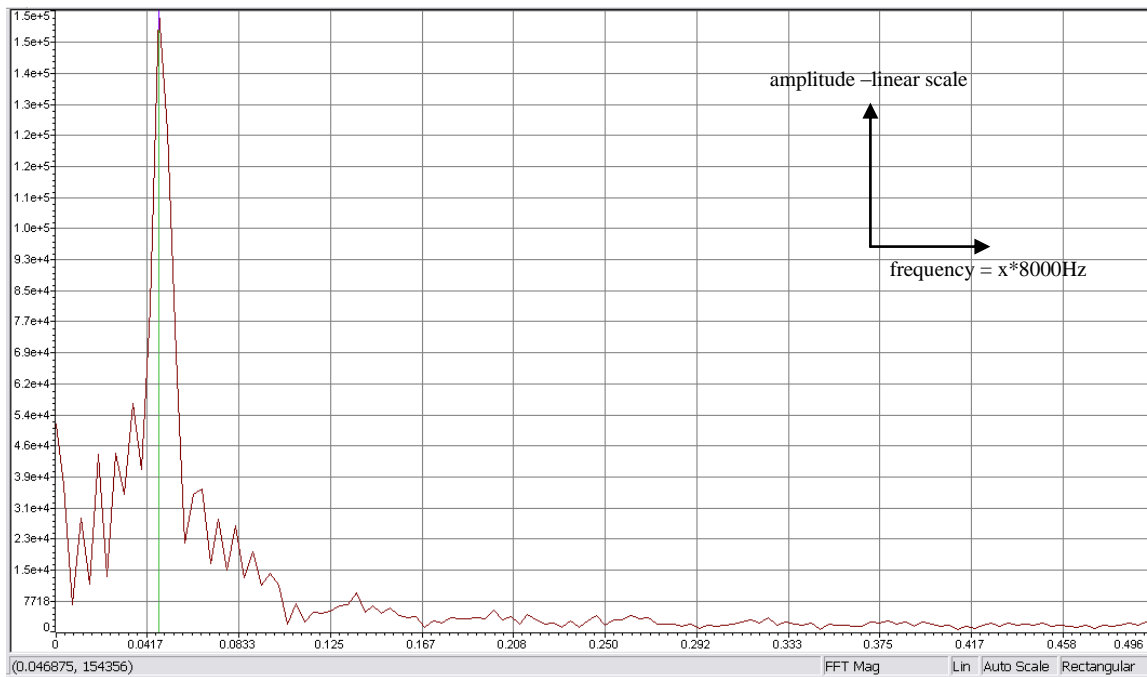


Figure 8.43 – Primary Noise for LMS Experiments for level-1 400 Hz signal

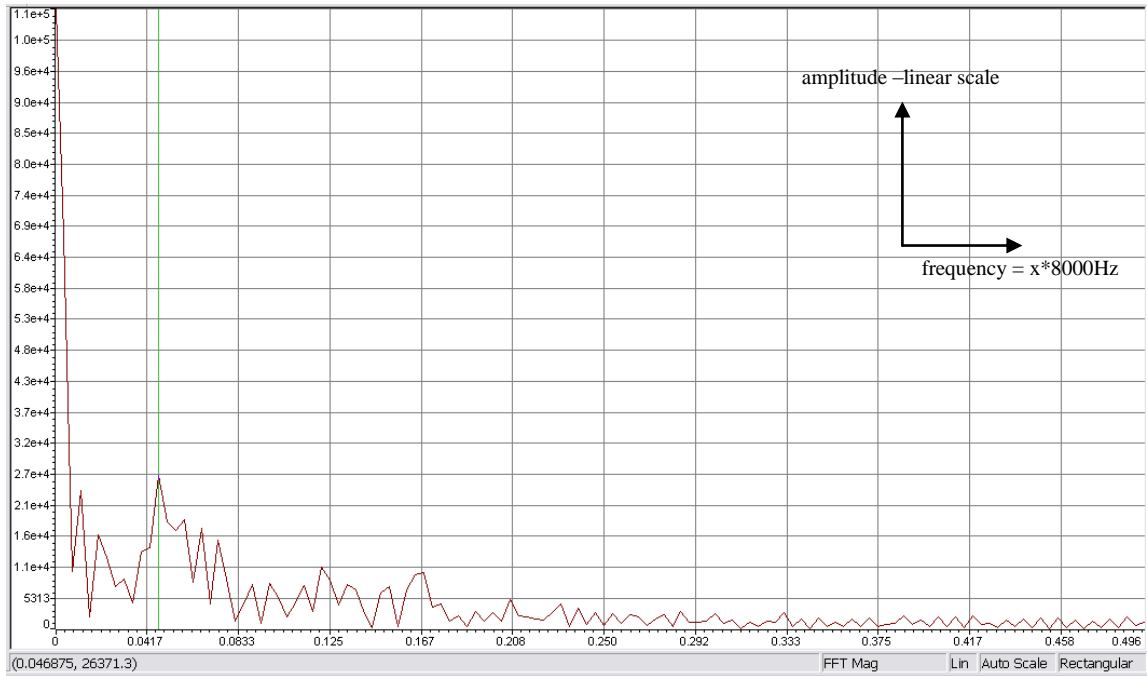


Figure 8.44 – Residual Error for NLMS Experiment for level-1 400 Hz signal

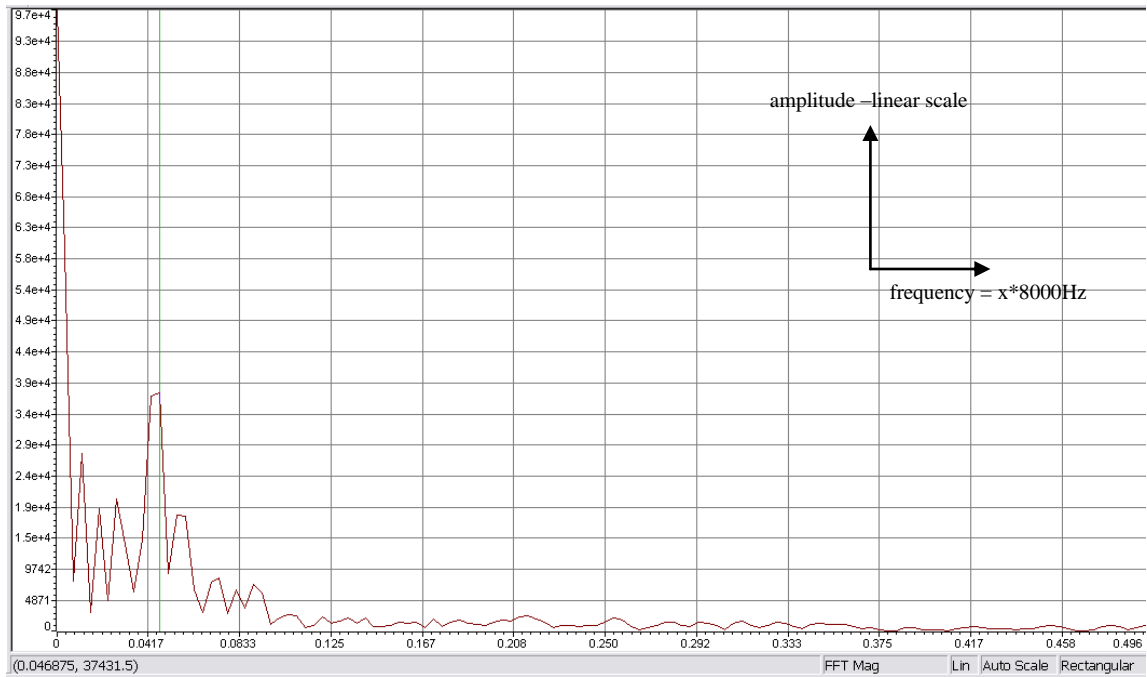


Figure 8.45 – Residual Error for LMS Experiment for level-1 400 Hz signal

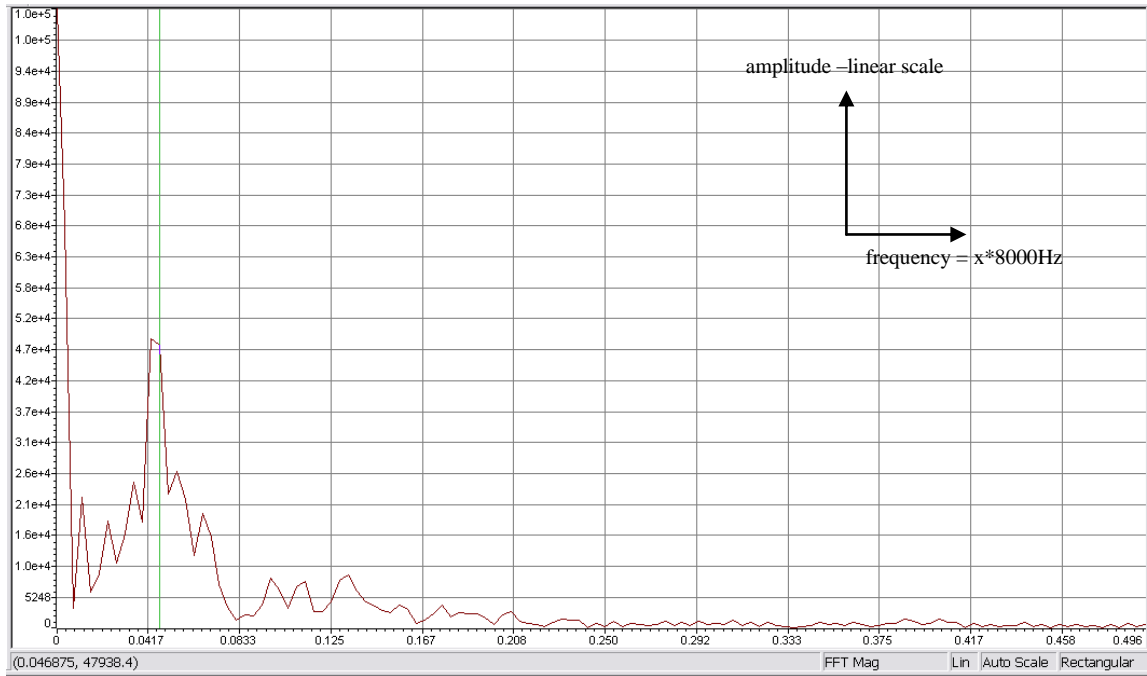


Figure 8.46 – Residual Error for Sign-Sign LMS Experiment for level-1 400 Hz signal

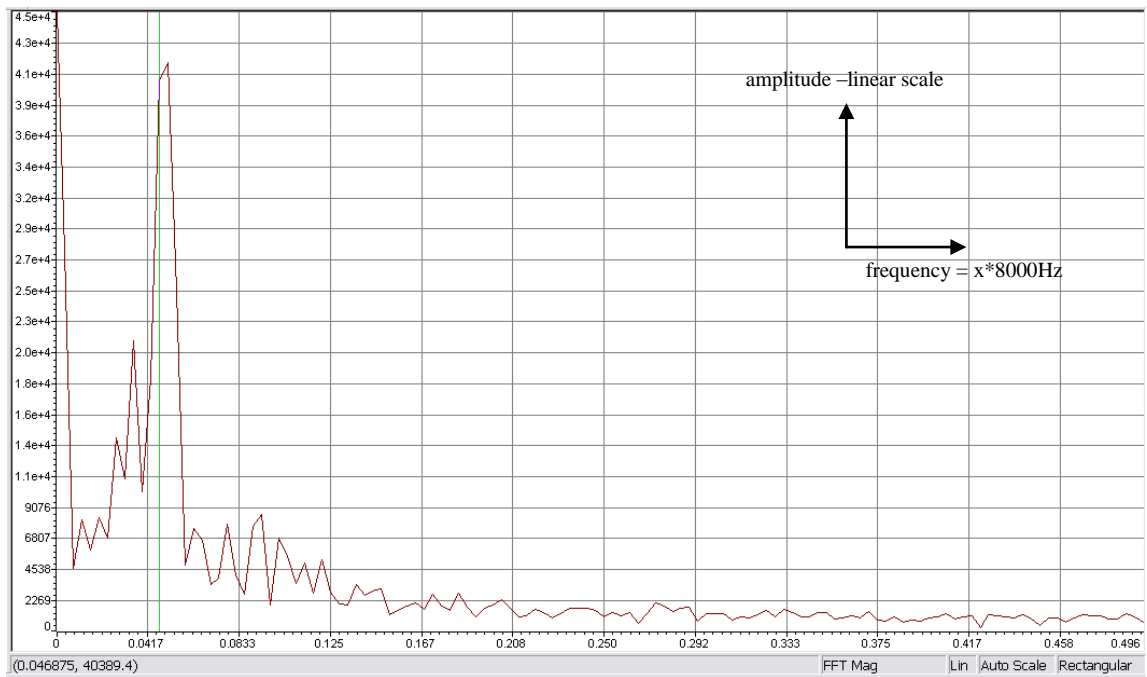


Figure 8.47 – Primary Noise for LMS Experiments for level-0 400 Hz signal

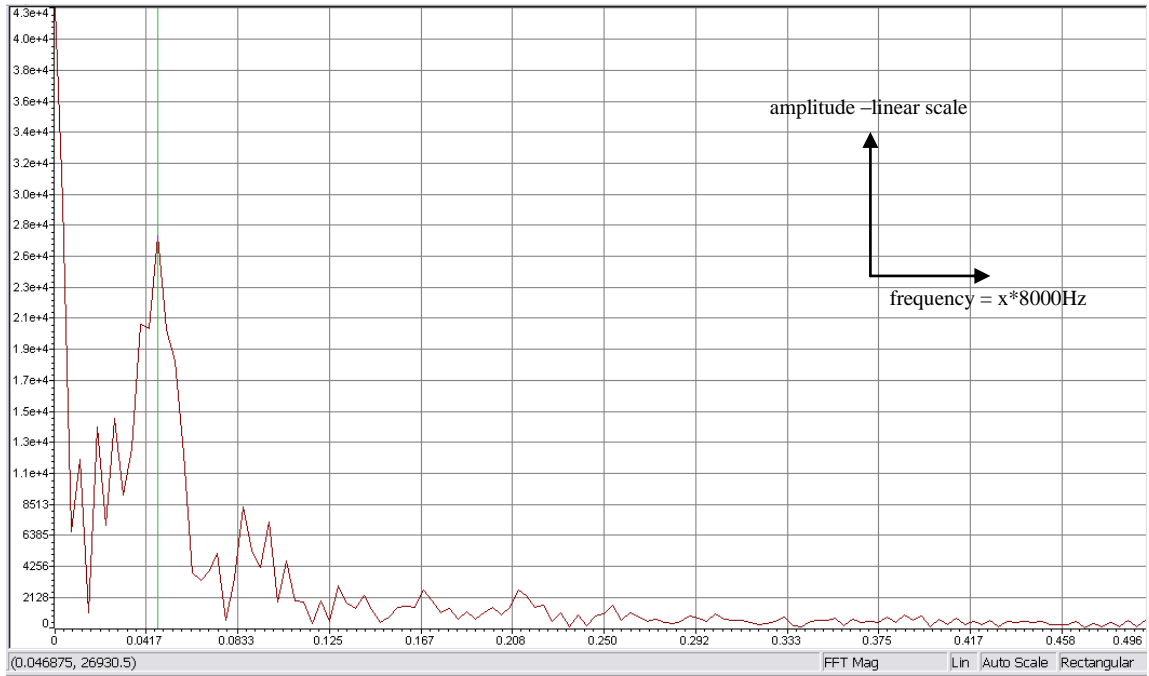


Figure 8.48 – Residual Error for NLMS Experiment for level-0 400 Hz signal

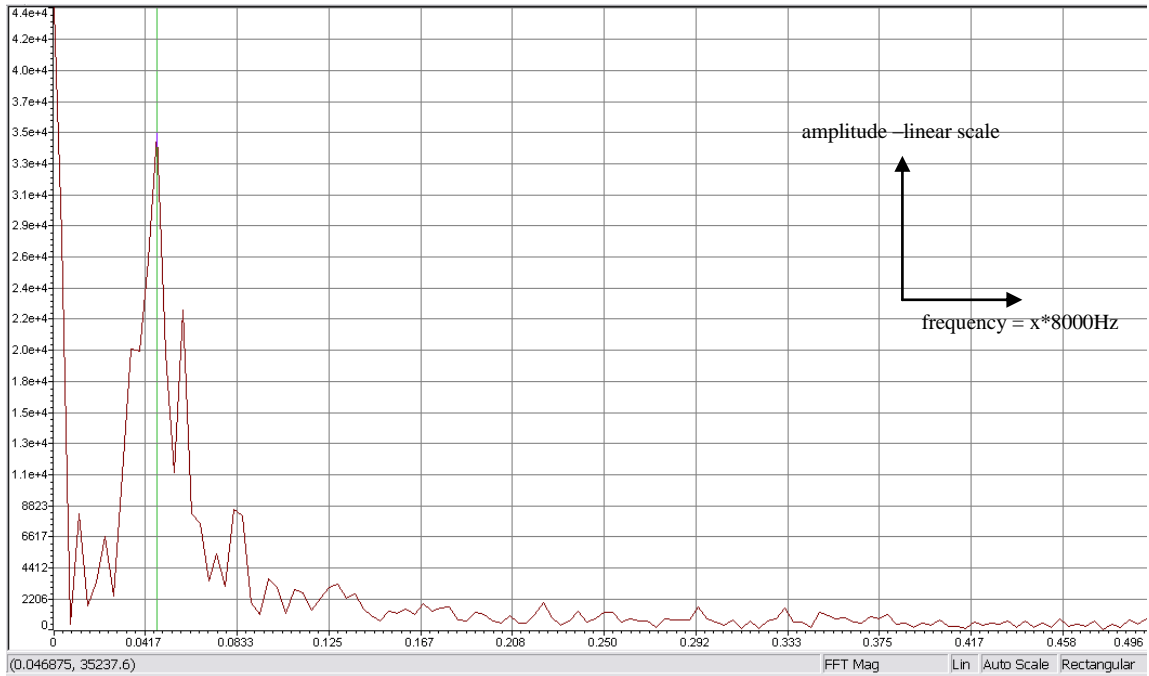


Figure 8.49 – Residual Error for LMS Experiment for level-0 400 Hz signal

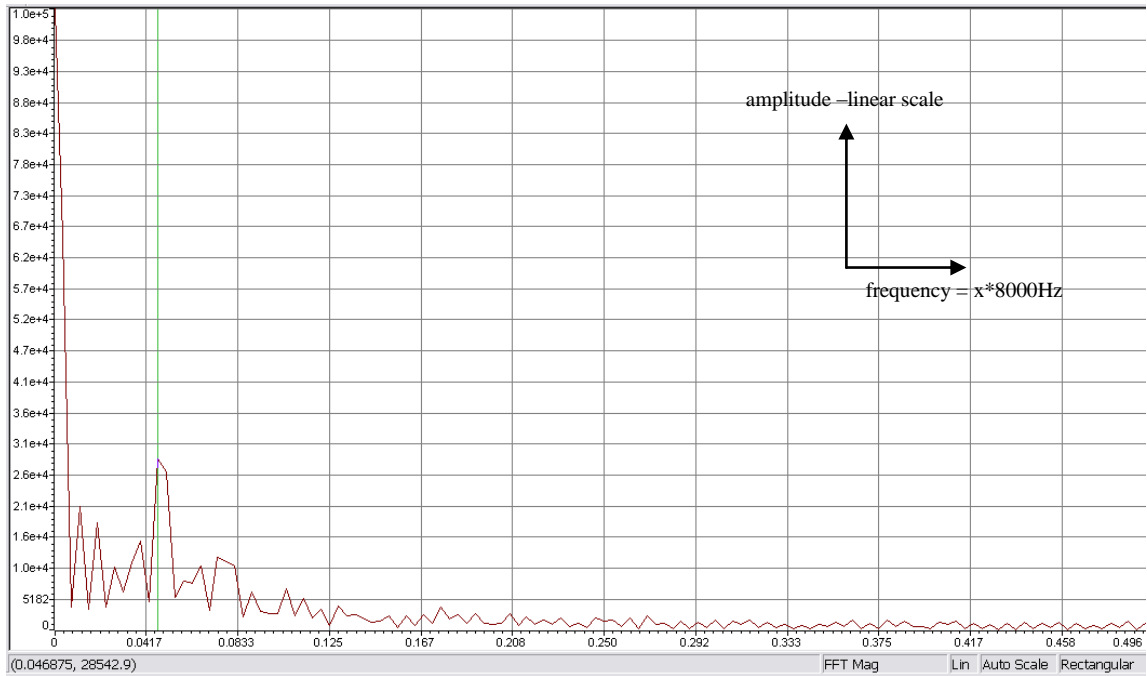


Figure 8.50 – Residual Error for Sign-Sign LMS Experiment for level-0 400 Hz signal

The results of these experiments showed that the digital residual error values are different for different adaptation algorithms. However, it is obvious that the attenuation levels are decreasing with decreasing primary noise levels in every algorithm. Moreover, below a determined primary noise level the adaptation ceases. It is seen that NLMS and SSLMS continues to attenuate even level-0 primary noise level, nevertheless LMS stops adapting at this level. It is experimentally seen that the slowdown phenomenon can be seen in fixed point environment when the primary noise signal is too low.

8.9 Drill Noise Experiment: Sub-band Filtering

How can the wideband drill noise be attenuated by digital system not only for its dominant frequencies but also for the other harmonics? To answer this question drill noise is filtered by a band pass filter whose pass band is 400 Hz - 500 Hz. The fourier transform of NLMS for drill noise around 400-500 Hz is given in Figure 8.51. The fourier transform of NLMS algorithm for band pass filtered drill noise is given in Figure

8.52. The attenuation of dominant frequency component at 450 Hz is 3 dB more than the attenuation in previous experiment. Moreover, some weaker harmonics around these dominant frequencies are attenuated only in this experiment. It is shown that total power attenuation is improved when the signal is made band limited. According to [25] sub-band filtering enhances the attenuation because of the decrease in eigenspread of each band limited primary noise piece. This result may be extended to dividing the signal in several bands around dominant frequencies and introducing individual adaptive filters for each band working in parallel.

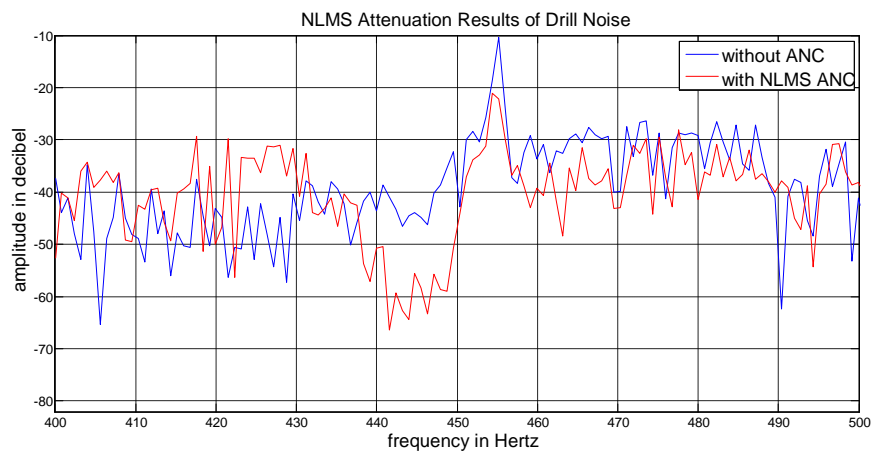


Figure 8.57 – The Attenuation of Normal Drill Noise by NLMS

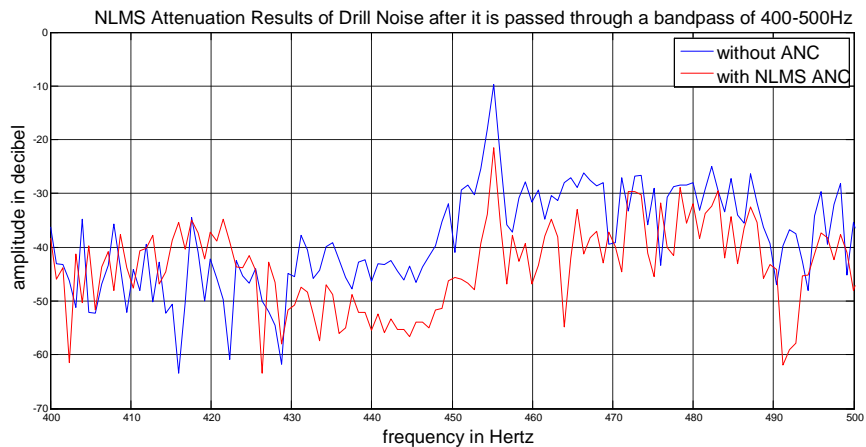


Figure 8.58 – The Attenuation of Bandpass Filtered Drill Noise by NLMS

8.10 Discussion of the Test Results of Digital ANC Headphone System

The digital system attenuation is about 25dB for single tones of 100Hz to 400 Hz. The attenuation levels are decreased for frequencies higher than 800 Hz down to 15 dB. The attenuation amount of each frequency component in a multi tone signal decreases as the dominance of this component in the overall signal decreases.

It is shown that NLMS is superior to other LMS algorithms in terms of convergence. The general attenuation levels of single tones are highest for LMS. SSLMS suffers from its slower convergence rate.

Digital systems are less effective than analog systems if the noise is distributed widely between 50Hz and 400 Hz, because the power reduction optimization of the adaptation algorithm causes the attenuation to be concentrated on dominant tones. Moreover, wideband noise is difficult to be attenuated by using only one adaptive filter. These insufficient attenuation levels of digital systems for wideband noises can be improved by a more qualitative filtering method: sub-band filtering.

DRE is inversely proportional to primary noise signal levels. Thus decreasing primary noise signals cause the adaptation process to terminate prematurely or continue with very small correction terms, i.e. the adaptation enters slowdown region.

The Bose Analog ANC Headphone is successful especially for wideband noises having frequency components lower than 300 Hz. However, it is insufficient for frequencies greater than 400 Hz. Moreover, analog ANC headphone starts to increase noises of frequencies greater than 700Hz - 800Hz. Its performance for very fast changing signals whose dominant frequency component is around 50Hz – 200Hz is superior to digital ANC headphone. On the other hand, it is obvious that slow changing signals within frequencies of around 300 – 800 Hz is tracked and more successfully attenuated by the digital ANC headphone system than the analog ANC headphone.

Another result is that successful mounting of analog ANC system on head contributes in noise cancellation. However, it should be noted that the mechanical attenuation is effective for frequencies higher than 400 Hz. It is experimentally seen in digital ANC system that the attenuation levels are increased when the headphone is tried to be tightly mounted on head. This action also increases the dynamic range as a result of the decrease in the error input to the microphone. As a result it can be said that a tighter mounting headphone should be selected for digital ANC system.

CHAPTER 9

CONCLUSION

In this thesis, the design and implementation of a portable fixed point digital ANC headphone system is achieved. The theoretical results of fixed point LMS are applied to real time ANC implementation.

LMS, normalized LMS and sign-sign LMS algorithms were studied. These algorithms were implemented as filtered input type. The problem of slowdown phenomenon in fixed point implementation has been examined. Step size selection in fixed point environment has been made. The delays inherent to digital systems and their importance in synchronization of the LMS adaptation algorithm were stated and necessary modifications are applied. A compact, noise immune and convenient card based on TMS320VC5416 Fixed point DSP was designed and produced. The card was designed such that further improvements or modifications can be done easily on hardware.

The performance of the digital device was compared with an analog ANC headphone with artificial signals as well as with natural signals. The tracking capability of the digital system was tested. Convergence rate of different LMS adaptation algorithms were compared. The digital residual error resulted from slowdown phenomenon was experimentally seen. Additionally, software adjustments for the practical usage of the digital system were introduced to prevent divergence of the system when the headphone is put off. The basis of further improvements in attenuation for digital ANC system was stated as sub-band filtering.

It is seen that the digital system is capable of attenuating frequencies from 80 Hz up to 1000 Hz especially when the noise is narrowband. The attenuation level is about

25 dB for narrow band signals between 80 Hz and 400 Hz. For higher frequencies up to 1000 Hz this attenuation level is about 15 dB.

Fixed analog controller in this study has a predefined optimum attenuation band. This optimum band is between 50 Hz and 400 Hz. The analog system is ineffective for frequencies higher than 400 Hz. Moreover, it increases frequency components higher than 700-800Hz. The attenuation levels of digital ANC system are much higher than the attenuation levels of analog system when the noise is narrowband. On the other hand, the attenuation level of digital ANC system is lower than analog ANC system for weaker frequency components when the noise is wideband, because filter coefficients are optimized to decrease the power of residual error and dominant frequency components are more effective on power of this error signal. One adaptation filter is insufficient when the noise is spread equally over a wide frequency band. It is experimentally seen that the adaptation of digital system can be improved for wideband noises by dividing the noise in sub-bands and applying individual filters for each partition.

It is seen that the digital system is affected by delays existing between analog and digital parts of headphone system. Digital residual error originating from fixed point implementation affects low level signal attenuation.

Normalized LMS algorithm is superior to other adaptation algorithms for its small digital residual error and high convergence rate. However, NLMS has a drawback for its inherent arithmetic complexity in fixed point implementation. Sign-sign LMS algorithm has the slowest convergence rate.

Unfortunately, the dynamic range of the designed digital system is not as good as analog ANC system. When the upper limit for primary noise signal is increased by decreasing step size the system becomes less sensitive to lower amplitude noise signals due to slowdown phenomenon whereas a larger step size increases results in divergence for high level primary noise signals. This problem can not be solved by increasing the

resolution because of increasing computational complexity. An educated step size sequence should be implemented such that the high level noises do not cause the system to diverge and low level noises do not create high digital residual error.

The mechanical design of the headphone was seen to be very critical to increase noise attenuation. Moreover, the tight mounting of the headphone resulted in the increase in dynamic range.

In conclusion, it is shown that adaptive ANC headphone system can be implemented digitally by using a fixed point processor. The attenuation levels can be increased by adaptive digital systems at about 10 dB compared with analog ANC systems when the noise is narrowband. Moreover, noise signals having frequency components higher than 400 Hz is attenuated in digital systems contrary to analog systems.

9.1 Future Work

The effectiveness of digital system should be extended to wider band noises by some additional improvements. It is seen that this improvement can be supplied by sub-band filtering which is achievable in the designed card of this study by an FPGA. FPGA is a suitable environment for such parallel synchronous operations. Actually a combination of DSP and FPGA controller can be used for optimized processing performance [26].

The mechanical design of digital ANC headphone should be improved. The tight mounting of headphone and mechanical attenuation is shown to be very important as a contribution to the overall attenuation.

The increase in clock rates of DSP and the resolution of CODECs results in much more computational capacity and decrease in the least significant digit values.

This makes fixed point limitations become less effective as the results of extended resolution, signal to noise ratio and total harmonic distortion.

An adaptive step size selection sequence increases the dynamic range of fixed point implemented LMS.

REFERENCES

- [1] C.M. Harris, Handbook of Acoustical measurements and Noise Control, 3rd ed. New York: McGraw-Hill, 1991
- [2] P. Lueg “Process of silencing sound oscillations” U.S. Patent 2,043,416 June 9, 1936
- [3] H. F. Olson and E. G. May, “Electronic sound absorber,” Acoust. Soc. Amer. vol. 25, pp. 1130–1136, Nov. 1953.
- [4] Sen M. Kuo and Dennis R. Morgan “Active Noise Control: A Tutorial Review” in Proceedings of the IEEE, vol. 87, no. 6 June 1999.
- [5] Dorey, A.P., S.F. Pelc, R.D. Rawlinson and P.D Wheeler. “The Development and Testing of an Active Noise Reduction System For use in Ear Defenders,” Proc. Inter-Noise 78. pp. 977-982, 1978.
- [6] Simon Haykin, “Adaptive Filter Theory”, Prentice Hall, 1996.
- [7] Simon Haykin, “Adaptive Filters”, Signal Processing Magazine, IEEE Computer Society, 1999.
- [8] Woon S. Gan, Sohini Mitra and Sen M. Kuo, “Adaptive Feedback Active Noise Control Headset: Implementation, Evaluation and Its Extensions” IEEE Transactions on Consumer Electronics, Vol. 51, No.3, August 2005.
- [9] Sen M. Kuo, Sohini Mitra and Woon-Seng Gan, “Adaptive Feedback Active Noise Control Headset: Implementation, Evaluation and Its Extensions” IEEE Transactions on Control Systems Technology , Vol. 14, No.2, March 2006.
- [10] D. R. Morgan, “An analysis of multiple correlation cancellation loops with a filter in the auxiliary path,” IEEE Trans. Acoust., Speech, Signal Processing, vol. ASSP-28, pp. 454–467, Aug. 1980.
- [11] S. J. Elliott and P. A. Nelson, “Active noise control,” IEEE Signal Processing Mag., Vol. 10, pp. 12–35, Oct. 1993.

- [12] Richard D. Gitlin, J. E. Mazo and Michael G. Taylor, "On the design of Gradient Algorithms for Digitally Implemented Adaptive Filters", IEEE Transactions On Circuit Theory, Vol. ct-20, No.2, March 1973.
- [13] Christos Caraiscos and Bede Liu, "A Roundoff Error Analysis of the LMS Adaptive Algorithm", IEEE Transactions on Acoustics, Speech and Signal Processing, Vol. ASSP-32, No.1, February 1984.
- [14] Neil J. Bershad, and Jose Carlos M. Bermudez, "New Insights on the Transient and Steady-State Behaviour of the Quantized LMS Algorithm", IEEE Transactions on Signal Processing, Vol. 44, No.10, October 1996.
- [15] Riten Gupta and Alfred O.Hero, "Power versus Performance Tradeoffs for Reduced Resolution LMS Adaptive Filters", IEEE Transactions on Signal Processing, Vol. 48, No.10, October 2000.
- [16] Neil J. Bershad, and Jose Carlos M. Bermudez, "A Nonlinear Analytical Model for the Quantized LMS Algorithm – The Power-of-Two Step Size Case", IEEE Transactions on Signal Processing, Vol. 44, No.11, November 1996.
- [17] Neil J. Bershad, and Jose Carlos M. Bermudez, "A Nonlinear Analytical Model for the Quantized LMS Algorithm – Arbitrary Step Size Case", IEEE Transactions on Signal Processing, Vol. 44, No.5, May 1996.
- [18] Nabil R. Yousef and Ali H. Sayed, "Fixed Point Steady-State Analysis of Adaptive Filters", International Journal of Adaptive Control and Signal Processing, Vol. 17, pp. 237-258, March 2003.
- [19] Sen M. Kuo and Dennis R. Morgan, "Active Noise Control Systems: Algorithms and DSP Implementations", John Wiley & Sons Inc., New York, 1996.
- [20] Texas Instruments, "TMS320VC5416 Fixed-Point Digital Signal Processor Data Manual", Literature Number: SPRS095O, January 2005.
- [21] Texas Instruments, "TMS320C54x DSP Reference Set Volume 1: CPU and Peripherals" Literature Number: SPRU131F, April 1999.
- [22] Texas Instruments, "TMS320C54x DSP Library Programmer's Reference" Literature Number: SPRU518C, August 2002.
- [23] Texas Instruments, "TLV320AIC20K Codec Data Manual" Literature Number: SLAS363D, April 2005.
- [24] Texas Instruments "TMS320C54x Chip Support Library API Reference Guide" Literature Number: SPRU420E, July 2003.

- [25] Victor DeBrunner, Linda S. DeBrunner and Longji Wang, “Sub-band Adaptive Filtering With Delay Compensation for Active Control”, IEEE Transactions on Signal Processing, Vol. 52, No.10, October 2004.
- [26] Reza Hashemian, “Design of an Active Noise Control System Using Combinations of DSP and FPGAs”, PLD Conference Proceedings, 1995.
- [27] Knowles Acoustics, SP0103NC Specification Document.
- [28] Markus Rupp and Ali H. Sayed “Robust FxLMS Algorithms with Improved Convergence Performance”, IEEE Transactions on Speech and Audio Processing, Vol. 6, No. 1, January 1998

APPENDIX A

HARDWARE DESIGN OF DIGITAL ANC HEADPHONE SYSTEM

Basic serial port connections between TLV320AIC20K CODEC and TMS320VC5416 CODEC can be seen in Figure A.1.

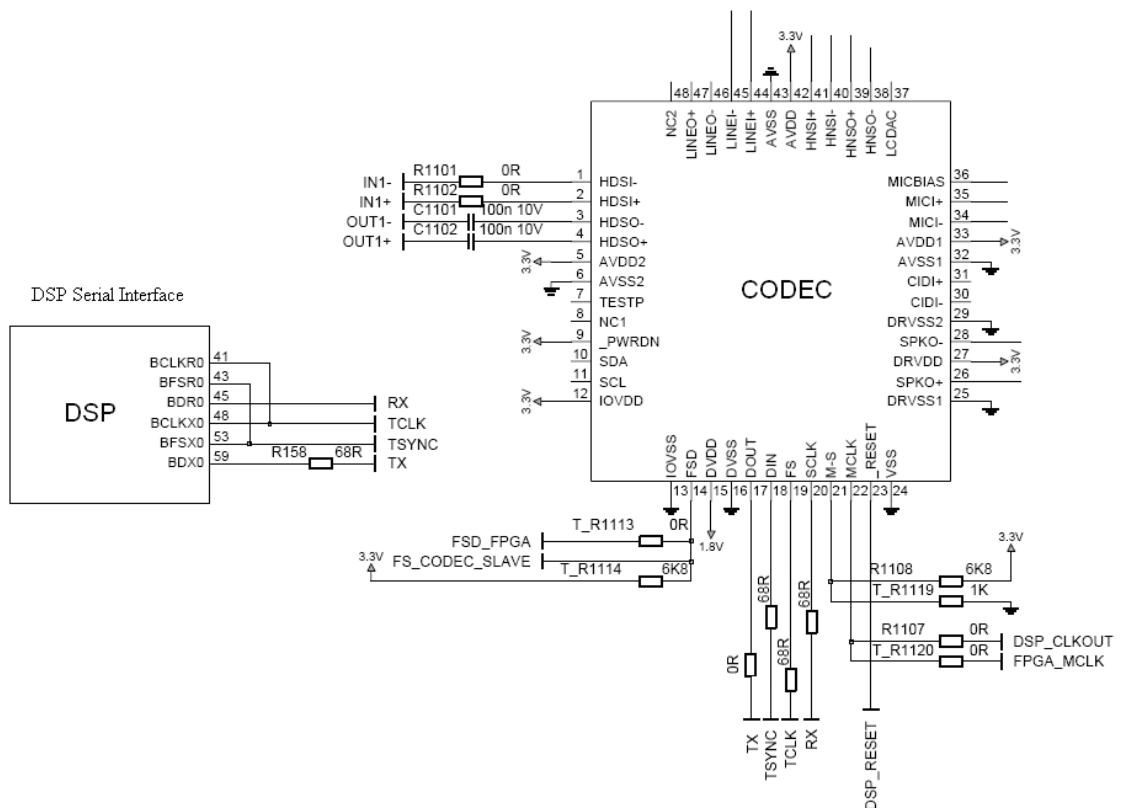


Figure A.1 – Serial Port Connections between TLV320AIC20K and DSP

An AMD29LV160DT-90EI flash-ROM is placed on card for the DSP to run independent of the emulator connection. The program is coded to the flash-ROM through emulator once and on each power-up the code is copied to the DSP. DSP starts to run from the starting point of this code.

Additionally, a Field Programmable Gate Array (Xilinx XC3S1000 FPGA) within a PROM (the code of RAM based FPGA resides on PROM) is placed on board for flexibility to develop other algorithms. Alternative paths from CODECs to the FPGA are supplied. There exists a parallel address/data bus between DSP and FPGA. The reason for this improvement is for possible future work. The advantages of FPGA based implementation considering some real implementation issue is explained in Chapter 9.

A second CODEC is placed on the card for some possible additional connections such as line-in.

The power management of the card is based on four MAXIM MAX1793 regulators which produce 3.3V, 1.8V, 1.5V and 1.2V for different components on the board. These regulators can work with voltages up to 5.5V as input.

The reset management is accomplished by MAX6707TKA-T reset supervisor. This component resets the intelligent devices on board when there exists a certain decrease in voltages 3.3V and 1.5V. The CODEC is reset through a general purpose output of the DSP by software.

The clock is supplied by an EC54 SMX7 24MHz clock oscillator and it passes through a Linear Technology LT1719IS6 operational amplifier for a clear square wave of 24 MHz. This clock is fed to the DSP and FPGA as the main clock sources. Inside the DSP, this rate is increased to 120MHz by the PLL. The 30MHz output clock of the DSP is given to the CODEC as its main clock. The 256 KHz clock and 8 KHz synchronization signal for the serial data and command interface between DSP and CODEC are supplied by the CODEC.

APPENDIX B

TMS320VC5416 DSP CONFIGURATION

As far as CPU registers are concerned, frequency of output clock signal of DSP can be set by CLKMD and BSCR registers. In addition, the frequency of CPU clock of the DSP can be set by CLKMD pins on hardware or by CLKMD registers on software. This input clock of 120MIPS DSP is supplied by a 24MHz clock and multiplied by 5 in internal PLL. By replacing the pin compatible TMS320VC5416PGE120 with TMS320VC5416PGE160 and 24MHz clock oscillator with 20 MHz clock oscillator the DSP can be run with 160 MHz CPU clock.

DSP provides three high-speed, full-duplex, multichannel buffered serial ports (MCBSPs) that allow direct interface to other C54x/LC54x devices, CODECS, and other devices in a system.

The McBSP consists of a data path and control path. The six pins, BDX, BDR, BFSX, BFSR, BCLKX, and BCLKR, connect the control and data paths to external devices. These are clock and synchronization signals of serial port. The implemented pins can be programmed as general-purpose I/O pins if they are not used for serial communication.

Control information in the form of clocking and frame synchronization is communicated by way of BCLKX, BCLKR, BFSX, and BFSR. The device communicates to the McBSP by means of 16-bit-wide control registers accessible via the internal peripheral bus. The control block consists of internal clock generation, frame synchronization signal generation and their control selection, but in this study DSP internal clock generation is not used. The control block sends notification of important events to the CPU and DMA by two interrupt signals, XINT and RINT, and two event

signals, XEVT and REVT. The interior block diagram of McBSP is given in Figure B.1. In this study DMA is not used, CPU directly interfaces with McBSP.

The CPU or the DMA controller reads the received data from the data receive register (DRR[1,2]) and writes the data to be transmitted to the data transmit register (DXR[1,2]). Data written to DXR[1,2] is shifted out to DX via the transmit shift register (XSR[1,2]). Similarly, receive data on the DR pin is shifted into the receive shift register (RSR[1,2]) and copied into the receive buffer register (RBR[1,2]). RBR[1,2] is then copied to DRR[1,2], which can be read by the CPU or the DMA controller. This allows simultaneous movement of internal and external data communications. DRR2, RBR2, RSR2, DXR2, and XSR2 registers are not utilized (written, read, or shifted) if the receive/transmit word length, R/XWDLEN[1,2], is specified for 8-, 12-, or 16-bit mode.

The control registers for the multichannel buffered serial port are accessed using the subbank addressing scheme. This allows a set or subbank of registers to be accessed through a single memory location. The McBSP subbank address register (SPSA) is used as a pointer to select a particular register within the subbank. The McBSP data register (SPSDx) is used to access (read or write) the selected register. Alternatively, one can benefit from chip support library to use predefined functions for register assignments.

The McBSP registers and their corresponding values specific to this study are as follows: SPCR1 register is set as the digital loopback mode disabled, receive interrupt is dedicated to RRDY signal and reset is applied to receive port. SPCR2 register is set to disable internal sample rate generator of TMS320VC5416, transmit interrupt is dedicated to XRDY signal and reset is applied to transmit port. The RCR and XCR registers are set as single-phase frames of 4 words consisting of 16 bits. Lastly, Pin Control Register is set as frame synchronization and clock signals are input. Frame synchronization signals are active high signals. PCR register configuration also dictates that the transmit clock, samples data at rising edges whereas the receive clock, samples data at falling edges.

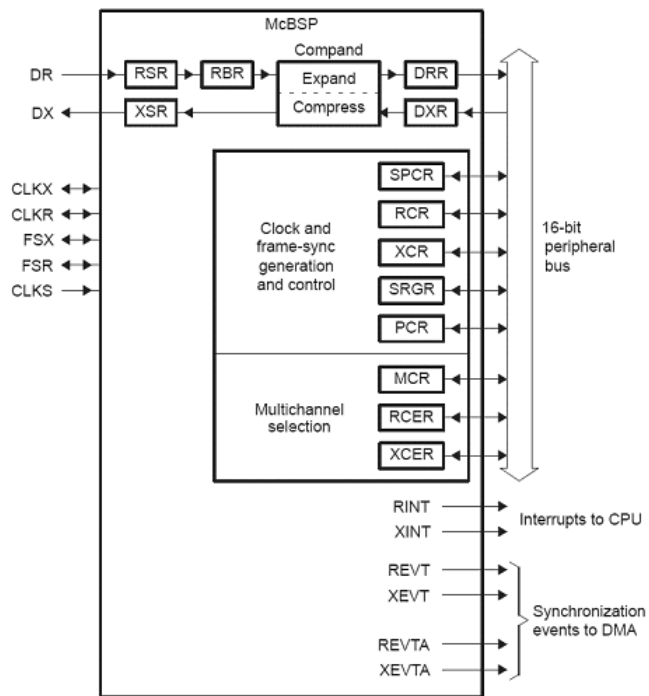


Figure B.1 – Block Diagram of Multichannel Buffered Serial Port in TMS320VC5416 DSP

APPENDIX C

TLV320AIC20K CODEC CONFIGURATION

TLV320AIC20K has several types of inputs and outputs for various load and source types such as Microphone / 8 Ohm Speaker, 600 Ohm Line In/ Line Out, 150 Ohm Headset In/ Headset Out, 150 Ohm Handset In / Handset Out. The block diagram of one channel of CODEC is in Figure C.1. Actually there exists another channel in TLV320AIC20K with same block diagram.

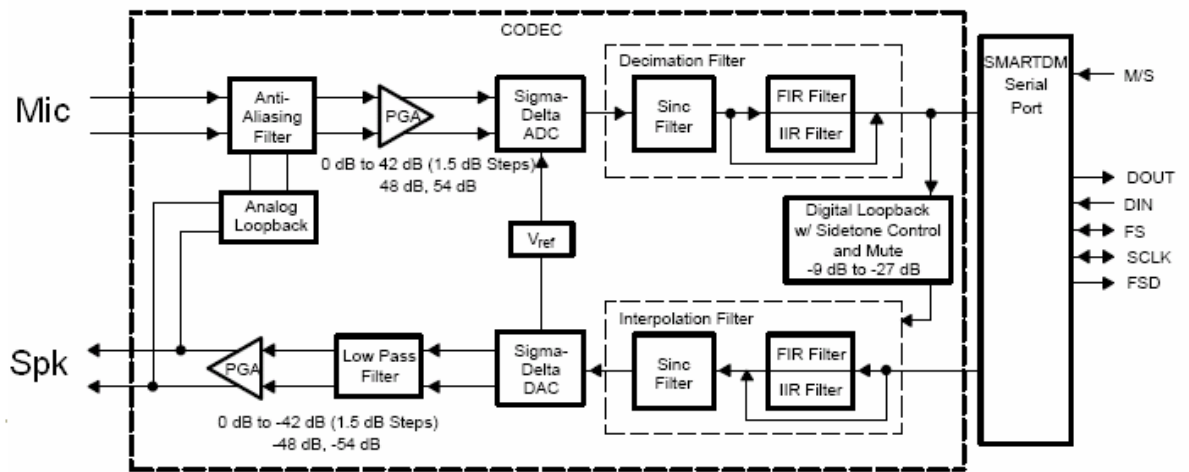


Figure C.1 – The Block Diagram of One Channel of TLV320AIC20K CODEC

The configuration of the codec defines the following parameters which are critical:

- The data rate of the serial port communication
- The sampling frequency of the ADC and DAC
- The input/output connections
- The amplifier gain for input/output
- The voltage level for Microphone Bias Output

- Interpolation / Decimation Filter disabling

Each channel in TLV320AIC20K contains 6 control registers that are used to program available modes of operation. All register programming is achieved by the control frame through DIN. New configuration takes effect after a delay of one frame synchronization signal. The serial interface is defaulted to programming mode upon power-up. 6th bit of Control Register-1 is set for continuous data transfer mode. The form of the registers to be written is in Table C.1 and crucial settings are given in Table C.2.

The configuration of TLV320AIC20K CODEC is made by TMS320VC5416 DSP through McBSP0 serial port which is also used for data communication. During configuration, as mentioned in DSP configuration, each frame consists of 4 words. The first and third words in this frame carry the configuration word for first and second channel of CODEC respectively. The second and fourth words carry corresponding data samples. Upon completion of the configuration, the serial port of DSP is reconfigured to carry 2 words in each frame which consists of only data samples.

Table C.1 – TLV320AIC20K CODEC Write Register Form

D15-D13	Control Register Address
D12	(0) write – (1) read
D11	broadcast (1)
D7 – D0	Register Content

Table C.2 - TLV320AIC20K CODEC Register Content

Register-1	00101001	The bias voltage of SP0103NC microphone is set to 2.35V.
Register-2	11100000	Decimation/Interpolation Filters are disabled
Register-3A	00011001	No power-down is chosen for the device to operate in normal mode.
Register-3B	01000000	Bandpass filter is disabled.
Register-3C	10000000	-
Register-3D	11000000	-
Register-4	11110101 and 00001010	Frame Synchronization signal is set to 8KHz by $FS = MCLK / MNP$ SCLK is 32xFS for continuous data transfer mode and 64xFS for programming mode
Register-5A	00010100	ADC gain is set to 42 dB
Register-5B	“01010100	DAC gain is set to -13.5 dB
Register-5C	10000000	-
Register-5D	11000000	-
Register-6A	00000001	Headset Input for CH1 / Handset Input for CH2
Register-6B	00000002	Headset Output for CH1 / Handset Output for CH2